

**INVESTIGATION OF RADIATION AND STRUCTURAL  
PROPERTIES OF BISMUTH-BARIUM-BOROSILICATE  
GLASS SYSTEM FOR DESIGN AS A GAMMA RAY  
SHIELDING MATERIALS**

**NATSUPON CHUTITHANAPANON**

**A THESIS SUBMITTED IN PARTIAL FULFILLMENT OF THE  
REQUIREMENTS FOR THE DEGREE OF DOCTOR OF PHILOSOPHY  
MAJOR IN PHYSICS  
FACULTY OF SCIENCE  
UBON RATCHATHANI UNIVERSITY  
ACADEMIC YEAR 2020  
COPYRIGHT OF UBON RATCHATHANI UNIVERSITY**

## ACKNOWLEDGEMENT

Foremost, I would like to express my sincere thanks to my thesis advisor, Assoc. Prof. Dr. Cherdsak Bootjomchai for invaluable help and constant encouragement throughout the course of this research. I am most grateful for his teaching and advice, not only the research methodologies but also the continuous support of my Ph.D. study and research, for his patience, motivation, enthusiasm, and immense knowledge. And also, I would not have achieved this far and this thesis would not have been completed without all the support that I have always received from him. In addition, I would like to thank the rest of my thesis committee: Prof. Dr. Tosawat Seetawan, Assoc. Prof. Dr. Reawat Loapaiboon, Asst. Prof. Dr. Tanin Nutaro, and Dr. Somkid Pencharee for their encouragement, insightful comments, and hard questions. I am grateful to Asst. Prof. Chadet Yenchai of the Nuclear Engineering Department, Faculty of Engineering, Chulalongkorn University for teach me about the geometry setup of the narrow beam transmission technique and opportunities for gamma-ray shielding testing.

Besides that, I would like to thank The Royal Golden Jubilee Ph.D. Program (grant no. PHD/0060/2560) for the continuous support of my Ph.D. study and financial support research.

Finally, thank all my fellow lab mates in Glass Technology Excellent Center (GTEC), Department of Physics, Ubon Ratchathani University for the discussions and for all the fun we have had in the last three years. I would like to thank my family for all their support throughout the period of this research and supporting me spiritually throughout my life.

Natsupon Chutithanapanon  
Researcher

## บทคัดย่อ

เรื่อง	: การศึกษาสมบัติทางรังสีและสมบัติทางโครงสร้างของแก้วระบบบิสมีท- แบเรียม-โบโรซิลิเกต เพื่อออกแบบเป็นวัสดุกำบังรังสีแกมมา
ผู้วิจัย	: ณัฏฐ์สุพล ชูติธนานนท์
ชื่อปริญญา	: ปรัชญาดุษฎีบัณฑิต
สาขาวิชา	: ฟิสิกส์
อาจารย์ที่ปรึกษา	: รองศาสตราจารย์ ดร.เชิดศักดิ์ บุตรจอมชัย
คำสำคัญ	: แก้วโบโรซิลิเกต, แบเรียมออกไซด์, วัสดุกำบังรังสี, เทคนิคอัลตราโซนิก

สำหรับงานวิจัยนี้ได้นำหลอดแก้วโซเดียมความดันสูง (high pressure sodium lamp glass) มารีเซเคิลและใช้แทนแก้วระบบโบโรซิลิเกต จากนั้นเตรียมให้อยู่ในระบบ  $(75-x)$  HPSg –  $(20)$  Na<sub>2</sub>O –  $5$  Bi<sub>2</sub>O<sub>3</sub> –  $(x)$  BaO โดยการเติมแบเรียมออกไซด์ เมื่อ  $x$  คือความเข้มข้นที่ 0, 5, 10, 15, 20, 25, 30, 35 mol% ด้วยเทคนิคการหลอมที่อุณหภูมิสูง หลังจากนั้นตัดและขัดชิ้นงานให้มีขนาด  $1 \times 1$  นิ้ว จากนั้นการศึกษาโครงสร้างของตัวอย่างแก้วจะถูกศึกษาด้วยหลายวิธีเช่น เทคนิคการใช้คลื่นเสียงอัลตราโซนิก ยูวีวิสซิเบิลสเปกโทรสโกปี (UV-Vis spectroscopy) และฟูเรียร์ทรานสฟอร์มอินฟราเรดสเปกโทรสโกปี (FTIR spectroscopy) สำหรับการศึกษาความเร็วคลื่นเสียงอัลตราโซนิก เราใช้ความเร็วคลื่นเสียงตามยาว (longitudinal velocity) และความเร็วคลื่นเสียงเฉือน (shear velocity) ซึ่งสามารถวัดได้โดยใช้เทคนิคพัลส์เอคโค่หรือวิธีการสะท้อนคลื่นเสียงกลับ (Pulse echo technique) โดยใช้หัววัดที่ความถี่ 4 MHz และวัดที่อุณหภูมิห้อง ผลจากการศึกษาพบว่าความเร็วคลื่นเสียงตามยาวและตามขวางลดลงเมื่อความเข้มข้นของแบเรียมออกไซด์เพิ่มขึ้น แสดงว่าแบเรียมไอออนอาจจะทำลายโครงสร้างของตัวอย่างแก้วจึงทำให้ความเร็วคลื่นเสียงลดลง หลังจากนั้นได้ศึกษาการดูดกลืนแสงขาวและอัลตราไวโอเล็ตด้วยยูวีวิสซิเบิลสเปกโทรสโกปีที่มีความยาวคลื่น 200 – 1100 nm พบว่าตัวอย่างแก้วมีการดูดกลืนแสงขาวน้อยในช่วง 400 nm นี้ทำให้ตัวอย่างแก้วโปร่งใส และจากผลการศึกษาสามารถนำไปคำนวณหาค่าแถบช่องว่างพลังงานได้ ซึ่งช่องว่างพลังงานจะอยู่ในช่วง 2.6-2.7 eV จากผลของแถบช่องว่างพลังงานสามารถนำไปคำนวณสมบัติทางแสงต่างๆได้ และพบว่าแบเรียมไอออนทำให้ตัวอย่างแก้วมีการนำไฟฟ้าเพิ่มขึ้นและมีความเป็นโลหะมากขึ้น การศึกษาโครงสร้างด้วยฟูเรียร์ทรานสฟอร์มอินฟราเรดสเปกโทรสโกปีจะวัดที่เลขคลื่น 400 - 2000 cm<sup>-1</sup> จากการศึกษาพบว่าการสั่นของ BO<sub>3</sub> และ BO<sub>4</sub> ซึ่งขนาดของการสั่นจะสัมพันธ์กับโครงสร้างตัวอย่างแก้วอีกทั้งยังเป็นการยืนยันผลจากการใช้เทคนิคความเร็วคลื่นเสียงอัลตราโซนิก สำหรับสมบัติทางรังสีเราสามารถวัดสัมประสิทธิ์การลดทอนเชิงเส้นโดยใช้เทคนิคการส่งผ่านลำรังสีแคบ (narrow beam

transmission method) ที่พลังงาน 662 keV, 1174 keV และ 1332 keV ของธาตุกัมมันตรังสี หลังจากนั้นสามารถคำนวณสัมประสิทธิ์การลดทอนเชิงมวล mfp และ HVL จากผลการทดลองพบว่า ตัวอย่างแก้วนั้นมีค่า HVL ที่พลังงาน 662 keV, 1174 keV และ 1332 keV ดีกว่าคอนกรีตทั่วไป เช่น คอนกรีตแบบแบไรต์ คอนกรีตแบบเซอร์เพนไทต์และคอนกรีตแบบโครไมท์ และเมื่อคำนวณสมบัติทางรังสีด้วยโปรแกรม Fluka และ WinXCom พบว่าผลจากทั้ง 2 โปรแกรมนี้กับผลจากการทดลองมีความใกล้เคียงกัน ซึ่งเป็นการยืนยันผลจากการทดลอง

## ABSTRACT

**TITLE** : INVESTIGATION OF RADIATION AND STRUCTURAL PROPERTIES OF BISMUTH-BARIUM-BOROSILICATE GLASS SYSTEM FOR DESIGN AS A GAMMA RAY SHIELDING MATERIALS

**AUTHOR** : NATSUPON CHUTITHANAPANON

**DEGREE** : DOCTOR OF PHILOSOPHY

**MAJOR** : PHYSICS

**ADVISOR** : ASSOC. PROF. CHERDSAK BOOTJOMCHAI, Ph.D.

**KEYWORDS** : BOROSILICATE GLASS, BARIUM OXIDE, SHIELDING MATERIAL, ULTRASONIC TECHNIQUES

In this research, high pressure sodium lamp glass (HPSg) was recycled and employed instead of borosilicate glass systems. The glass samples were prepared in  $(75-x)$  HPSg –  $(20)$   $\text{Na}_2\text{O}$  –  $5$   $\text{Bi}_2\text{O}_3$  –  $(x)$   $\text{BaO}$  by adding barium oxide (where  $x$  is 0, 5, 10, 15, 20, 25, 30, and 35 mol%) through the melt-quenching method. After that, the glass samples were cut in  $1 \times 1$  square inch and polished by different grades of silicon carbide. Next, structural properties of the glass samples were studied by way of several methods such as ultrasonic techniques, UV-Vis spectroscopy, FTIR spectroscopy. For ultrasonic techniques, we use ultrasonic velocities such as longitudinal velocity and shear velocity which were measured by using the pulse-echo technique at 4 MHz frequency and at room temperature. The results found that longitudinal and shear velocity decreased when adding barium oxide to the glass system. These results indicate that barium ions may destroy the glass structure leading to a decrease in longitudinal and shear velocity. Then, absorption of visible light and ultraviolet was studied by UV-Vis spectroscopy and recorded in a wavelength range of 200 – 1100 nm. We found that the glass samples absorbed less visible light and ultraviolet in the range of 400 nm. This result shows that the glass samples are transparent. In addition, we can calculate optical properties from the energy band gap and found that the energy band gap is 2.6-2.7 eV. Adding barium ions in the glass system leads to increase in electric conduction and metallization. FTIR spectroscopy was measured in wave number range 400 - 2000

$\text{cm}^{-1}$ . The results found that the glass network is absorbing and vibrating in the various modes of the functional group of  $\text{BO}_3$  and  $\text{BO}_4$  for which the quantity of absorption is related to the structure of glass and confirms the results from ultrasonic techniques. For radiation properties, the linear attenuation coefficient was measured by using a narrow beam transmission method at the energy of isotope source of 622 keV, 1174 keV, and 1332 keV. Then, we calculated the mass attenuation coefficient, mfp, and HVL. The results found that the glass samples have a value of HVL at 622 keV, 1174 keV, and 1332 keV better than ordinary concrete, barite concrete, serpentite concrete, and chromite concrete. As we determined radiation properties from the Fluka and WinXCom program, we found that the theoretical value and experimental data are in solid agreement and confirm the experiment's results.

## CONTENTS

	PAGE
<b>ACKNOWLEDGEMENTS</b>	<b>I</b>
<b>THAI ABSTRACT</b>	<b>II</b>
<b>ENGLISH ABSTRACT</b>	<b>IV</b>
<b>CONTENTS</b>	<b>VI</b>
<b>LIST OF TABLES</b>	<b>VIII</b>
<b>LIST OF FIGURES</b>	<b>IX</b>
<b>CHAPTER 1 INTRODUCTION</b>	
1.1 Introduction	1
1.2 Objective	2
1.3 Advantage of research	3
1.4 Scope of research	3
<b>CHAPTER 2 THEORETICAL BACKGROUND</b>	
2.1 Glass materials	4
2.2 Gamma shielding measurements	31
2.3 High pressure sodium lamp	42
2.4 literature reviews	42
<b>CHAPTER 3 MATERIALS AND METHODS</b>	
3.1 Instrumentation	46
3.2 Chemical and materials	46
3.3 Experimental technique	47
<b>CHAPTER 4 RESULTS AND DISCUSSIONS</b>	
4.1 Color of glass samples	51
4.2 Density and molar volume of glass samples	51
4.3 Physical properties of glass	54
4.4 Elastic properties	55
4.5 Infrared spectral studies	67

**CONTENTS (CONTINUED)**

	<b>PAGE</b>
4.6 Optical properties	69
4.7 Radiation properties	73
<b>CHAPTER 5 CONCLUSION</b>	
5.1 Structural properties	92
5.2 Optical properties	93
5.3 Radiation properties	93
<b>REFERENCES</b>	<b>96</b>
<b>APPENDICES</b>	
A Tools	108
B Publication and proceeding	116
<b>VITAE</b>	<b>117</b>



## LIST OF TABLES

TABLE		PAGE
2.1	Chemical composition of high-pressure sodium lamps glass	42
4.1	The chemical composition of all glass sample	53
4.2	The chemical composition of all glass sample in the previous research	54
4.3	Ion concentration, Polaron radius, interatomic distance, and field strength as a function of BaO in glass system	55
4.4	Density, molar volume, longitudinal velocity, and shear velocity as a function of Bi <sub>2</sub> O <sub>3</sub> in glass system for the previous research.	57
4.5	Experimental elastic moduli of glass samples	60
4.6	Experimental elastic moduli of glass samples	66
4.7	Theoretical elastic moduli of glass samples	67
4.8	Refractive index, dielectric constant, optical dielectric constant, reflection loss, molar refractivity, metallization, and molar polarizability as a function of BaO in glass system.	73
4.9	Chemical compositions of concretes	79
4.10	The value of linear attenuation coefficient and mass attenuation coefficient	80
4.11	The value of the mean free path and HVL	81
4.12	The value of mass attenuation coefficients between WinXcom and Fluka data	84
4.13	The value of mean free path between WinXcom and Fluka data	87
4.14	The value of half value layer between WinXcom and Fluka data	91

## LIST OF FIGURES

FIGURE	PAGE
2.1 Schematic specific volume and temperature relationships for the crystallization and glass formation	5
2.2 Structures of a typical solid in 2D (a) and glass (b)	6
2.3 Glasses and crystals have the same building blocks	7
2.4 Schematic representation of the classical rates for nucleation and crystallization	8
2.5 Metastable immiscibility diagram for the sodium silicate system	9
2.6 Schematic representation of two tetrahedra of silica (a) and random arrangement of silica tetrahedra (b)	11
2.7 Structure of boroxal units	12
2.8 Schematic plot of electron energy versus interatomic separation for an aggregate of 12 atoms	19
2.9 The various electron band structures in solids at 0 K	20
2.10 The transmission of light through a transparent medium	24
2.11 Basic component in Fourier transform infrared spectrometer	24
2.12 Measurement of the pulse-echo technique	26
2.13 Longitudinal modulus in materials	26
2.14 Shear modulus in materials	27
2.15 Bulk modulus in materials	27
2.16 Young's modulus in materials	28
2.17 Poisson's ratio in materials	29
2.18 Alpha particle is emitted from a nucleus	33
2.19 Beta particles	33
2.20 Gamma decay	34
2.21 Schematic representation of photoelectric effect process	35
2.22 Schematic representation of Compton scattering	37

## LIST OF FIGURES (CONTINUED)

FIGURE	PAGE
2.23	Pair production process39
3.1	Experimental setup of narrow beam transmission method49
3.2	Schematic diagram of the divergent beam50
4.1	All glass sample with different the concentration of BaO51
4.2	Density and molar volume of glass samples as a function of BaO contents53
4.3	Longitudinal and shear velocity as a function of BaO contents for (75-x) HPSg – (20) Na <sub>2</sub> O – 5 Bi <sub>2</sub> O <sub>3</sub> – (x) BaO system with x = 0, 5, 10, 15, 20, 25, 30 and 35 mol%.56
4.4	Longitudinal and shear modulus as a function of BaO contents for (75-x) HPSg – (20) Na <sub>2</sub> O – 5 Bi <sub>2</sub> O <sub>3</sub> – (x) BaO system with x = 0, 5, 10, 15, 20, 25, 30 and 35 mol%.58
4.5	Young’s modulus and bulk modulus as a function of BaO contents for (75-x) HPSg – (20) Na <sub>2</sub> O – 5 Bi <sub>2</sub> O <sub>3</sub> – (x) BaO system with x = 0, 5, 10, 15, 20, 25, 30 and 35 mol%.59
4.6	Softening temperature and Debye temperature as a function of BaO contents for (75-x) HPSg – (20) Na <sub>2</sub> O – 5 Bi <sub>2</sub> O <sub>3</sub> – (x) BaO system with x = 0, 5, 10, 15, 20, 25, 30 and 35 mol%.61
4.7	Poisson’s ratio as a function of BaO contents for (75-x) HPSg – (20) Na <sub>2</sub> O – 5 Bi <sub>2</sub> O <sub>3</sub> – (x) BaO system with x = 0, 5, 10, 15, 20, 25, 30 and 35 mol%.61
4.8	Micro-hardness as a function of BaO contents for (75-x) HPSg – (20) Na <sub>2</sub> O – 5 Bi <sub>2</sub> O <sub>3</sub> – (x) BaO system with x = 0, 5, 10, 15, 20, 25, 30 and 35 mol%.62
4.9	Longitudinal modulus compare with theoretical and experimental data.64

## LIST OF FIGURES (CONTINUED)

FIGURE	PAGE
4.10 Shear modulus compare with theoretical and experimental data.	64
4.11 Young's modulus compare with theoretical and experimental data	65
4.12 Bulk modulus compare with theoretical and experimental data	65
4.13 Poisson's ratio compare with theoretical and experimental data.	66
4.14 The IR spectra of (75-x) HPSg – (20) Na <sub>2</sub> O – 5 Bi <sub>2</sub> O <sub>3</sub> – (x) BaO glass system	96
4.15 Absorption spectra as a function of wavelength for (75-x) HPSg – (20) Na <sub>2</sub> O – 5 Bi <sub>2</sub> O <sub>3</sub> – (x) BaO system with x = 0, 5, 10, 15, 20, 25, 30 and 35 mol%.	70
4.16 Direct band gap of glass samples	71
4.17 Indirect band gap of glass samples	71
4.18 Comparison the mass attenuation coefficient between the glass samples in previous work and doped with BaO at 662, 1174, and 1332 keV	74
4.19 Comparison of mfp of glass samples with different concentration of barium oxide and mfp of previous work	75
4.20 Comparison of HVL of glass samples with different concentration of barium oxide and HVL of previous work	76
4.21 The variation of HVL of glass samples compare to different concrete with different concentration of barium oxide at 662 keV.	78
4.22 The variation of HVL of glass samples compare to different concrete with different concentration of barium oxide at 1174 keV.	78
4.23 The variation of HVL of glass samples compare to different concrete with different concentration of barium oxide at 1332 keV.	79
4.24 Comparison of the mass attenuation coefficients between experimental data, WinXcom data, and Fluka data at the energy of 662 keV	82

## LIST OF FIGURES (CONTINUED)

FIGURE	PAGE
4.25 Comparison of the mass attenuation coefficients between experimental data, WinXcom data, and Fluka data at the energy of 1174 keV	83
4.26 Comparison of the mass attenuation coefficients between experimental data, WinXcom data, and Fluka data at the energy of 1332 keV	84
4.27 Comparison of the mean free path between experimental data, WinXcom data, and Fluka data at the energy of 622 keV	85
4.28 Comparison of the mean free path between experimental data, WinXcom data, and Fluka data at the energy of 1174 keV	86
4.29 Comparison of the mean free path between experimental data, WinXcom data, and Fluka data at the energy of 1332 keV	87
4.30 Comparison of the half value layer between experimental data, WinXcom data, and Fluka data at the energy of 622 keV	88
4.31 Comparison of the half value layer between experimental data, WinXcom data, and Fluka data at the energy of 1174 keV	90
4.32 Comparison of the half value layer between experimental data, WinXcom data, and Fluka data at the energy of 1332 keV	90

# **CHAPTER 1**

## **INTRODUCTION**

### **1.1 Introduction**

Nowadays, nuclear technology is used extensively and very important for industry, medical and agriculture such as insect pest control by the sterile insect technique (SIT) led to a declining pest population, plants genes mutation for plant breeding, irradiation technology for food preservation using gamma rays, x-rays, or electron beams source and radiography in medicine. In addition, one of the nondestructive testing (NDT) is radiographic testing (RT) that involves the use of either x-rays or gamma rays to view the internal structure of a component. In the petrochemical industry, radiographic testing is often used to inspect machinery, such as pressure vessels and valves, to detect for flaws and then also used to inspect weld repairs [1-3]. Thus, radiation protection and radiation dosimetry have been interested from many researchers around the world. Normally, the most commonly materials for shielding radiation are concrete due to it's an effective, versatile and economic material. The high density of concrete shield by adding heavy materials has the ability to reduce the energy of gamma rays. However, concrete has some disadvantage such as water permeability, susceptible to cracking and being opaque to visible light. Glass material has been interesting for use as a radiation shielding materials. Because of some advantage of glass such as very high-water resistance, high resistant to chemical corrosion and excellent transparency. Therefore, glass materials can be instead of conventional concrete for radiation shielding materials. The adding some transition metal oxides into glass structure has an influence on the properties of glass. For example, the glass systems doped with lead oxide (PbO) can be used for nuclear radiation shielding application [4-5]. Moreover, borosilicate glass is one of the interesting systems due to high refractive index, high resistance to chemical, strong resistance to temperature, excellent transparency, and low thermal expansion. Borosilicate glass widely used in many fields such as laboratory glassware, scientific lenses, the semiconductor fabrication industry for modern electronics and radiation shielding material. Atul Khanna et al. [6] reported that the increase in number of non-

bridging oxygens is related to the ion of  $\text{Bi}^{3+}$  in the glass network. Bismuth ions acts as a network former at higher concentration, while it acts a network modifier at low concentrations. Thomas Maeder [7] discovered that the lead can be replaced by bismuth in thick film, and it are therefore actually replacing them in many applications such as material for electronics, sensors, sealing glasses, solar cells, architectural and automotive glass. Moreover, Heavy glasses containing bismuth and lead have useful in the field of nuclear technology. Murat Kurudirek et al. [8] reported that the successful fabrication of the new glass system recycled by high pressure sodium lamp. the adding bismuth oxide in glass network are increased in the gamma ray shielding capability and fast neutrons. In addition, the concentration of bismuth oxide in the glass network can create the formation of number of non-bridging oxygens. Reza Bagheri et al. [9] discovered that the barium - bismuth - borosilicate glasses have a gamma ray shielding capability with 662 keV, 1173 keV and 1332 keV. The results from XCOM, MCNP and experiment data are good agreement with each other. Sarawut Burinram [10] reported that the glass system in  $(80-x) \text{HPSg} - (20) \text{Na}_2\text{O} - (x) \text{Bi}_2\text{O}_3$  can be used in the field of radiation shielding and also the adding in bismuth ions can created the formation of number of non-bridging oxygens in this glass network. The aim of this research is producing the new glasses system in gamma-ray radiation shielding. High pressure sodium lamp (HPSg) has been recycled and were prepared in  $(75-x) \text{HPSg} - (20) \text{Na}_2\text{O} - 5 \text{Bi}_2\text{O}_3 - (x) \text{BaO}$  (where x is 0, 5, 10, 15, 20, 25, 30 and 35 mol%) by the melt quenching method. Borosilicate glass were replaced by high pressure sodium lamp glass due to high pressure sodium lamp glass has a high percentage of  $\text{B}_2\text{O}_3$ . The glass samples were investigated on structural properties, elastic properties, optical properties, and radiation properties. Elastic properties can be calculated by the value of ultrasonic data and elastic moduli were studied to reveal the resistance to deformation of network structure.

## 1.2 Objectives

1.2.1 Development of the glass system for a high efficiency radiation shielding materials

1.2.2 Investigation of the glass system on structural properties, optical properties, elastic properties, and radiation properties

1.2.3 Investigation on the influence of barium ions on this glass system

### **1.3 Advantage of research**

1.3.1 Knowledge of the recycling of the high pressure sodium lamp glass by melt quenching method

1.3.2 Knowledge of the influence of barium ions on barium - bismuth - borosilicate glass system

1.3.3 Knowledge of structural properties, optical properties, elastic properties, and radiation properties in this glass system

### **1.4 Scope of research**

1.4.1 Preparation of all glass samples from high pressure sodium lamp glass doped with  $\text{Bi}_2\text{O}_3$ ,  $\text{BaO}$  and  $\text{Na}_2\text{O}$  in  $(75-x) \text{HPSg} - (20) \text{Na}_2\text{O} - 5 \text{Bi}_2\text{O}_3 - (x) \text{BaO}$  (where  $x$  is 0, 5, 10, 15, 20, 25, 30 and 35 mol%) by the melt quenching method.

1.4.2 Ultrasonic velocity measurement were measured by using ultrasonic detector at 4 MHz (SONATEST Sitescan 230).

1.4.3 Fourier transform infrared spectroscopy measurement for investigation on structural properties of glass samples and investigate the optical band gaps of glass samples.

1.4.4 Mass attenuation coefficient can be measured by using narrow beam transmission method.



## **CHAPTER 2**

### **THEORETICAL BACKGROUND**

#### **2.1 Glass materials**

##### **2.1.1 Definition of Glass**

Glass is an amorphous solid. The term is usually applied to inorganic solids and not to plastics or other organics. Glasses do not have a crystalline internal structure. It's like a cross between a solid and a liquid with some of the crystalline order of a solid and some of the molecular randomness of a liquid. They usually are hard and brittle solids. It is composed mainly of approximately 77-80% sand (silica) and some an alkali. The glass made from ordinary sand which is mostly made of silicon dioxide and heated until it melts and turns into a liquid. Normally, the melting point of silica is approximately 1700-1900°C. When molten sand cools, it becomes a kind of frozen liquid or what materials scientists refer to as an amorphous solid. In addition, American Society for Testing and Materials (ASTM) defined the definition of glass which states "a glass is an inorganic product of fusion which has cooled to a rigid condition without crystallization" [11-14].

##### **2.1.2 Glass formation**

It is known that the glass materials have some properties such as a good transparent, possessing the properties of hardness, rigidity, brittleness, and, apart from transparency, these are the typical properties one normally associates with a solid. The glass formation is best understood by examining Figure 2.1, in which the specific volume is plotted against its temperature. Point A shows that a liquid starts at a high temperature and the reduces of heat causes the state to move along the line AB, as the liquid concurrently cools and shrinks in specific volume. The crystallization can create from a finite amount of the supercooling liquid, but there must below the freezing point B, which is also the melting point. Crystallization is the solidification of atoms or molecules into a highly structured form called a crystal and indicated by line BC. Where  $T_g$  is glass transition temperature and  $T_m$  is melting point temperature.

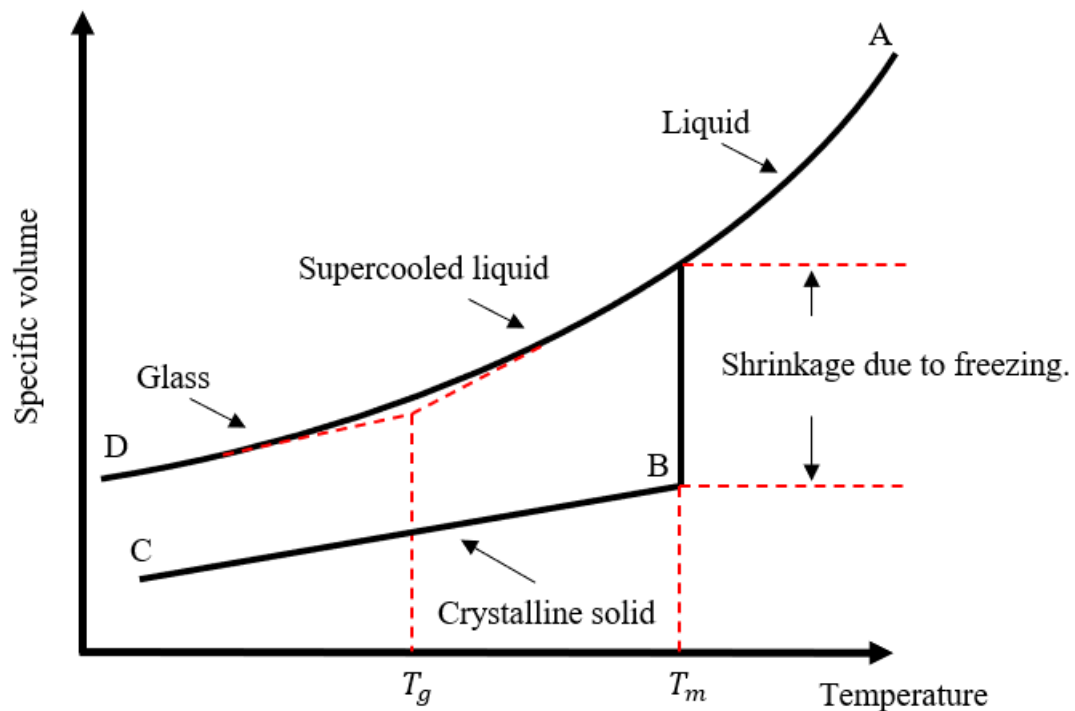


**Figure 2.1 Schematic specific volume and temperature relationships for the crystallization and glass formation**

However, if cooling is conducted quickly enough, crystallization will not take place. In line AD curve, the volume shrinking is continuously decreasing with falling temperature and its viscosity rising enormously. At last, supercooled liquid will become very viscous that its volume will shrink at a slower rate, and it will become a seemingly rigid solid called glass [15,17].

### **2.1.3 Atomic structure of glass**

Normally, there are three distinct states of matter: gas, liquid, and solid. The atoms or molecules of a gas are randomly arranged and widely separated. A gas has a fill all the available space inside a container. The molecules of a liquid are also randomly arranged, but they are closer together than a gas and they move relative to one another. The last state of matter is solid, which can impose having a fixed shape and can be classified as either crystalline or non-crystalline. crystals are concerned with interatomic bonding, interatomic distances, the environment of the ions, and long-range ordering (except non-crystalline materials such as glass). Thus, crystal has an ordering on the

lattice—long-range order whilst Glass has short-range order. But liquid has a no order to short-range order [16-17]. Glasses are essentially non-crystalline or amorphous solids often obtained by freezing supercooled liquids and as shown in Figure 2.2.

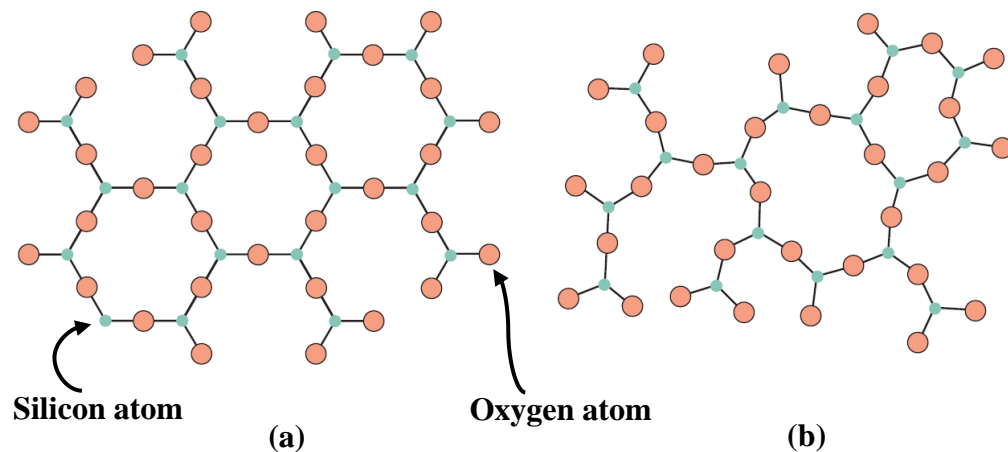


**Figure 2.2 Structures of a typical solid in 2D (a) and glass (b) [16]**

#### 2.1.3.1 Random network theory

Random network theory is originally based on the ideas of Zachariasen's model. Before Zachariasen, Glass structure was believed to be comprised of nanocrystals ( $\sim 20$  Å size) given the broadening of diffraction patterns. Mechanical properties of glass have similar between glasses and crystals, and so expected similar structural energies. It's similar underlying atomistic building blocks and as shown in Figure 2.3. Zachariasen's rules for glass formation based on an empirical observation on oxides [19]

- 1) An oxygen atom should be linked to not more than two glass-forming atoms (two cations).
- 2) The cation coordination number of glass-forming atoms is low, 4 or less.
- 3) Oxygen polyhedra share corners, not edges, or faces.
- 4) For 3D networks, at least three corners must be shared.

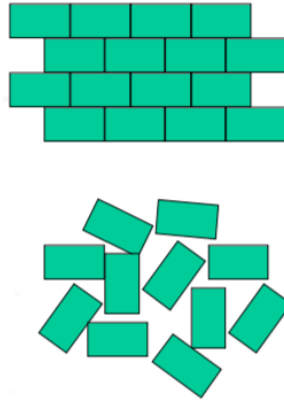


**Figure 2.3 Glasses and crystals have the same building blocks [18]**

Normally, the four rules should be satisfied for glass formation to occur. Low cation coordination numbers, corner-sharing rules imply that the formation of glass is more likely with open which it's low density polyhedral structures. For example,  $\text{SiO}_2$ ,  $\text{GeO}_2$  are good a glass former due to the coordination numbers of  $\text{SiO}_2$  and  $\text{GeO}_2$  is equal to 4. While  $\text{V}_2\text{O}_5$  and  $\text{MgO}$  are not good a glass former due to the coordination numbers of  $\text{V}_2\text{O}_5$  and  $\text{MgO}$  is equal to 5 and 6, respectively. The open network structures of the glass-forming oxides are sometimes classified as glass modifier oxide or intermediate oxides. This behavior is depending on their structural roles [17,19].

#### 2.1.3.2 Kinetic theory

The kinetic theory discussed above considers only the relative ease of glass formation. glasses are formed by melt quenching method from some temperature above the material crystallization temperature down through the  $T_g$  and into the solid state. Thus, glass formation will occur if crystallization can be avoided when a melt is cooled. In a crystal nucleus, the atoms in a melt must reorganize to form an ordered crystal structure and in a supercooled liquid, the crystalline solids are thermodynamically preferred over the disorganized melt. therefore, the nucleation rate has been calculated by using the next relations [19]:

$$I = \frac{A}{\eta} \exp\left(\frac{B\gamma^3}{\Delta G_v T}\right) \quad (1)$$

Where  $A$  and  $B$  are constants,  $\Delta G_v$  is the free energy difference between the liquid and crystal.  $\eta$  is viscosity of glass,  $\gamma$  is surface energy for create crystal nuclei, and  $T$  is temperature. Crystallization process will start from stable nuclei in melts below  $T_m$  at a rate ( $U$ ) given by [19,20]

$$U = \frac{CT}{\eta} \left[ 1 - \exp\left(-\frac{\Delta G_v}{kT}\right) \right] \quad (2)$$

Where  $C$  is constants and  $k$  is Boltzmann's constant. Figure 2.4 is shown A schematic representation of the temperature dependences of nucleation and crystallization rates described by equations (1) and (2)

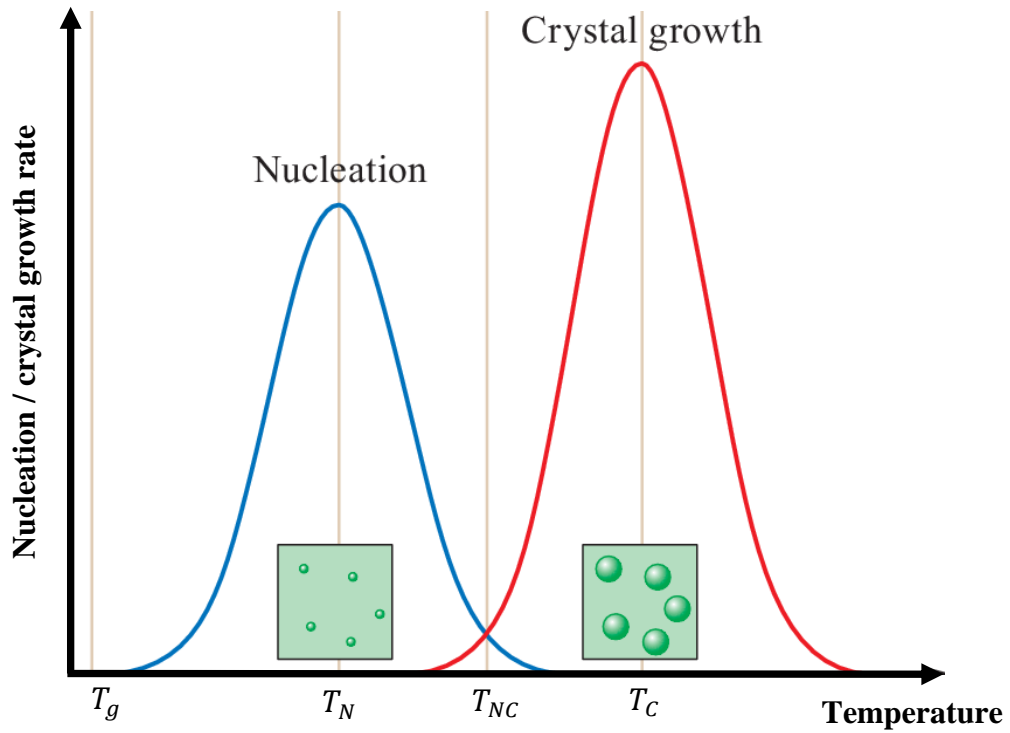


**Figure 2.4 Schematic representation of the classical rates for nucleation and crystallization [20]**

### 2.1.4 Amorphous phase separation

Amorphous phase separation (APS) is an important phenomenon of the glasses. Phase separation at above the glasses melting point (the liquidus line) is known as stable immiscibility and temperatures below the liquidus line are known as metastable immiscibility. There are two paths to the formation of discrete phases by metastable phase separation. The first path is either by spinodal decomposition and the second path is either by nucleation and growth process. However, the path taken depends on the free energy of the mixing of the system [21].

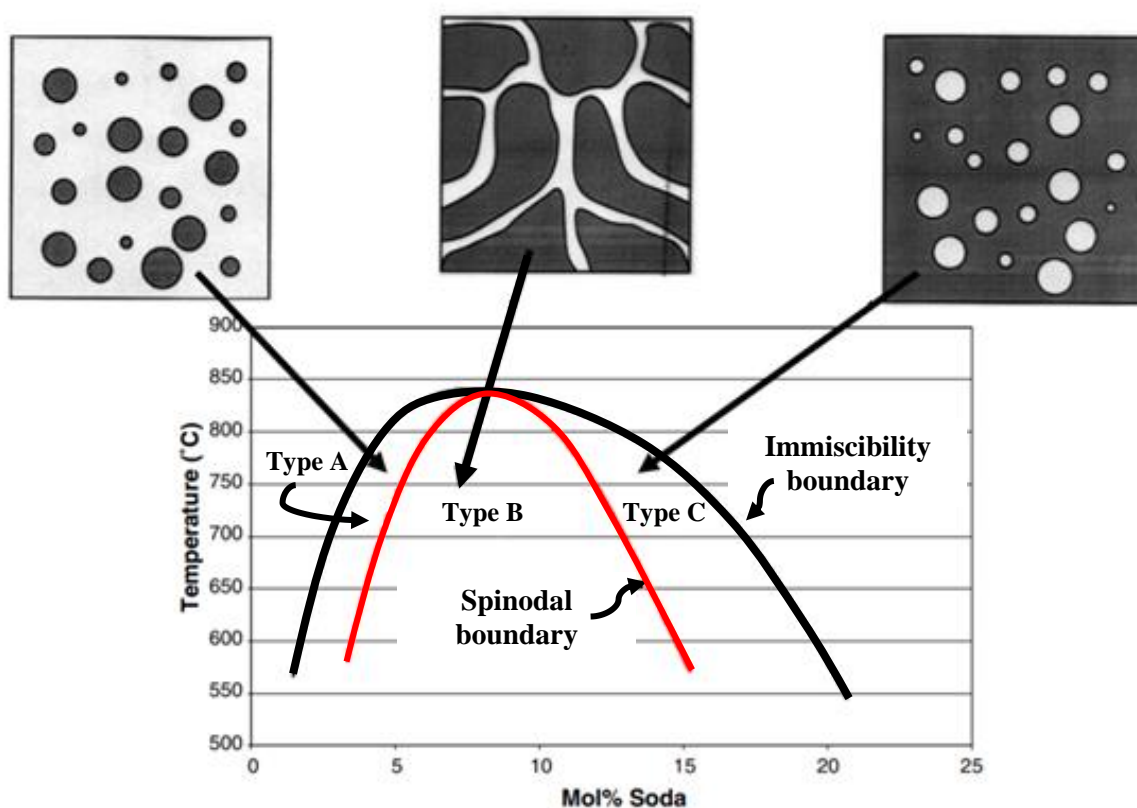


**Figure 2.5 Metastable immiscibility diagram for the sodium silicate system [22]**

In Figure 2.5, dark phase shows a sodium-rich composition and light phase denotes a silica-rich composition. While region in type A and type C of phase separation are in a binodal region and undergo amorphous phase separation by nucleation and growth process. However, the region in type B is within the spinodal region and undergoes amorphous phase separation by spinodal decomposition. When reducing temperature often involves passing from one region to another during the cooling

process. If sufficient time is allowed, phase separation will occur during cooling and an originally homogeneous melt will yield a phase-separated glass. The size of separated regions and their compositions will be given by the interaction of the cooling rate.

### **2.1.5 Type of glass**

It is known that the glasses can be classified in different groups according to their chemical composition such as soda-lime glass or commercial glass, lead glass, aluminosilicate glass, and borosilicate glass, etc. Silica or silicon dioxide ( $\text{SiO}_2$ ) is the most important for the glass former and silicate glasses represent more than 95% of industrial glass production. However, the silica in glass former oxide can be replaced by boron oxide and phosphorus pentoxide, etc.

#### **2.1.5.1 Soda-lime glass or silicate glasses**

Soda-lime glass is the most prevalent type of glass since comparatively inexpensive, amenable to recycling, chemically stable, reasonably hard, and extremely workable. A typical composition of this glass is 70 percent silica (silicon dioxide), 15 percent soda (sodium oxide), and 9 percent lime (calcium oxide), with much smaller amounts of various other compounds. Moreover, a low percentage of other reagents can be added for specific properties and application requirements. The structure of soda-lime glass consists of well-defined  $\text{SiO}_4$  tetrahedra connected to another neighboring tetrahedron through each corner. The distance bond of Si-O in the tetrahedron is 0.162 nm and the bond of O-O distance is 0.262 nm, the same dimensions as found in crystalline silica [23,24]. Atomic structure of amorphous silica as shown in Figure 2.6.

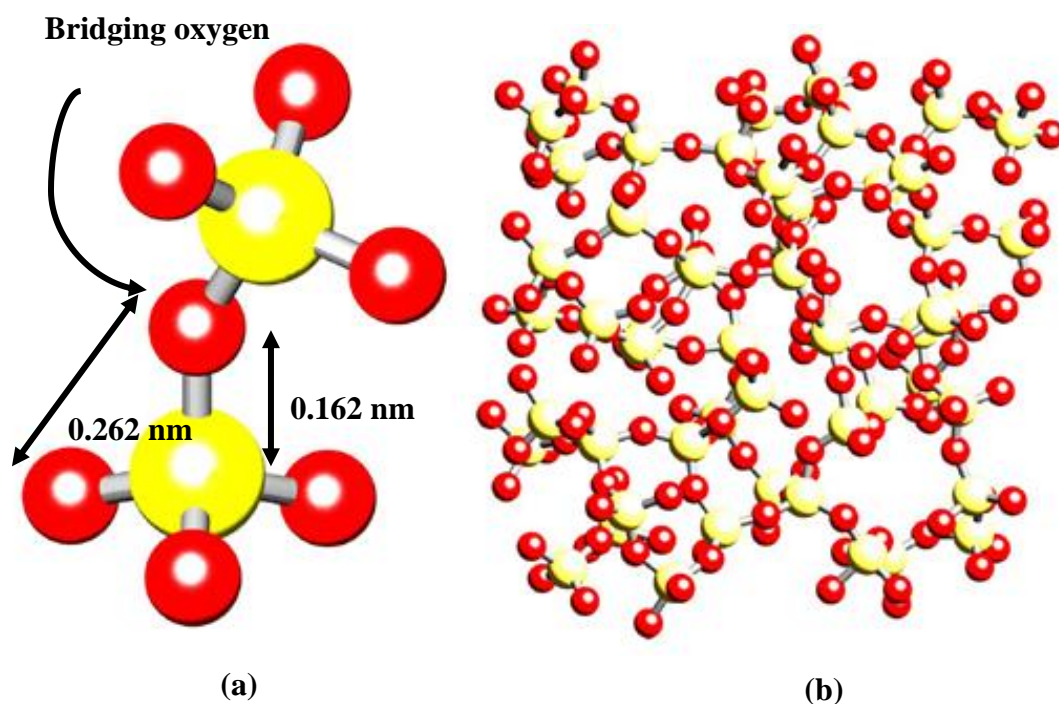


**Figure 2.6 Schematic representation of two tetrahedra of silica (a) and random arrangement of silica tetrahedra (b) [23]**

In addition, the alkali silicate glasses structure also consists of a network of  $\text{SiO}_4$  tetrahedra, but some of the corners are now occupied by non-bridging oxygens (NBOs) that are linked to the modifying polyhedral. Increasing the concentration of modifying oxide ( $\text{R}_2\text{O}$ ) led to an increase in the relative fraction of non-bridging oxygens associated with the glass network. Hence, the melting temperature of the mixture and viscosity will extremely reduce while the thermal expansion coefficient and ionic conductivity are increase. Soda-lime glass is produced on a large scale and used for immense applications in various fields such as light bulbs, windowpanes, bottles, art objects, UV-transmitting optics, IR-transmitting optics, lenses, mirror substrates, trays and boats and metrology components.

#### 2.1.5.2 Borosilicate glasses

Borosilicate glass is one of the types of glass with silica ( $\text{SiO}_2$ ) and boron trioxide ( $\text{B}_2\text{O}_3$ ) as the main glass-forming constituents. The main components of borosilicate glass are typically composed of composed of 70 – 80 wt%  $\text{SiO}_2$ , 7 – 13 wt% of  $\text{B}_2\text{O}_3$ , 4 – 8 wt% of  $\text{Na}_2\text{O}$  or  $\text{K}_2\text{O}$ , and 2 – 8 wt% of  $\text{Al}_2\text{O}_3$  [25-29]. Vitreous  $\text{B}_2\text{O}_3$



structure consists of planar triangular  $\text{BO}_3$  units that link to form larger units (boroxol rings) and show in Figure 2.7.

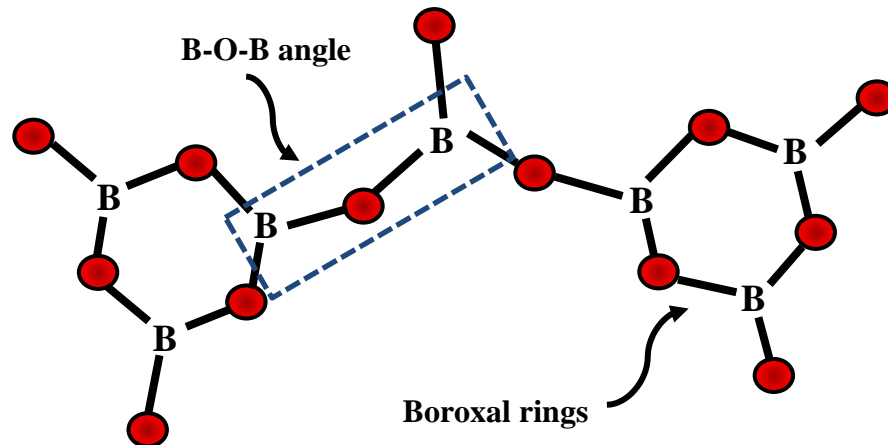


**Figure 2.7 Structure of boroxal units**

When adding the  $\text{B}_2\text{O}_3$  in silicate glasses, these led to the increase in glass transition temperature and a decrease in the thermal expansion coefficient. These glasses are also used for dielectric and insulating materials and it is known that borosilicate glass behaves as a good shield against gamma radiation when adding lead oxide [30]. However, borosilicate glass is widely used in several fields. Because of their good heat resistant properties, thermal shock resistance they are used in the chemical industry, domestic kitchen cooking utensils, structural integrity due to low thermal expansion, and good resistance to chemical attack.

#### 2.1.5.3 Aluminosilicate glasses

Aluminosilicate glass is a type of glass that contains aluminum oxide ( $\text{Al}_2\text{O}_3$ ) and boron oxide ( $\text{B}_2\text{O}_3$ ). The chemical of aluminosilicate glass contains 52 – 58 wt% of  $\text{SiO}_2$ , 15 – 25 wt% of  $\text{Al}_2\text{O}_3$ , and 4 – 18 wt% of  $\text{CaO}$ . The difference in type of aluminosilicate glass depends on their chemical compositions, with a focus on the metal oxide composition. Aluminosilicate glass has become useful in numerous industrial, commercial, and personal applications. Because of them has properties similar to borosilicate glass but has better chemical resistance. However, when compared to the borosilicate glass and aluminosilicate glass, aluminosilicate glass is more difficult to manufacture.

#### 2.1.5.4 Lead glasses

Lead glass is like silicate glasses but has lead oxide (replace in lime position). Normally, lead glasses typically contain  $\text{SiO}_2$  (54-65%),  $\text{PbO}$  (18-38%)  $\text{Na}_2\text{O}$  (13-15%), and other oxides in a few proportions. If the adding of lead oxide content is less than 18% in the glass it is called crystal glass but lead oxide content more than 65% can be used for radiation shield (x-rays and gamma-rays in medical, technical, and research work). Furthermore, lead glass is normally used in various industries such as glassware, jewelry, optical lenses, enamels, lacquers, and used in the electronics industry to encapsulate diodes [29].

#### 2.1.5.5 Phosphate glasses

Phosphate glass is widely used in optical technology such as in high energy laser applications. In general, phosphate glass is composed of metal phosphates of various metals, and the forming of the glass structure is based on phosphorus pentoxide ( $\text{P}_2\text{O}_5$ ). These glasses were found to be having superior optical properties such as low dispersion, comparatively high refractive indices as that of silicate-based optical glasses and highly resistant to hydrofluoric acid. If the adding iron oxide in phosphate glasses act as efficient heat absorbers. Furthermore, phosphate glasses have a low melting temperature in the range of 950 – 1150 °C and have an extremely low glass transition temperature, typically below 400 °C.

#### 2.1.5.6 Germanate glasses

Germanate glasses have potential applications and used in many fields of industry such as optical fibers and telecommunications. The angle of  $\text{Ge} - \text{O} - \text{Ge}$  bond is like to the  $\text{Si} - \text{O} - \text{Si}$  bond angle and germanium ion is larger in diameter than the silicon ion ( $\text{Ge} - \text{O}$  bond is 0.173 nm). Of all types of glasses, the germanate glasses allow the optimum combination of transmission, physical, and chemical properties. In addition, some properties of germanate glasses can be varied somewhat to fit a particular application due to the size of glass-forming areas for germanates is smaller than that for silicates. When compared the germanate glass with silicate and borosilicate glass systems, in germanate glass have a high refractive index (1.80 or more) with low concentrations of the heavy elements oxides.

#### 2.1.5.7 Chalcogenide glasses

Chalcogenide glasses refer to the element in VIA column of the periodic table such as sulfur, selenium, and tellurium, but excluding oxygen. While Polonium is also a chalcogen but is not used because of its strong radioactivity. Chalcogenide glasses are formed by the addition of some elements such as Ge, As, Sb, Ga, etc. In addition, these glass lower energy band gaps contribute to very dissimilar optical and electrical properties. The optical band gaps of chalcogenide glasses are 1-3 eV and accordingly they can be regarded as amorphous semiconductors [31].

#### 2.1.5.8 Halide glasses

Halide glasses refers to glasses in which the anions are from elements in Group VIIA of the periodic table.  $\text{BeF}_2$  and  $\text{ZnCl}_2$  is the halide glasses and have been known for a long time. However, these glasses ( $\text{BeF}_2$  and  $\text{ZnCl}_2$ ) are found to be hygroscopic and undergo crystallization. The structure of halide glasses ability which requires the creation of a strong covalent bond is characteristic of a few highly charged cations as found in oxides. Therefore, their structures are like those of  $\text{SiO}_2$  and  $\text{GeO}_2$  [32].

### 2.1.6 Properties of glass

At room temperatures, the glass is perfectly elastic solid, electrical insulator, and excellent thermal insulator. The network structure of glass systems is ultimately responsible for many of the properties that distinguish glass from other solids. It is well known that the adding of some oxide led to the change in the network structure of glass systems. Thus, the properties of glass depending on the metal oxide with adding in the glass network.

#### 2.1.6.1 Physical properties

##### 1) Density and molar volume

In general, the density of a material is a characteristic property of a substance and defined as the mass per unit of volume. Density of glass is given by [19]

$$\rho = \frac{m}{V} \quad (\text{kg/m}^3) \quad (3)$$

where  $\rho$  is the density of material,  $m$  is the mass, and  $V$  is the volume of the sample material. In this work, the densities of glass material were

determined by Archimedes' principle using n-hexane as an immersion liquid and applying the relation [33]

$$\rho = \rho_l \left( \frac{w_a}{w_a - w_b} \right) \quad (kg/m^3) \quad (4)$$

where  $\rho_l$  is density of n-hexane (0.661 g/cm<sup>3</sup>).  $w_a$  and  $w_b$  are the sample weights in air and in n-hexane, respectively. The molar volume is the volume occupied by one mole of material and is obtained by dividing the molecular weight by its density of material [34]:

$$V_m = \frac{M_w}{\rho} \quad (m^3) \quad (5)$$

Where  $M_w$  is the molecular weight of the substance or molecular weight of glass system.  $V_m$  is the molar volume and  $\rho$  is the density of the material or glass.

## 2) Viscosity

Viscosity is one of an important property of glass which it is a measure of the resistance of a liquid to shear deformation and given by the expression [29]:

$$\mu = \frac{Fd}{Av} \quad (N \cdot s/m^2) \quad (6)$$

where  $\mu$  is dynamic viscosity,  $F$  is applied force,  $A$  is applied to two parallel planes of area,  $d$  is separation distance, and  $v$  is the relative velocity. The glass processing requires the viscosity to be in a certain range of approximately  $10^3$ -  $10^7$  dPa at a certain temperature which we called that the working point. If the viscosity of glass reaches  $10^{7.6}$  dPa is defined as the softening point. In this point, the glass deforms rapidly and is used for glass blowing or sintering. If viscosity the and the upper limit  $10^{13}$  dPa is called the annealing point. The viscosity of glass is increased, and the

structure becomes frozen-in(quasi-solid) when the temperature as below the glass transformation temperature point.

### 3) Physical parameters

In addition, the physical properties also include ion concentration, polaron radius, internuclear distance and field strength can be calculated by using the following formula [36]

Ion concentration ( $N$ ):

$$N = \frac{\text{mole \% of doped} \times \text{density of glass} \times N_A}{\text{average molecular wight of glass}} \quad (cm^{-3}) \quad (7)$$

Polaron radius ( $r_p$ ):

$$r_p = \frac{1}{2} \left( \frac{\pi}{6N} \right)^{1/3} \quad (\text{\AA}) \quad (8)$$

Internuclear distance ( $r_i$ ):

$$r_i = \left( \frac{1}{N} \right)^{1/3} \quad (\text{\AA}) \quad (9)$$

Field strength ( $F$ ):

$$F = \left( \frac{Z}{r_p^2} \right) \quad (cm^2) \quad (10)$$

Where  $Z$  is the valence number of the dopants,  $N_A$  is Avogadro's number ( $6.02214076 \times 10^{23}$ ).

#### 2.1.6.2 Thermal properties

##### 1) Heat capacity

In a solid material, heat capacity is one of a property that is indicative of a material's ability to absorb heat from the external environment. heat capacity is expressed as follows:

$$C = \frac{dQ}{dT} \quad (J/mol.K) \quad (11)$$

Where  $dQ$  is the energy required and  $dT$  is temperature. In addition, there are two paths for measurement in this property at the environmental conditions accompanying the transfer of heat. First, heat capacity while maintaining the specimen volume constant is  $C_v$  and is for constant external pressure, which is denoted  $C_p$ . In this work,  $C_v$  can be calculated by using eq. (12)

$$C_v = \frac{12}{5} \left( \frac{\pi^4 N_A k_B T^3}{\theta_D^3} \right) \quad (12)$$

And  $C_p$  is given by eq. (13)

$$C_p = 3R \left[ 1 - \exp \left( -1.5 \frac{T}{\theta_D} \right) \right] \quad (13)$$

Where  $N_A$  is Avogadro's number,  $k_B$  is Boltzmann's constant,  $T$  is temperature,  $\theta_D$  is Debye temperature, and  $R$  is gas constant.

## 2) Thermal expansion coefficients

Thermal expansion is the behavior of materials to change its shape, area, and volume in response to the difference in temperature. The curve of thermal expansion can be measured by using three important properties. The three important properties are the thermal expansion coefficient, glass transformation temperature, and softening temperature. In the glass material, thermal expansion coefficients are measured in one-directional which the measured value is called linear thermal expansion coefficient. Normally, the value of thermal expansion coefficients is measured over a specified temperature range which the measured in range of from 0 to 300 °C, 20 to 300 °C, or 25 to 300 °C [29].

### 2.1.6.3 Electrical properties

It is well known that glasses are excellent insulating properties, while the most metal oxide are ionic conductor. However, most metal oxide is extremely poor electrical conductor due to low numbers of free monovalent ions. Due to the glass is excellent insulating properties, it is widely used in the field of electrical and electronic engineering to produce seals, high-voltage insulators, microelectronic packaging, high-vacuum tubes, lamps, etc.

### 1) Resistivity of glass

The electrical conductivity of the glass depends on the mobility of ions. In general, the addition of alkali metal oxide in the based glass led to increasing conductivity of glass but adding two or more alkali metal oxide (mixed-alkali effect) is an effect to decreases in the conductivity. Furthermore, the electrical conductivity also depends on temperature. At room temperature, the mobility of ions increases with the increasing temperature, and resistivity also decreases.

### 2) Dielectric properties

Dielectric properties consist of dielectric constant and dissipation factors while dielectric constant is used to describe the dielectric characterization of a material. Normally, the dielectric constant usually lies between 4.5 and 8.0 which is within the range of other electrically insulating material [34]. Because of the dielectric constant depends on the electronic and ionic polarization and increases with temperature.

### 3) Energy band structures in solids

The energy band structure is a correlation between the energy and momentum of a carrier in the material and has been used to explain many physical properties of solids such as optical properties, electrical properties, and understanding of all solid-state devices (transistors, solar cells, etc.). Each individual atom has existed discrete energy levels which may be occupied by electrons. Where the shell is designated by integers (1, 2, 3, etc.) and subshell is designated by letters (s, p, d, and f). The most electron in atoms fill only the states having the lowest energies. these are in accordance with the Pauli exclusion principle.

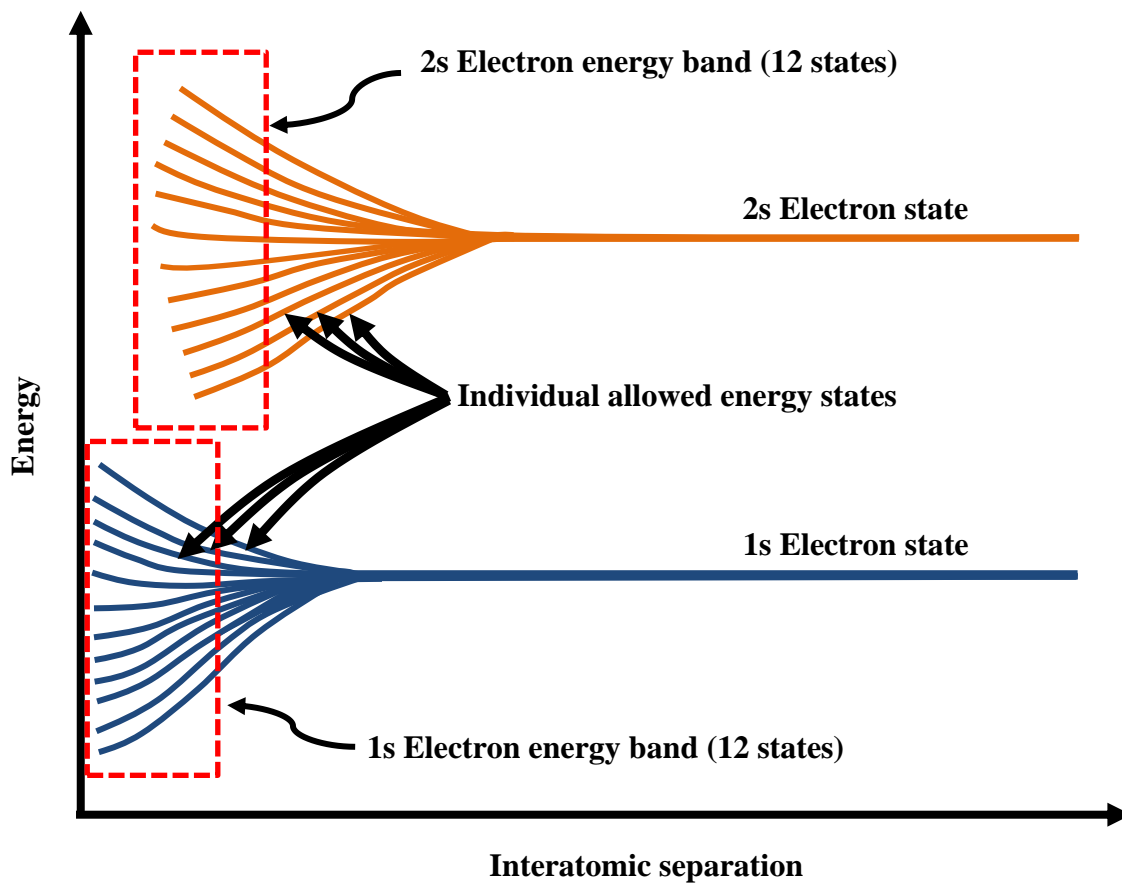


**Figure 2.8 Schematic plot of electron energy versus interatomic separation for an aggregate of 12 atoms**

When the atoms come within proximity of one another, The electrons are perturbed. This influence shows that the atomic state split into a series of closely spaced electron states in the solid which the form is called an electron energy band. The electrical properties of solids are a consequence because of electron band structure. In the Figure 2.9 (a), the electron band gap in metal such as copper is available electron states above and adjacent to filled states or valence band. Figure 2.9 (b) show that the electron band gap of magnesium is an overlap of filled and empty outer bands. Figure 2.9 (c) represents the large electron band gap of insulators in which the valence band is separated from the conduction band. Figure 2.9 (d) shows the electron band gap of semiconductors.



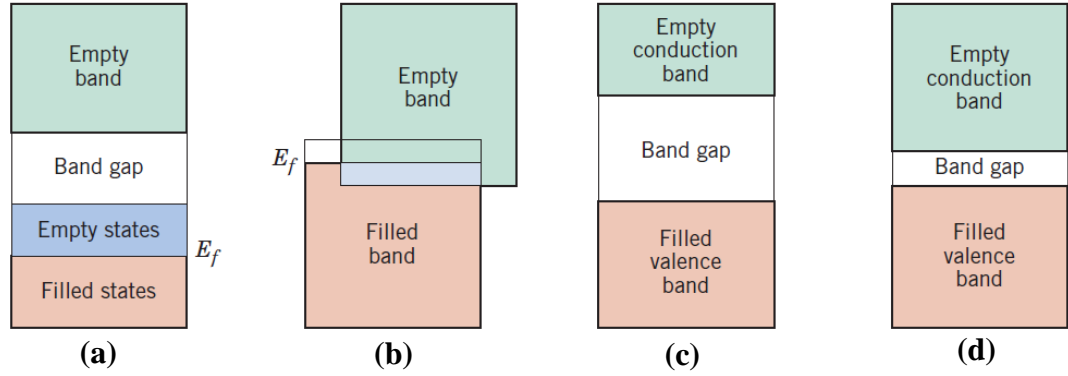


**Figure 2.9** The various electron band structures in solids at 0 K [16]

#### 2.1.6.4 Optical properties

The optical properties are one of the important properties due to the structure of glass that can be studied by using UV-vis spectroscopy. In general, optical properties mean a material's response to exposure to electromagnetic wave and in particular to visible light. In this work, the UV-vis absorption spectra are recorded in the wavelength range 200 – 2000 nm by UV-vis spectroscopy. The absorption coefficient ( $\alpha_{(\omega)}$ ) can be calculated by Mott and Davis relation [36]

$$\alpha_{(\omega)} = \frac{B(\hbar\omega - E_{opt})^n}{\hbar\omega} \quad (14)$$

Where  $\alpha_{(\omega)}$  is absorption coefficient for electronic transitions based on the value of  $n$  ( $n=1/2$  for direct transition and  $n=2$  for indirect transition) and is a function of photon energy ( $\hbar\omega$ ).  $B$  is the band tailing parameter and  $E_{opt}$  is the optical band gap.

##### 1) Refraction of light

when the light passes through in the transparent materials, the velocity of light is a decrease and bent at the interface. this phenomenon is the refraction of light. The refractive index is defined as the ratio of the speed of light in a vacuum to that in a second medium of greater density.

$$n = \frac{c}{v} \quad (15)$$

The refractive index of materials is one of important parameters on optical properties. Where  $n$  is refractive index of matter.  $c$  is light velocity ( $3 \times 10^8 \text{ m/s}$ ) and  $v$  is the velocity of light traveling in the matter. In this work, refractive index of the glass can be calculated by the Dimitrov and Sakka relation [37]

$$\frac{n^2 - 1}{n^2 + 1} = 1 - \sqrt{\frac{E_{opt}}{20}} \quad (16)$$

Where  $n$  is the value of refractive index and  $E_{opt}$  is the optical band gap. Furthermore, the larger of atoms or ions such as barium and lead ions have an important influence on the electronic polarization. For example, the glass systems containing lead oxide approximately 90 wt% have an index of refraction of approximately 2.1. The molar refraction ( $R_m$ ) can be calculated by the Lorentz-Lorentz equation as [38, 39]

$$R_m = \left[ \frac{n^2 - 1}{n^2 + 1} \right] V_m \quad (cm^{-3}) \quad (17)$$

Where  $V_m$  is the molar volume of glass. The molar refraction depends on the electronic polarizability in materials and related to the structure of glass. The electronic polarizability ( $\alpha_m$ ) can be calculated using the relation [40, 41]:

$$\alpha_m = \left( \frac{3}{4\pi N_A} \right) R_m \quad (nm) \quad (18)$$

The reflection loss can be determined by [40, 42]:

$$R_L = \left( \frac{n - 1}{n + 1} \right)^2 \quad (19)$$

Moreover, from the value of refractive index of the glass samples can be calculated the dielectric constant ( $\varepsilon$ ) and optical dielectric constant, respectively [43,44].

$$\varepsilon = n^2 \quad (20)$$

optical dielectric constant of glass is obtained by the relation.

$$P \frac{dt}{dp} = (\varepsilon - 1) = (n^2 - 1) \quad (21)$$

The metallization ( $M$ ) can be obtained from following the relation eq.19 and depended on the refractive index of materials. However, the value of metallization has a value in the range of 0 – 1. If the value of metallization close to 0 represent that the material is metal and close to 1 show that the material is an insulator [40,42].

$$M = 1 - \frac{R_m}{v_m} \quad (cm^{-6}) \quad (22)$$

## 2) Absorption

Normally, the transparent material often appears colored. These results due to the visible light is absorbed by two mechanisms. One of the mechanisms is electronic polarization which it is important at light frequencies in the vicinity of the relaxation frequency of the constituent atoms. The last mechanism is related to the conduction band electron transitions that depend on the electron energy band structure of the material. The excitation energy is related to the absorbed photon frequency through eq. (20).

$$\Delta E = h\nu \quad (J) \quad (23)$$

Where  $E$  is photon energy,  $h$  is a universal constant called Planck's constant ( $6.63 \times 10^{-34} J \cdot s$ ) and  $\nu$  is the frequency of electromagnetic radiation. If the material has impurities that lead to the donor and acceptor levels of the

electron levels are created within the energy band gap. In addition, the intensity of the absorption can be calculated by the relation

$$I = I_0 e^{-\mu x} \quad (24)$$

Where  $I$  is the intensity of the non-absorbed radiation incident radiation,  $I_0$  is the intensity of the non-reflected incident radiation,  $\mu$  is absorption coefficient, and  $x$  is thickness of material.

### 3) Transmission

The absorption, reflection, and transmission of the material can be applied to the route of light through a transparent solid and as shown in Figure 2.10. The transmitted intensity of light radiation can be calculated by using the following formula

$$I = I_0(1 - R)^2 e^{-\mu x} \quad (25)$$

Where  $R$  is the reflectance,  $I$  is the transmitted intensity at the back face,  $I_0$  is the intensity of the incident beam,  $\mu$  is absorption coefficient, and  $x$  is thickness of material. In addition, the reflectivity, absorptivity, and transmissivity are depending on the light wavelength. In this work, we used Fourier transform infrared (FTIR) spectroscopy to investigate the absorptivity and transmissivity of the glass samples. FTIR spectroscopy has been considered as one of the most effective techniques to study and understand the determination of the functional groups with possible molecular bonds between chemical compounds. In Figure 2.11 show the schematically of the main component of a simple FTIR spectrophotometer.

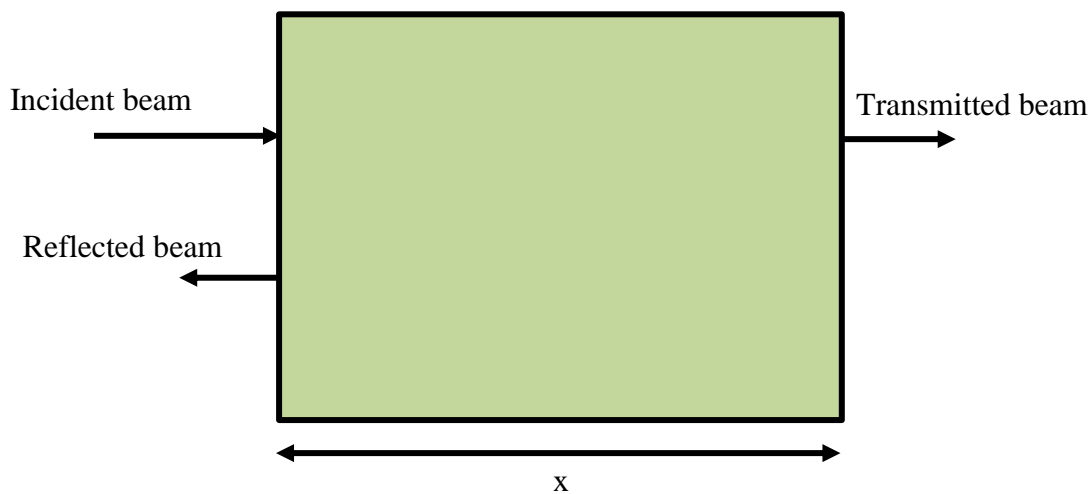


**Figure 2.10 The transmission of light through a transparent medium**

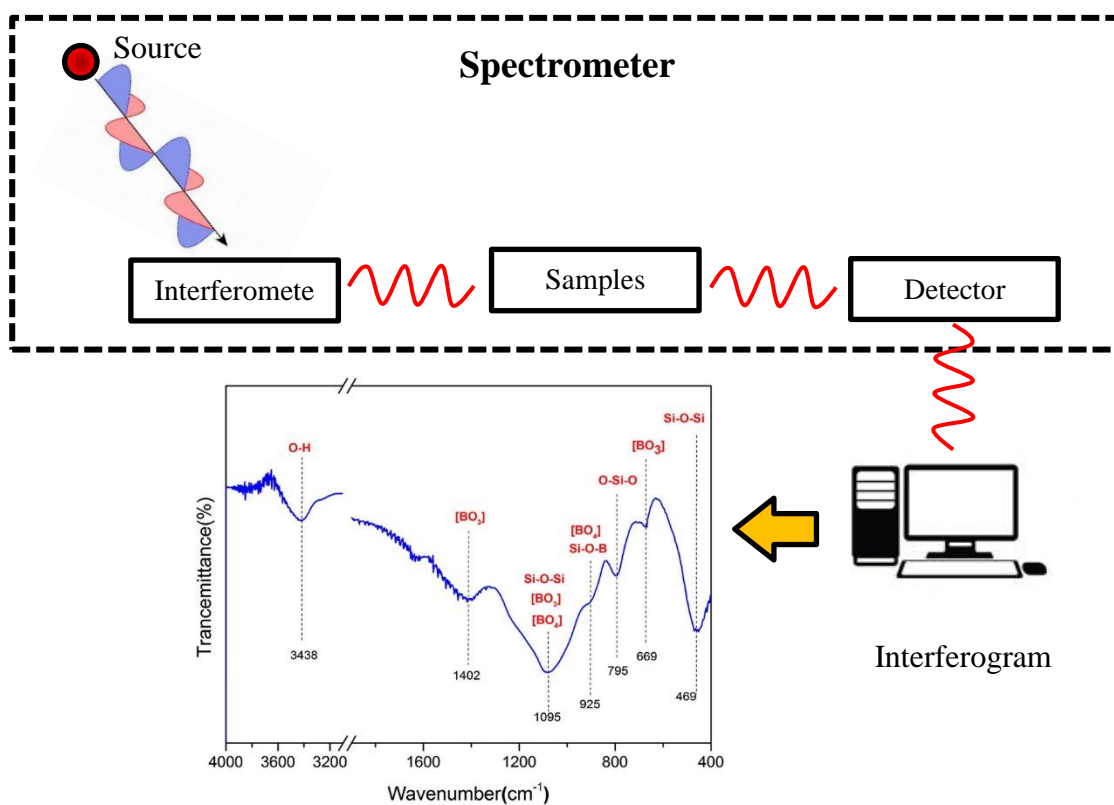


**Figure 2.11 Basic component in Fourier transform infrared spectrometer [86]**

The FTIR spectra of the glass samples were recorded in the wavenumber range of 400 - 2000  $\text{cm}^{-1}$ . The changes in vibrational energy state for many functional groups are located in the mid-IR region which has the wavenumber approximately 400 - 4000  $\text{cm}^{-1}$ . Typically, functional groups in the glass structure are the range of approximately 400 – 1000  $\text{cm}^{-1}$ .

#### 2.1.6.5 Elastic properties

Elastic properties are one of the important properties for solids. Because of elastic properties are related to the interatomic potentials. Additionally, there are also linked thermodynamically to the specific heat, thermal expansion, Debye temperature, etc. In the framework of this research, the glass samples were measured the value of ultrasonic velocities by a pulse-echo technique in which the elastic moduli can be calculated by the value of ultrasonic velocities. Receiver and transducer detector are used at 4 MHz frequency and at room temperature and as shows in Figure 2.12. However, the receiver and transducer detector are acting as a transmitter-receiver at the same time and the value of ultrasonic velocity can be determined by the relation [45]

$$v = \frac{2x}{\Delta t} \quad (m/s) \quad (26)$$

Where  $x$  is the thickness of the glass samples,  $v$  is the velocity of materials and  $t$  is the time interval in material.

The elastic moduli such as longitudinal modulus, shear modulus, bulk modulus, Young's modulus, Poisson's ratio, and micro-hardness have been studied in this work. The longitudinal modulus can be determined by using the value of density and ultrasonic velocity measured. This valuable property tells us ahead of time how stiff a material is to deformation and as shows in Figure 2.13. The longitudinal modulus is the value of resistance to longitudinal compression in materials needed to deform a material and can be calculated by the relation [46]

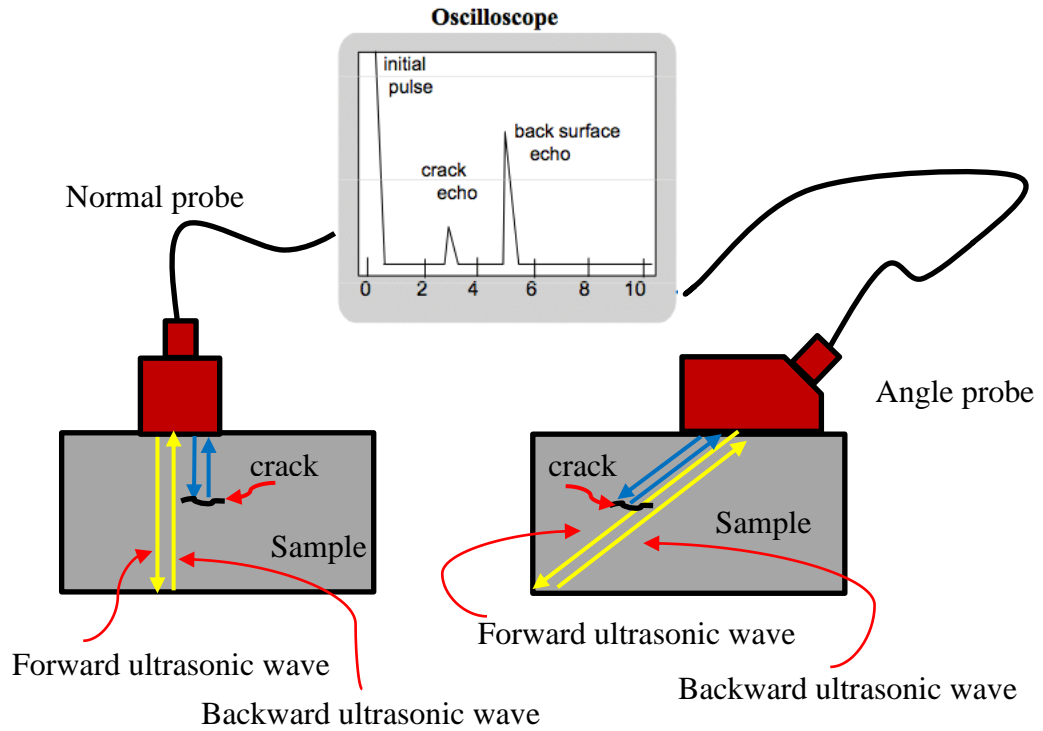


**Figure 2.12 Measurement of the pulse-echo technique**



**Figure 2.13 Longitudinal modulus in materials**

$$L = \rho v_L^2 \quad (Pa) \quad (27)$$

Where  $\rho$  is density of the glass sample,  $v_L$  is longitudinal velocity of glass sample and  $v_s$  is shear velocity. And then, the shear modulus is the ratio the shear stress needed to deform a material by a given angle and denoted by  $G$ . It is well known that the shear modulus tells us in advance how resistant a material is to shearing deformation. Figure 2.14 show the shear modulus diagram in material and can be expressed in terms of shear velocity and density as:

$$G = \rho v_s^2 \quad (Pa) \quad (28)$$

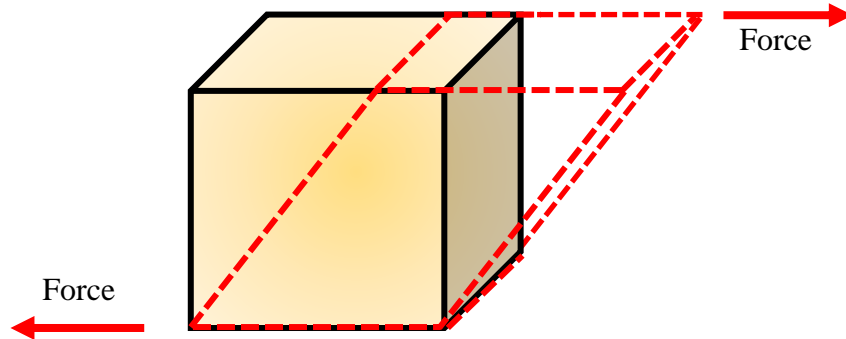


**Figure 2.14 Shear modulus in materials**

Bulk modulus describes the elastic properties of a solid when it is under pressure on all surfaces or the describes how resistant a substance is to compression. Normally, the bulk modulus is denoted by  $K$  in equations and as show in Figure 2.15. The value of bulk modulus depends on the longitudinal modulus and shear modulus and can be used to predict compression. In addition, it indirectly indicates the types of chemical bonding within a substance. The value of bulk modulus is shown in Pascals units (Pa) or newtons per square meter ( $N/m^2$ ).

$$K = L - \frac{4}{3}G \quad (Pa) \quad (29)$$

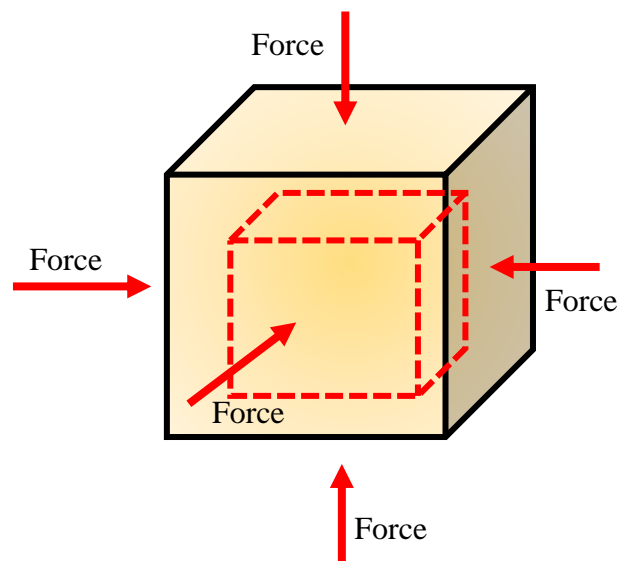


**Figure 2.15 Bulk modulus in materials**



Figure 2.16 is present Young's modulus diagram and is one of the elastic moduli we use for deformation which takes place or the ratio of stress to strain. when we must lengthen or shorten the glass samples without actually breaking it, the greater the value of Young's modulus, the larger the stress that is needed to achieve the deformation. The Young's modulus is defined as the eq. (26) in Pascals unit.

$$E = (1 + \sigma)2G \quad (Pa) \quad (30)$$

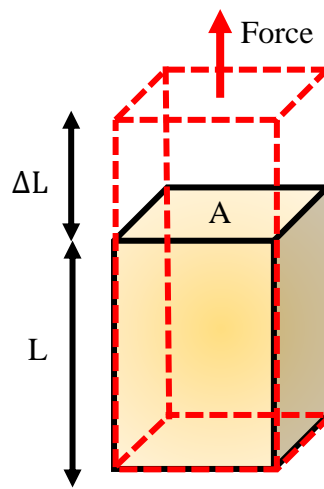


**Figure 2.16 Young's modulus in materials**

Poisson's ratio ( $\sigma$ ) is the ratio of the transverse contraction strain to longitudinal extension strain in the direction of the applied load and as show in Figure 2.17. And then, Poisson's ratio is related to elastic moduli such as bulk modulus, Young's modulus, longitudinal modulus, and shear modulus. Basically, the value of Poisson's ratios for common materials is in the range of 0 - 0.5. However, the value of Poisson's ratio may be a negative value because of compressive deformation and maybe a positive Poisson's ratio when materials deformed by tensile. The Poisson's ratio is determined by the relation below.

$$\sigma = \frac{L - 2G}{2(L - G)} \quad (31)$$

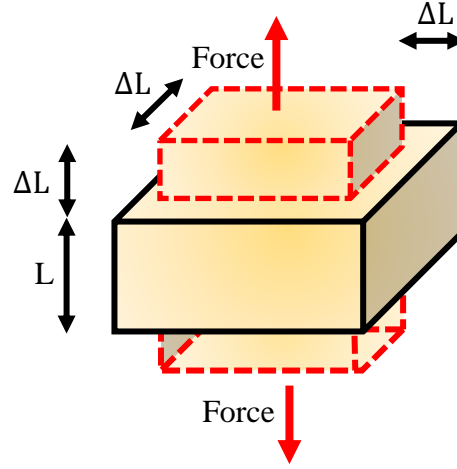


**Figure 2.17 Poisson's ratio in materials**

Hardness is one of the properties of a material that enables it to resist plastic deformation. Normally, the microhardness measurement can be measured with the most popular test (Knoop hardness test and the Vickers hardness test). However, micro-hardness measured in this work can be calculated by elastic moduli data and determined by eq. (28) in Pascals unit.

$$H = \frac{(1-2\sigma)E}{6(1+\sigma)} \quad (Pa) \quad (32)$$

The softening point is the temperature at which a material softens beyond some arbitrary softness. In this work, we study the softening temperature ( $T_s$ ) of the glass samples. Softening temperature is maximum temperature of glass before it permanently deforms. Debye temperature ( $\theta_D$ ) is one of important parameter for materials. Debye temperature will determine the elastic moduli and atomic vibrations and defined as eq. (30).

$$T_s = \frac{v_s^2 M}{C^2 \psi} \quad (K) \quad (33)$$

And then, the last parameter is Debye temperature and calculated according to this equation

$$\theta_D = \left(\frac{h}{k_B}\right) \left(\frac{3\psi N_A}{4\pi V_m}\right)^{1/3} \quad (K) \quad (34)$$

Where  $v_s$  is shear velocity,  $M$  is molecular weight of the glass,  $c$  is constant equal to  $0.5074 \times 10^5 \text{ cmk}^{-1/2}\text{s}$ ,  $\psi$  is number of atoms in chemical formula,  $h$  is Plank's constant,  $k_B$  is Boltzmann's constant,  $N_A$  is Avogadro's number, and  $V_m$  is molar volume of glass.

Moreover, the elastic moduli result from the ultrasonic measurement compared with the elastic moduli calculation by Makishima-Mackenzie's model. Makishima-Mackenzie's theory has derived the following relationships for calculating the dissociation energy per unit volume and packing density [87]. This model determines the elastic moduli such as shear modulus, Young's modulus, bulk modulus, and Poisson's ratio of the glass sample. The equation used to calculate the elastic moduli are listed below:

Young's modulus is given by eq. (35)

$$E_{th} = 2V_t G_t \quad (GPa) \quad (35)$$

Where  $V_t$  is packing density,  $G_t$  is dissociation energy per unit volume and in addition,  $x_i$ ,  $V_i$  and  $G_i$  are the respective molar fraction, packing factor and dissociation energy per unit volume from their chemical composition.

Bulk modulus is given by eq. (36)

$$K_{th} = 1.2V_t E_{th} = 2.4V_t^2 G_t \quad (GPa) \quad (36)$$

Shear modulus is given by eq. (37)

$$G_{th} = \frac{3E_{th}K_{th}}{9K_{th} - E_{th}} \quad (GPa) \quad (37)$$

Poisson's ratio is given by eq. (38)

$$\sigma_{th} = \frac{E_{th}}{2G_{th}} - 1 \quad (38)$$

Longitudinal modulus is given by eq. (39) [88-89]

$$L_{th} = K_{th} + \left(\frac{4G_{th}}{3}\right) \quad (GPa) \quad (39)$$

Where  $G_t$  and  $V_t$  can be calculated by the following equation

$$V_t = \frac{\rho}{M} \sum_i x_i V_i \quad (cm^3) \quad (40)$$

$$G_t = \sum_i G_i x_i \quad (kcal/cm^3) \quad (41)$$

## 2.2 Gamma shielding measurements

### 2.2.1 Radiation

Basically, radiation is the process of energy emission as either particles or waves that come from the source or travels through space may be able to penetrate various materials such as visible light, radio, microwaves, etc. Radiation is classified as ionizing radiation and non-ionizing radiation which it depends on energy to knock an electron off an atom.

#### 2.2.1.1 Non-ionizing radiation

Non-ionizing radiation is referred to the electromagnetic radiation that does not carry photon energy to ionize atoms or molecules. When the non-ionizing radiation passing through matter and has sufficient energy only for excitation, an electron in the atom is the move to a higher energy state. However, radio and microwave energy have low frequencies and it is harmful only to the extent of the amount of heat energy it transfers to whatever it hits.

##### 1) Microwave and radio interactions with matter

The photon energy of microwave is in the order  $10^{-3}$  eV and the range in these energies can separate the quantum states of molecular rotation and torsion.

The molecules will be to rotate and produce the heat because of that molecular motion. However, the photon energy of the microwave has lower than the energy of the x-ray approximately a million times.

## 2) Infrared interaction with matter

The photon energy of infrared radiation is in the order of  $10^{-2}$  eV. These energies can be separate the quantum states of molecular vibrations. The absorption of infrared is stronger than microwaves. this leads to the heating in tissue since it increases molecular vibrational activity.

## 3) Visible light Interaction with matter

When the light hits the material, the material is absorbed visible light. If the photon has the required energy, the atom or molecule will be raised from a low energy state to one of higher energy. After a short time, the atom or molecule falls back to a lower state and the energy difference is emitted as a photon. The energy of visible light is in the range of 1.7 - 3.1 eV and in the wave range approximately 400 – 700 nm. However, visible light does not cause ionization with its risks.

### 2.2.1.2 Ionizing radiation

Ionizing radiation is given off energy to knocking electrons off atoms that cause the atoms to have a charge (ion). Ionizing radiation is a high-energy radiation that leads to damage to cells and their genetic material. DNA damages from ionizing radiation is an effect to comprise cellular DNA repair mechanisms which is an established risk factor for cancer. However, ionizing radiation has many types that is categorized by the nature of the particles such as alpha particles, beta particles, and electromagnetic waves such as higher ultraviolet (UVC), x-ray, and gamma-ray.

#### 1) Alpha particles

Alpha particles or alpha rays are consisting of two protons and two neutrons tightly bound together into a particle identical to a helium - 4 nucleus. Normally, alpha ray is emitted from radioactive decay, called alpha-decay. They have a velocity in the vicinity of 5% the speed of light and have a kinetic energy of about 5 MeV. Because of alpha ray have highly ionizing that leads to unable to penetrate extremely far through matter (a few centimeters of air). Alpha particles emitted from a nucleus and as shows in Figure 2.18.

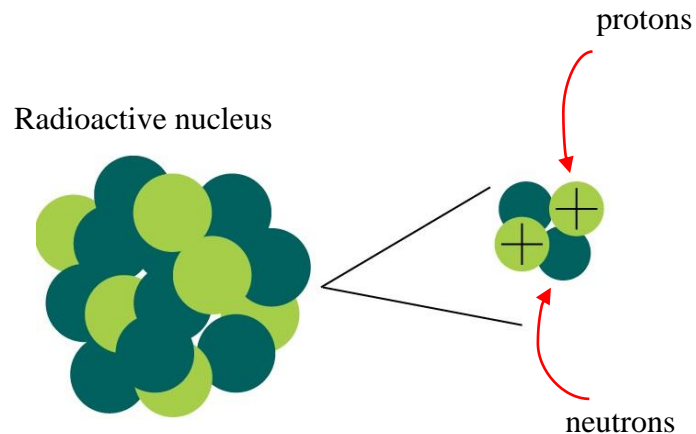


**Figure 2.18 Alpha particle is emitted from a nucleus.**

## 2) Beta particles

Beta particles or beta ray is a high energy and high speed of an electron or positron which they are emitted by the radioactive decay, called beta-decay. This process will decrease the neutrons by one and an increase in the number of protons by one. The effect of the number of protons in the nucleus determines the difference in element. Beta ray has an energy of 0.5 MeV, and they can travel a range of about one meter in the air which depends on the particle energy, but less ionizing than alpha particles. Figure 2.19 present the beta particles emitted by the radioactive decay.

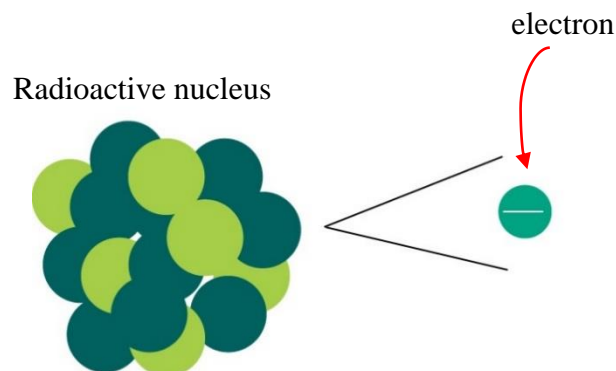


**Figure 2.19 Beta particles**

### 3) Ultraviolet radiation

Ultraviolet radiation or UV rays are electromagnetic radiation that comes from the sun and can be made by humans. UV rays have more energy than visible light, but not as much as x-rays. There are many types of UV rays that based on how much energy they have. At the high-energy, UV rays is ionizing radiation and can produce harmful physiological effects ranging from sunburn to skin cancer. However, at low-energy, UV ray is not considered an ionizing radiation. Because of photons lack the energy to ionize atoms. This causes can create chemical reactions and causes many substances to glow or fluoresce.

### 4) Gamma radiation

Gamma radiation or gamma rays is a penetrating electromagnetic wave occur from the radioactive decay and as shows in Figure 2.20. Gamma rays have a very high-energy and travel at the speed of light that can cover hundreds to thousands of meters through the air before expending their energy. In addition, they have so much penetrating power and can easily pass through the human body. The shielding to stop them must lead or several centimeters of concrete.



**Figure 2.20 Gamma decay**

#### 4.1) Interaction of gamma ray with matter

Gamma interactions with matter are important for the shielding application material. there are three mechanisms for the interaction of gamma rays such as photoelectric effect, Compton scattering, and pair production. Each of the mechanism depends on the intensity, energy, and the type of radiation. Furthermore, gamma ray shielding application is used to medical field, nondestructive testing, etc. [48-52].

#### 4.1.1) Photoelectric effect

Figure 2.21 present the photoelectric process in an atomic Shell. When the incident photon hits an electron in the orbit, the kinetic energy of the incident photon is transfer to an electron that effect to an electron has increased in the energy and change to the excited state. These results lead to a vacancy in a primitive position, and it is promptly filled by one of the outer electrons. After that the electromagnetic radiation, characteristic x-ray, emitted by the electron transit to the electron hole.

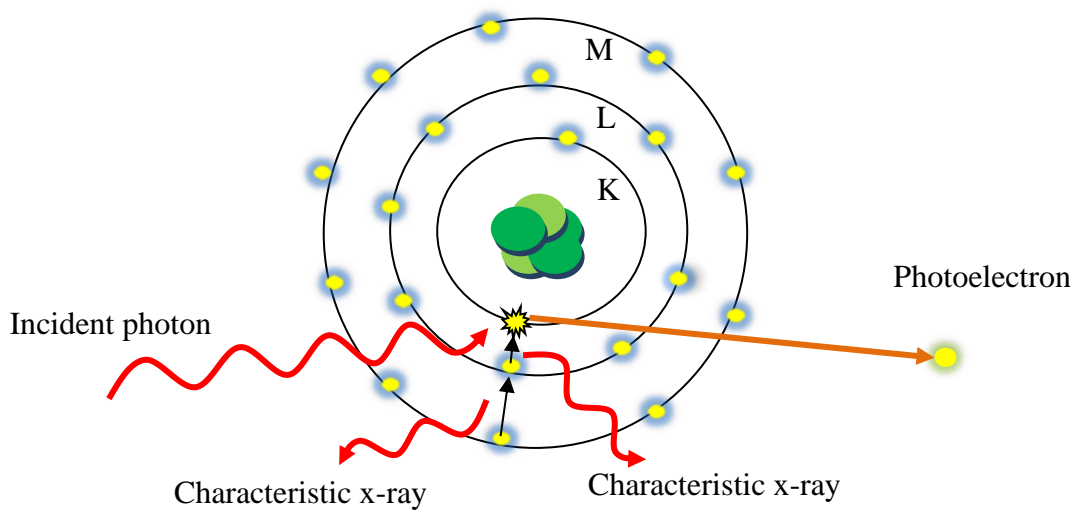


**Figure 2.21 Schematic representation of photoelectric effect process**

The kinetic energy of photoelectron can determine by the relation

$$E_k = h\nu - E_B \quad (42)$$

Where  $h\nu$  is the energy of incident photon,  $E_B$  is the binding energy of the electron in the atom which it equal to the excitation energy of the atom after electron ejection for K-shell. In addition, the probability of photoelectric effect is given approximately by the expression



$$\sigma_{PE} \propto \frac{Z^n}{E^3} \quad (43)$$

Where  $n$  is the exponent between 3 and 4 over the gamma-ray energy region of interest. Photoelectric effect probability depends on the atomic number ( $Z$ ) and  $E$  is energy of incident photon. Moreover, the process creates predominant interaction for low-energy of gamma ray, x - ray, and characteristic x-ray or bremsstrahlung [48-52].

#### 4.1.2) Compton scattering

Compton scattering is the most process for the interaction of gamma radiation with matter. Figure 2.22 shows the Compton scattering process. Incident photon collides with an electron that transfers the part of its kinetic energy to the electron. The recoil electron is called Compton electron. The velocity of Compton electron is depending on the energy transferred to the electron. the incident photon is deflected through an angle  $\theta$  with respect to its original direction and the direction of Compton electron deflected through an angle  $\phi$ . This process is most important for energy absorption in the range from 100 keV to 10 MeV. The energy of scattered electron can be determined by the relation [48-53]

$$E_e = E_\gamma - E'_\gamma \quad (44)$$

Where  $E_e$  is the energy of scattered electron,  $E_\gamma$  is the energy of incident photon, and  $E'_\gamma$  is the energy of scattered photon. The conservation of energy and momentum can be determined by using the relationship

The conservative of energy:

$$E_\gamma + E_0 = E'_\gamma + (E_0^2 + c^2 P^2)^{1/2} \quad (45)$$

The conservative of momentum

$$\frac{\vec{E}_\gamma}{c} = \frac{\vec{E}'_\gamma}{c} + \vec{P} \quad (46)$$

Where  $E_0 = m_0c^2$  is total energy when it is at rest (0.511 MeV),  $m_0$  is rest mass of electron,  $c$  is light velocity and  $P$  is momentum. The equation of vector in the conservation of momentum can explain from the below equation.

$$\frac{E_\gamma}{c} = \frac{E'_\gamma}{c} \cos \theta + P \cos \phi \quad (47)$$

and

$$0 = -\frac{E'_\gamma}{c} \sin \theta + P \sin \phi \quad (48)$$

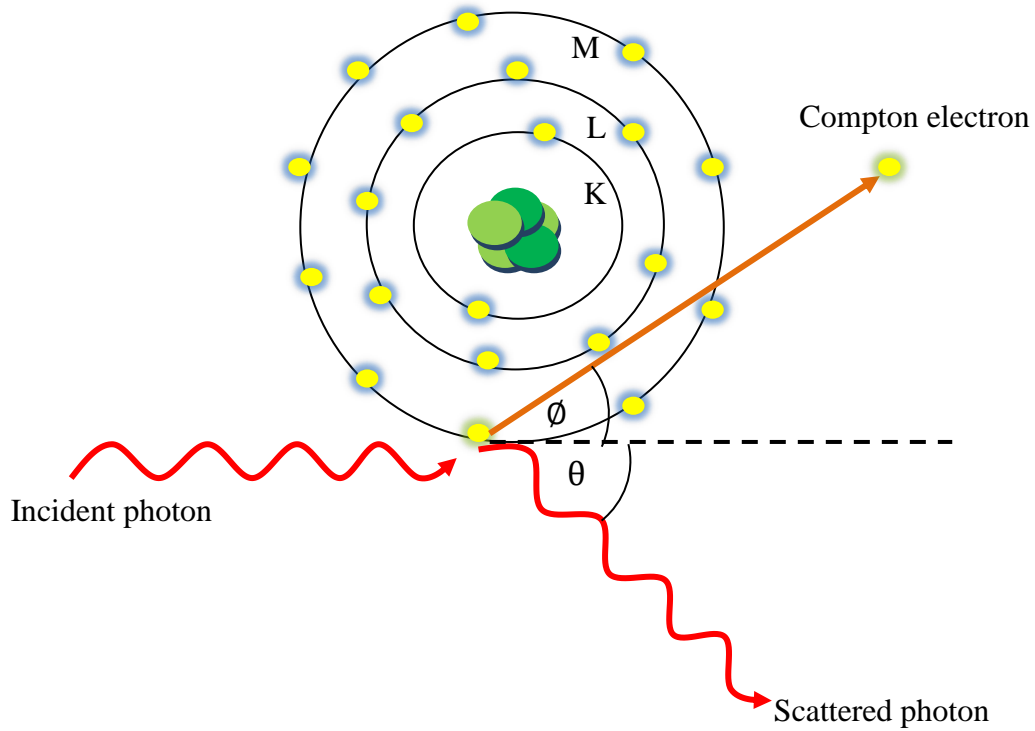


**Figure 2.22 Schematic representation of Compton scattering**

Therefore, the result is

$$P^2 c^2 = E_\gamma^2 - 2E_\gamma E'_\gamma \cos \theta + E_\gamma'^2 \quad (49)$$

and then, substitution the eq. (38) into eq. (34)

$$\frac{1}{E'_\gamma} - \frac{1}{E_\gamma} = \frac{1 - \cos \theta}{E_0} \quad (50)$$

So, the last equation is expressed as

$$\Delta\lambda = \lambda' - \lambda = \lambda_0(1 - \cos \theta) \quad (51)$$

Where  $\lambda_0 = \frac{h}{m_0 c}$  is Compton wavelength of electron,  $\theta$  is angle of scattering photon.  $\lambda$  and  $\lambda'$  is the wavelength of photon before and after scattering.

#### 4.1.3) Pair production

When an incident photon has the energy at least 1.022 MeV, an electron and positron are created under the influence of the strong electromagnetic fields in the vicinity of a nucleus and as shows in Figure 2.23. The nucleus in this process received an exceedingly small amount of recoil energy to conserve momentum. However, the nucleus is otherwise unchanged and incident photon disappears. If the photon energy is more than 1.022 MeV, 1.022 MeV goes to create an electron and positron pair which each particle is received the energy in 0.511 MeV. The remain of incident photon energy is divided as kinetic energy among the electron and positron. The kinetic energy of the electron produced can be expressed as [48-52]

$$E_{electron} + E_{positron} = h\nu - 1.022 \text{ MeV} \quad (52)$$

The probability of this process depends on the increasing photon energy and atomic number.

$$\sigma_{pp} \approx Z^2 \quad (53)$$

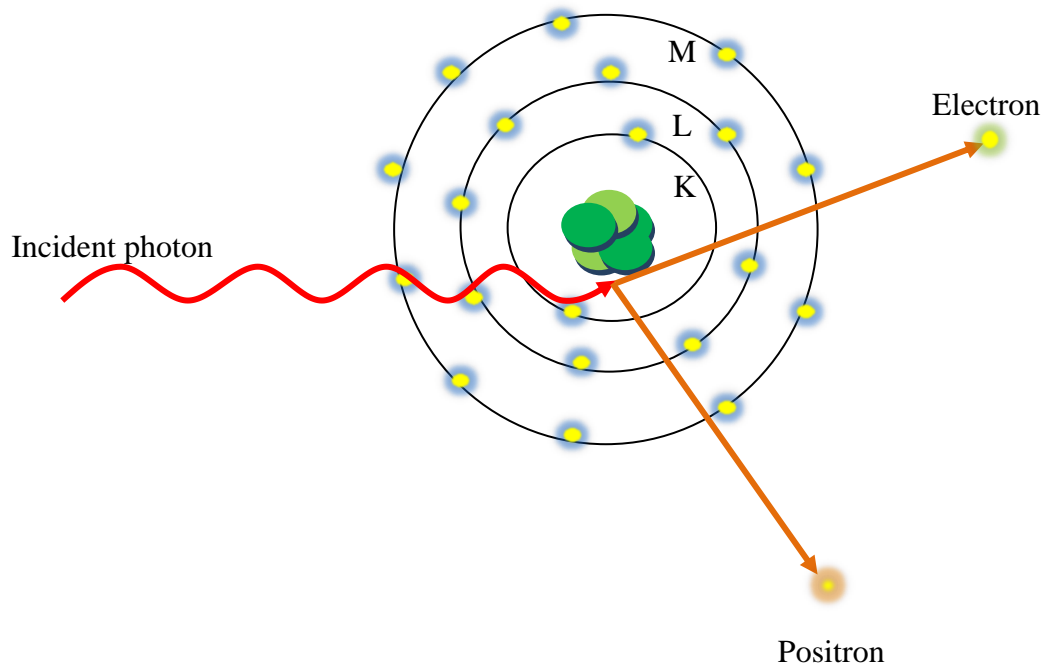


**Figure 2.23 Pair production process(a)**

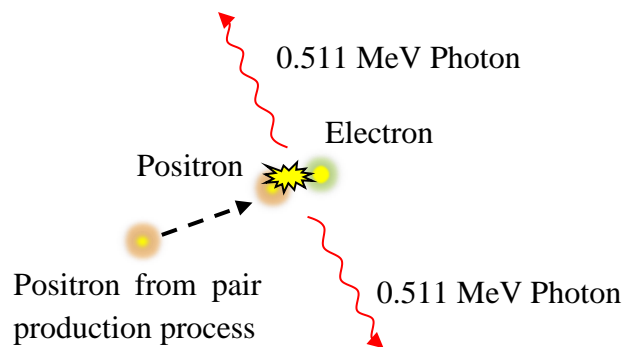


**Figure 2.23 Annihilation process(b)**

### 2.2.2 The fundamental law of gamma attenuation

When gamma-ray ( $I_0$ ) is incident on an absorber of thickness ( $x$ ), the transmitted intensity ( $I$ ) which is given by the Beer–Lambert law

$$I = I_0 e^{-\mu x} \quad (54)$$

Where  $x$  is the thickness of the absorber,  $I_0$  is intensity of incident gamma ray,  $I$  is intensity of gamma ray transmitted, and  $\mu$  is linear attenuation coefficient. The linear attenuation coefficient is explaining the fraction of the x-rays or gamma radiation which is absorbed per unit thickness of the absorber. Moreover, the value of the linear attenuation coefficient increases as the atomic number of the absorber increases and decreases with the energy of the gamma rays for all materials [48-52].

### 2.2.3 Mass attenuation coefficient

The linear attenuation coefficient is independent of the density of a material, the mass attenuation coefficient is always reported for convenience. The mass attenuation coefficient is defined as the ratio of the linear attenuation coefficient to the density of absorber and its units are  $\text{cm}^2/\text{g}$ . The mass attenuation coefficient value can be converted by the value of the linear attenuation coefficient and given by the following relation [48-52]

$$\mu_m = \frac{\mu}{\rho} \quad (\text{cm}^2/\text{g}) \quad (55)$$

### 2.2.4 Half value layer (HVL)

Half-value layer (*HVL*) is the thickness of an absorbing material required to reduce the energy of an x-ray or gamma-ray to half its original value. The value of half value layer depends on atomic number and the energy of x-ray or gamma-ray which decreases with the atomic number of the absorber increases and increases with the photon energy. Thus, if the incident photon energy is 1 and transmitted energy is 0.5 that substitute into the eq. (43) or Beer–Lambert law [48-52].

$$HVL = \frac{\ln 2}{\mu} = \frac{0.693}{\mu} \quad (m) \quad (56)$$

### 2.2.5 Mean free path (*mfp*)

Mean free path is the average distance of the photon particle which travels through before interacting [54].

$$mfp = \frac{1}{\mu} \quad (m) \quad (57)$$

### 2.2.6 Effective atomic number and electron density

The value of effective atomic number can be determined using the total atomic and electronic cross sections data. Basically, cross-section is the probability from measurement a collision of two particles which is usually denoted  $\sigma$  and expressed in terms of the transverse area. The total atomic cross section can be determined from the following equation [54]

$$\sigma_{t,a} = \frac{1}{N_A} \sum_i f_i A_i \left( \frac{\mu}{\rho} \right)_i \quad (58)$$

Where  $N_A$  is Avogadro's number,  $f_i$  is the fractional abundance of element,  $A_i$  is the number of formula units and the atomic weight,  $Z_i$  is atomic number and  $(\mu/\rho)_i$  is the mass attenuation coefficient of the element. The total electronic cross sections are expressed by the following formula

$$\sigma_{t,el} = \frac{1}{N_A} \sum_i \frac{f_i A_i}{Z_i} \left( \frac{\mu}{\rho} \right)_i = \frac{\sigma_{t,a}}{Z_{eff}} \quad (59)$$

and effective atomic number can be calculated by using the relation

$$Z_{eff} = \frac{\sigma_{t,a}}{\sigma_{t,el}} \quad (electron/atom) \quad (60)$$

The effective electron number or electron density is given by

$$N_e = \frac{(\mu/\rho)}{\sigma_{t,el}} \quad (electron/g) \quad (61)$$

### 2.3 High pressure sodium lamp

High-pressure sodium lamps are a high-intensity discharge lamp that uses sodium in an excited state to create the light at the wavelength approximately 589 nm and widely used in industrial lighting and many public outdoor areas. Because of high efficiency around 100 lumens per Watt and long life. Normally, there are consist of the mixture between xenon, sodium, and mercury within a compact arc tube. Xenon gas in the tube can simply be ionized that encourage striking the arc under the voltage. The vapor of mercury and sodium were created by heat generated from the arc. the light was produced by the gas pressure and the voltage from mercury vapor and sodium vapor when the pressure within the arc tube is adequate. The operating characteristics of the high-pressure sodium lamp have an efficacy between 70 to 120 lumens/watt, the color temperature is in the range of 1900 K to 2100 K and lifetime is approximately 10,000 - 24,000 hrs [55].

**Table 2.1 Chemical composition of high-pressure sodium lamps glass [90]**

Compound	Percentage
B <sub>2</sub> O <sub>3</sub>	20.20
Al <sub>2</sub> O <sub>3</sub>	17.35
SiO <sub>2</sub>	48.51
Na <sub>2</sub> O	8.21
K <sub>2</sub> O	5.73

### 2.4 literature reviews

In 1996 Kulwant Singh et al. [56] reported the gamma ray attenuation coefficients of borate glasses that adding the bismuth oxide into glass based. The density and mass attenuation coefficients increase with the concentration of bismuth oxide added in glass system. Basically, the amount of the boron oxide in the glass network can absorb the slow neutrons. When adding the bismuth oxide are improve the radiation properties of borate glass. Next, in 2011 K. Kirdsiri et al. [57] studies on radiation shielding, and optical properties of silicate glasses doped with metal oxides such as lead oxide, bismuth oxide, and barium oxide. They were found that the mass attenuation coefficients

increase with the increase of lead oxide and bismuth oxide. This result is an effect on the photoelectric effect and increases in their process. In addition, lead oxide (PbO) can be replaced by bismuth oxide ( $\text{Bi}_2\text{O}_3$ ) for radiation shielding material. For barium oxide (BaO), half value layer is better than ordinary concrete. This report indicates that the glass exhibits radiation shielding properties and will open the new feasibility for lead-free shielding applications. And then, in 2019 Y. Al-Hadeethi et al. [58] studies the borosilicate glass system doped with heavy metal such as  $\text{TiO}_2$ ,  $\text{Bi}_2\text{O}_3$ , and BaO for radiation shielding material. The radiation shielding properties were investigated by using the Geant4 simulation code. They are select the borosilicate glass system for the investigation of radiation shielding properties because  $\text{B}_2\text{O}_3$  can act the network former and leads to some properties such as low melting point, transparency, high refractive index, and low viscosity. The density of glass doped with  $\text{Bi}_2\text{O}_3$  has a value more than the glass doped with BaO and  $\text{TiO}_2$ . The value of mass attenuation coefficients in the glass doped with  $\text{Bi}_2\text{O}_3$  higher than both glasses. These results show that the concentration of  $\text{Bi}_2\text{O}_3$  has a significant effect on the gamma-ray shielding properties in the borosilicate glasses. After that, in 2004 Narveer Singh et al. [59] reported the gamma-ray shielding of lead borate glass and bismuth lead borate glass systems. For the density, bismuth lead borate glass has more value than lead borate glass. In the radiation properties parameter, mass attenuation coefficients have increased, and more than lead borate glass at the 511 keV of the photon energy while the value of half value layer decrease in both glasses systems. Furthermore, gamma-ray shielding properties are better than ordinary concrete, barite concrete, and iron concrete. It has been also observed that bismuth lead borate can be a substitute for lead in order to improve the gamma-ray shielding properties of material. In 2012 Cherdasak bootjomchai et al. [60] studies on gamma-ray shield properties of barium bismuth borosilicate glasses. They used borosilicate glass system because there is low thermal expansion, excellent transmission to visible light, and resistance to thermal shock. The results have shown that it is improved gamma-ray shielding properties when doped with the concentration of bismuth oxide in the glass system. Because the glass system has a high atomic number from barium and bismuth. In addition, the value of gamma-ray shielding parameters such as mass attenuation coefficient, effective atomic number, and electron density are a good agreement between the data of experiment and theoretical data by WinXCom



program. Next, in 2018 Reza Bagheri et al [61] reported that the mass attenuation coefficient of silicate glass system doped with barium, bismuth, and lead oxide has the value more than ordinary concrete and barite concrete. Gamma-ray shielding properties were studied at the energy range of 10 keV - 10 MeV by using XCOM, MCNP-4P code, and XMuDat program. At 622 keV photon energy, the mass attenuation coefficient of silicate glass doped with lead oxide has higher than both glass systems and concrete (ordinary concrete and barite concrete). Moreover, when a comparison between MCNP, XCOM, XuDat, and experimental value, the value of the mass attenuation coefficient is a good agreement. After that, in 2017 Reza Bagheri et al [62] reported the gamma-ray shielding properties of barium-bismuth-borosilicate glasses by using XCOM, MCNP-4C code, and experimental data. The results show that the mass attenuation coefficient at the energy 662 keV, 1173 keV, and 1332 keV has increased when adding the concentration of bismuth oxide, and a good agreement between theoretical value and experiment data. The half value layer and mean free path decreases with the increasing of bismuth oxide in the mol%. While the effective atomic number and electron density are increase with the adding of bismuth oxide in the glass system. In addition, the value of gamma-ray shielding parameter is higher than ordinary concrete and barite concrete. In 2018 M. Kurudirek et al. [63] also studied the effect of bismuth oxide on gamma-ray shielding properties of high-pressure sodium lamp glass recycled. High-pressure sodium lamp glass was used instead of borosilicate glasses because the chemical composition of high-pressure sodium lamp glass is similar to the borosilicate glass system. From the results data, the mass attenuation coefficient is depending on the concentration of  $\text{Bi}_2\text{O}_3$  and photon energy. Furthermore, the adding of  $\text{Bi}_2\text{O}_3$  into the glass system are create the number of non-bridging oxygens in the glass network but they improve the gamma-ray shielding properties. In 2020 Abolfazl Khodadadi and Reza Taherian [64] reported the gamma-ray shielding properties of lead silicate glass doped with ZnO and BaO. The results show that they are increase in mass attenuation coefficient while HVL and MFP are decrease with the adding of modifier oxide (ZnO and BaO). Gamma-ray shielding properties were improved by using the adding of ZnO and BaO. it's a 8% improvement for containing ZnO in 15 mol% and 5% improvement for containing BaO in 15 mol%. In addition, in 2017 N. Chanthima et al. [65] reported the radiation shielding properties of the BaO-ZnO- $\text{B}_2\text{O}_3$  glass system. The density of the glass sample is increase with the

BaO content. They measure the mass attenuation coefficient at the photon energy in the range of 220 - 662 keV. The results show that the main interaction is Compton scattering when the photon pass-through into the glass samples. HVL were decreased with the BaO content. Besides, HVL at the 20% of BaO is better than hematite-serpentine, ilmenite-limonite, basalt-magnetite concrete. Moreover, in 2014 S. Kaewjaeng et al. [66] studied the optical, structural and radiation shielding properties of barium oxides in  $\text{SiO}_2 - \text{B}_2\text{O}_3 - \text{Al}_2\text{O}_3 - \text{CaO} - \text{Na}_2\text{O}$  glasses system. From the results, it was found that it was found that half value layer has decrease and better than the ordinary concrete and commercial window at the photon energy of 622 keV. Furthermore, the concentration of BaO are led to the dominant Compton scattering and related to the mass attenuation coefficient. And then, in 2019 O. Agar et al. [67] studied the radiation shielding properties of BaO and  $\text{MoO}_3$  on  $\text{P}_2\text{O}_5$  based glasses by using MCNPX code. The mass attenuation coefficient decreases with the increase in photon energy. However, it is increase at 0.02 MeV because of K absorption of Mo for the sample 5 -8 and increase at 0.04 because of K absorption of Ba for the sample 1 -4. HVL and MFP is lower than the ordinary concrete and commercial window. In addition, the results are a good agreement between WinXCom program and MNCPX code.

From the literature reviews in many researches found that the glass can be used to radiation shielding material applications. Borosilicate glasses system has many advantages when compared to the silicate glasses system such as higher the density, higher reflective index, low melting point, and higher resistance to the chemical. In addition, the adding of  $\text{Bi}_2\text{O}_3$  in the borosilicate glass system can improve the radiation shielding properties because of increasing the probability of interaction. for example, HVL and MFP decrease with the concentration of  $\text{Bi}_2\text{O}_3$  in the glass system and increase with the increases in photon energy while the value of the mass attenuation coefficient increases with the concentration of  $\text{Bi}_2\text{O}_3$ . Moreover, when adding the barium oxide in the glass system can increase the probability of photoelectric effect and Compton scattering and they are non-toxic when comparison with lead oxide and bismuth oxide.

## **CHAPTER 3**

### **MATERIALS AND METHODS**

#### **3.1 Instrumentation**

In this work, structural properties, elastic properties, optical properties, and radiation properties were measured by using many instruments of Ubon Ratchathani University. The instruments for this work have below as

3.1.1 Electronic balance (Precisa d05M-200A) have the accuracy in the order of 0.0001 g.

3.1.2 Compound clay crucibles

3.1.3 Electric furnace was developed by GTEC, Physics Department, Faculty of science, Ubon Ratchathani University. The maximum temperature of electric furnace is approximately 1800 degrees Celsius.

3.1.4 Annealing furnace was developed by GTEC, Physics Department, Faculty of science, Ubon Ratchathani University.

3.1.5 Cutter machine (Herbert Arnold)

3.1.6 Polishing machine was developed by GTEC, Physics Department, Faculty of science, Ubon Ratchathani University.

3.1.7 Ultrasonic flaw detector (SONATEST: Sitiescan 230) and ultrasonic testing probe at the frequency of 4 MHz.

3.1.8 NaI(Tl) detector and isotope source ( $^{137}\text{Cs}$  and  $^{60}\text{Co}$ .) were used for this work by Nuclear Engineering, Faculty of Engineering, Chulalongkorn University.

3.1.9 Ultraviolet-visible spectrophotometer (PerkinElmer/Lambda35) at Chemistry Department, Faculty of science, Ubon Ratchathani University

3.1.10 Fourier Transform Infrared Spectrophotometer (ANTRRIS II FT-NIR Analyzer) at Scientific Instrument Center, Ubon Ratchathani University

#### **3.2 Chemical and materials**

3.2.1 High pressure sodium lamp glass

3.2.2 N-hexane 95% of purity (Fisher scientific)

3.2.3 Sodium carbonate ( $\text{NaCO}_3$ ) was used to replace sodium oxide. (Riedel-de Haën)

3.2.4 Bismuth oxide ( $\text{Bi}_2\text{O}_3$ ) 99.99% of purity (Fluka)

3.2.5 Barium oxide ( $\text{BaO}$ ) 99% of purity (Riedel-de Haën)

### **3.3 Experimental technique**

#### **3.3.1 Glass preparation**

Glass samples in  $(75-x)$  HPSg –  $(20)$   $\text{Na}_2\text{O}$  –  $5$   $\text{Bi}_2\text{O}_3$  –  $(x)$   $\text{BaO}$  glass system (where  $x$  is 0, 5, 10, 15, 20, 25, 30, and 35 mol%) are prepared by using the melt quenching technique. The high-pressure sodium lamp glass was used to instead the borosilicate glasses system because the amount of  $\text{B}_2\text{O}_3$  close to borosilicate glasses and as shown in the Table 2.1. The chemical composition was weighed using a digital balance and mixed until homogeneity in compound clay crucibles. Next, the mixture of the glass composition was heated at the temperature  $1250^\circ\text{C}$  for 4 hr. and then annealed at  $650^\circ\text{C}$  for 2 hr. and after that cool down to room temperature. The glass sample was cut and polished by using different silicon carbide grades.

#### **3.3.2 Density measurement**

In this work, the value of density was determined by using Archimedes' principle and used n-hexane as the immersion liquid (density of n-hexane is  $0.661 \text{ g/cm}^3$ ). The immersion liquid (n-hexane) was used for this work because they do not create a chemical reaction with glass samples.

#### **3.3.3 Ultrasonic velocity measurement**

The velocity of glass can be measured by pulse echo technique. The ultrasonic wave was generated from a ceramic transducer with a resonant frequency at 4 MHz and acting as a transmitter-receiver at the same time. In this work, the ultrasonic velocity detector uses two types such as normal probe for the measurement of longitudinal velocity and angle probe for the measurement of shear velocity. Elastic properties can be calculated by the ultrasonic velocity data.

### 3.3.4 UV-Vis spectroscopy

When the light pass-through the glass samples, the glass absorbs some of the light and transmitted. The intensity of the transmitted light is correlated to absorbance. Normally, the intensity absorbance was recorded in the wavelength range of 200 – 2000 nm at department of chemistry, Ubon Ratchathani University. Next, energy band gap of glass samples can be calculated by using absorbance data.

### 3.3.5 FTIR spectroscopy

Basically, the glass absorbs infrared spectra at the wavenumber approximately 400 - 600  $\text{cm}^{-1}$ . In this work, infrared spectra were measured at room temperature in the wavelength range 400–2000  $\text{cm}^{-1}$  by using a Fourier Transform infrared spectrometer from Scientific Instrument Center, Ubon Ratchathani University. The glass samples must thin enough to allow light to pass through and transparency.

### 3.3.6 Radiation measurement

In this work, we use a narrow beam transmission method for measuring the attenuation of gamma-ray. The experimental setup of the narrow beam transmission method as shown in Figure 3.1. The glass samples were placed 18 cm away from isotope source and were placed between the isotope source and radiation detector. the distance of the isotope source with the detector is 27 cm and as shown in Figure 3.1. The isotope source was enclosed in a lead container with one face a small aperture about 5 mm. The narrow beam is characterized by the scatter acceptance angle ( $\theta_{sc}$ ), which is the sum of the incident beam divergence ( $\theta_{in}$ ) and the angle subtended by exit collimation ( $\theta_{out}$ ). Figure 3.2 shows the Schematic diagram of the divergent beam. The radiation detector is a NaI(Tl) scintillation detector with a resolution of 8.5% at the energy of 622 keV and the multichannel analyzer (MCA) for the record of the pulse-height spectra of isotope sources. The energy at 622 keV, 1174 keV, and 1332 keV was emitted through by  $^{137}\text{Cs}$  and  $^{60}\text{Co}$ . When the gamma-ray pass through a glass sample, the intensity of gamma-ray is determined by the Lambert-Beer law.

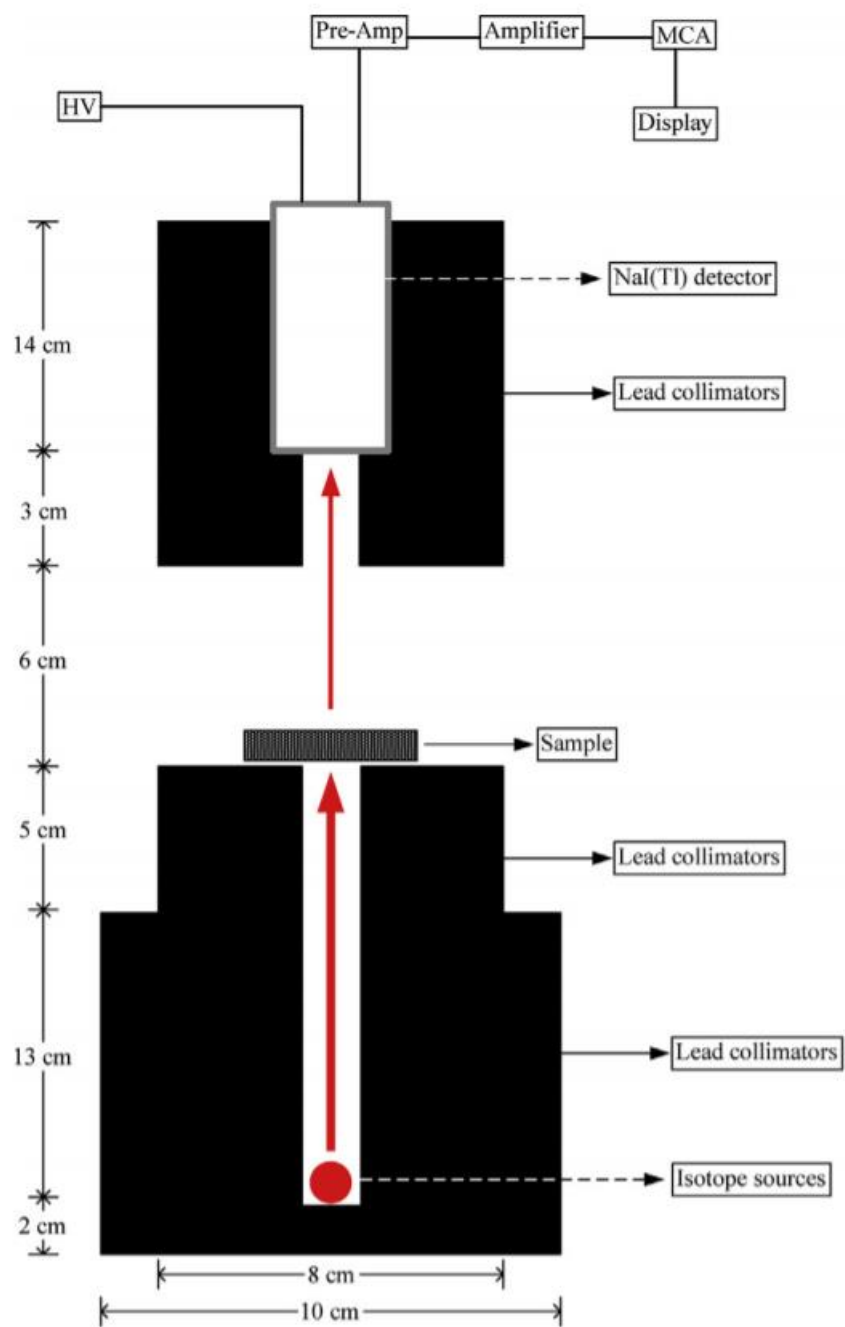


**Figure 3.1 Experimental setup of narrow beam transmission method**

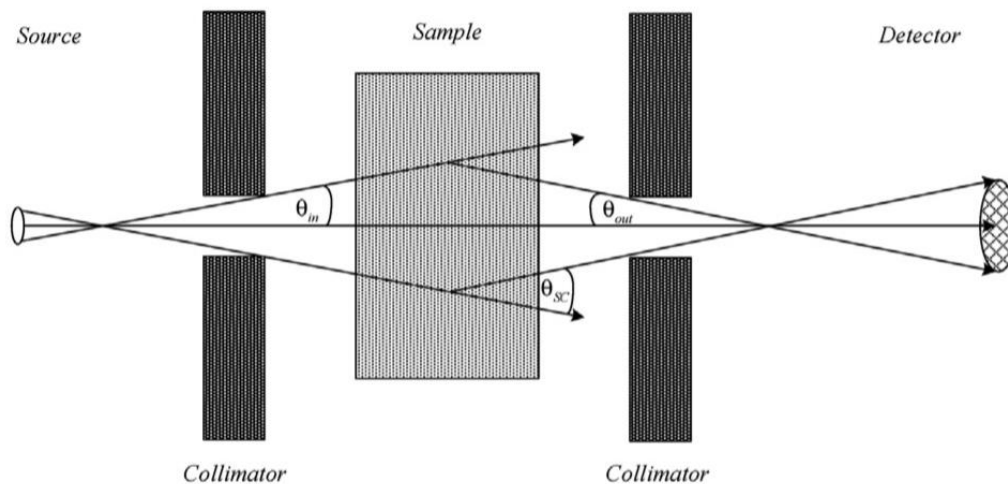


**Figure 3.2 Schematic diagram of the divergent beam**

### 3.3.7 Theoretical calculations

First, we calculate the elastic moduli of glass samples from Makishima-Mackenzie's model. Makishima-Mackenzie's theory has derived the following relationships for calculating the dissociation energy per unit volume and packing density. And in addition, dissociation energy is related to bridging oxygen in the network structure. Next, we compare elastic moduli between experimental data and theoretical value.

Second, the radiation shielding parameter can be calculated by using the WinXcom program and Fluka program. In this work, the shielding properties of the glass have been studied in three ways (narrow beam transmission method, WinXcom, and Fluka program) at the energy of 622 keV, 1174 keV, and 1332 keV. WinXcom program is used widely in radiation shielding fields and used to estimate the mass attenuation coefficient for a material composed of different elements. Moreover, Fluka program is one of the powerful ways for visualizing and understanding the attenuation of the photons pass through the glass samples and calculated at the energy of 622 keV, 1174 keV, and 1332 keV. After that, we compared the value of the shielding parameter between experimental data and theoretical data.

## CHAPTER 4

### RESULTS AND DISCUSSIONS

#### 4.1 Color of glass samples

The glass sample were prepared in  $(75-x)$  HPSg –  $(20)$  Na<sub>2</sub>O –  $5$  Bi<sub>2</sub>O<sub>3</sub> –  $(x)$  BaO (where  $x$  is 0, 5, 10, 15, 20, 25, 30 and 35 mol%) by using the melt quenching method. Chemical composition of glass samples as show in Table 4.1. The chemical composition of glass and was mixed until homogeneity. And then, the chemical composition of all glass was poured carefully into the compound clay crucible. This filled compound clay crucible is heated at the temperature 1250°C for 4 hr. and annealed at 650°C for 2 hr. Next, glass sample were cut and polished using different silicon carbide grades. The all-glasses sample is transparent, and they have a yellow-green color. We called lemon lime color and hexadecimal color code is e3ff00. This color has an approximate wavelength of 567 nm [68]. In BaO at 0 mol%, The glass sample has a clear and without bubbles inside the glass. While the color goes out towards the yellow-green color increases with the adding the concentration of BaO in the glass network because barium oxide gives a slightly green and bismuth give a light yellow. Thus, Color mixing occurs between slightly green and light yellow is leads to the yellow-green color in the glass sample and increases with adding the concentration of BaO.

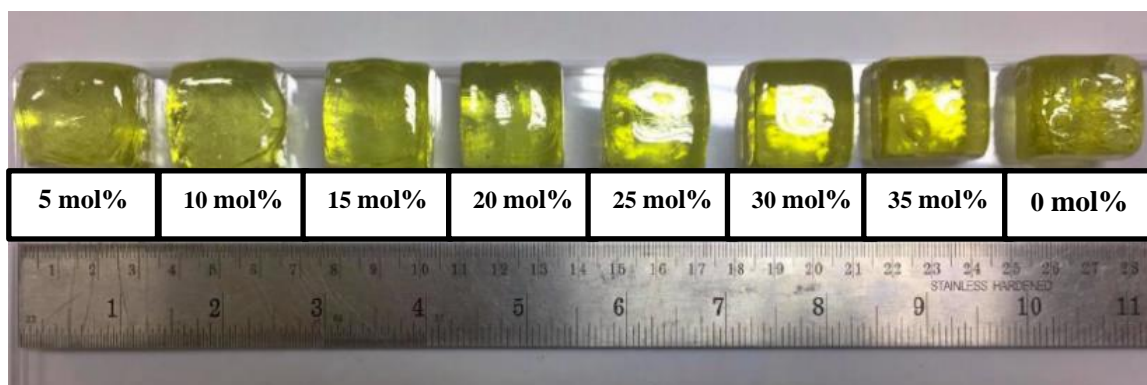


**Figure 4.1 All glass sample with different the concentration of BaO**



However, the yellow color of glass samples not generated from barium oxide, but the yellow color may be probably from bismuth oxide in the glass system. From previous research, it can be seen that the glass samples in (80)HPSg – (20)Na<sub>2</sub>O – (0)Bi<sub>2</sub>O<sub>3</sub> have a clear colorless and without bubbles inside the glass at 0 mol% of Bi<sub>2</sub>O<sub>3</sub>. When adding the bismuth oxide in the glass network is leads to the light-yellow color in the glass samples. Thus, the yellow color in glass samples was caused by bismuth oxide [91-93].

#### 4.2 Density and molar volume of glass samples

Density is one of the parameters for physical properties in this work. Density is a characteristic property of a material and related to the mass of atoms, their size, and how they are arranged to determine the density of a material. In this work, the density of glass can be calculated by using Archimedes' principle and used n-hexane as the immersion liquid (density of n-hexane is 0.661 g/cm<sup>3</sup>). The value of density and molar volume as shown in Figure 4.2. It can be seen that the value of density increases from 3.23 g/cm<sup>3</sup> to 3.67 g/cm<sup>3</sup>. Because barium oxide (BaO) has a high molecular weight more than silica (SiO<sub>2</sub>) in HPSg and high molecular compared to the other compounds added all together. The molecular weight is 153.3 g/mol and 60.09 g/mol of BaO and SiO<sub>2</sub>, respectively [69-70]. Furthermore, the density was greatly increased from the previous research. In previous research, when not filled the barium oxide, we vary the concentration of bismuth oxide in the glass system from 0 - 5 mol% of bismuth oxide. The chemical composition of glass in previous research is shows in Table 4.2. The value of density increases from 2.54 to 3.22 g/cm<sup>3</sup> with the increase of concentration of bismuth oxide in glass systems. It is known that adding a higher atomic number of the element into a glass system leads to an increase in the density of glass. Thus, the density increased are due to the concentration of bismuth oxide, and also added from barium oxide. The density of glass can be identified as structural alterations in the network structure. The value of density and molar volume of the previous research as show in Table 4.4.

When we are adding barium oxide in the base glass, the molar volume of glass samples is increase from 27.57 cm<sup>3</sup>/mol to 32.04 cm<sup>3</sup>/mol with increasing of BaO content in the glass system. According to Shelby reported that molar volume depends on the ionic radius of the modifier [19]. It is due to the ionic radius of the modifier in the network structure of glass. Ionic radius of Ba<sup>2+</sup> larger than Si<sup>4+</sup>, Bi<sup>3+</sup> and Na<sup>+</sup>. The

ionic radius of  $\text{Ba}^{2+}$ ,  $\text{Si}^{4+}$ ,  $\text{Bi}^{3+}$  and  $\text{Na}^{+}$  are 1.35 Å, 0.40 Å, 1.03 Å and 1.02 Å , respectively [71-72]. In addition, the increase in molar volume led to an increase in the interstitial size of network structure and decrease in compactness of glass network with increasing the concentration of BaO [73-75].

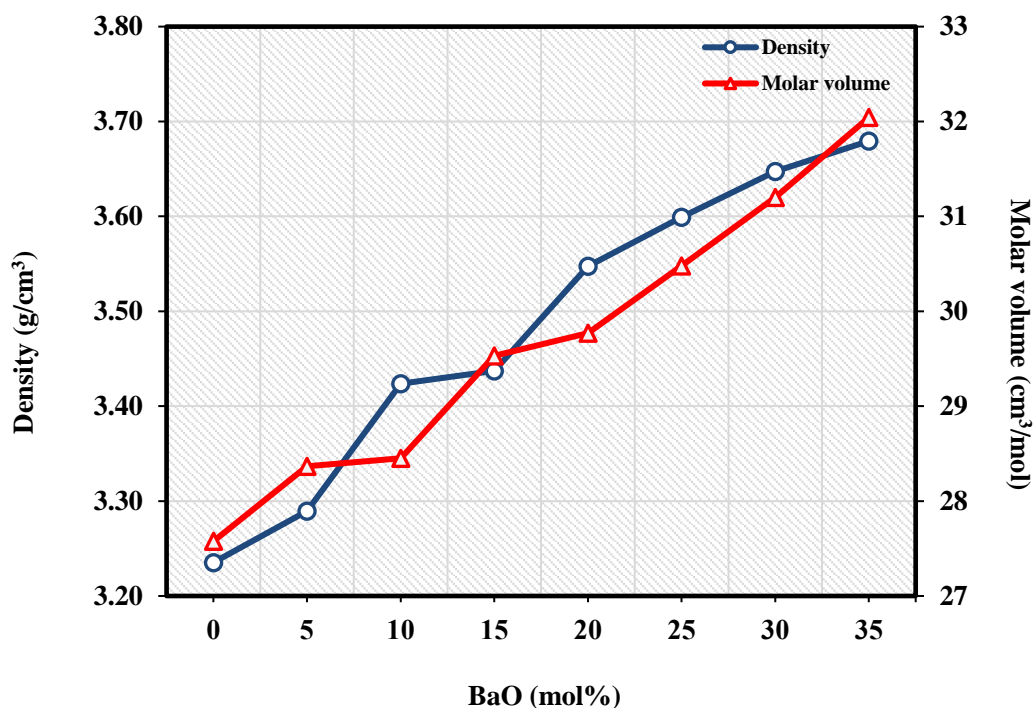


**Figure 4.2** Density and molar volume of glass samples as a function of BaO contents

**Table 4.1** The chemical composition of all glass sample

Glass samples	Composition of glass (mol%)			
	HPSg	Na <sub>2</sub> O	Bi <sub>2</sub> O <sub>3</sub>	BaO
S1	75	20	5	-
S2	70	20	5	5
S3	65	20	5	10
S4	60	20	5	15
S5	55	20	5	20
S6	50	20	5	25
S7	45	20	5	30
S8	40	20	5	35

**Table 4.2 The chemical composition of all glass sample in the previous research**

Glass samples	Composition of glass (mol%)			
	HPSg	Na <sub>2</sub> O	Bi <sub>2</sub> O <sub>3</sub>	BaO
S-0	80	20	0	-
S-1	79	20	1	-
S-2	78	20	2	-
S-3	77	20	3	-
S-4	76	20	4	-
S-5	75	20	5	-

### 4.3 Physical properties of glass

The physical properties of glass such as ion concentration, polaron radius, interatomic distance and field strength can be calculated by using the value of density and related to the concentration of dopants in the glass system. The value of the physical properties of the glass sample is given in Table 4.3. The ion concentration of the dopant is an important parameter that influences the glass base has been determined by using eq. (7-10). Ion concentration is related to the average molecular weight of glass system, the density of glass and mole fraction of dopant. A considerable increase in the ion concentration with the increase of BaO concentration may be due to an increase in the density of glass with increasing the concentration of BaO in the glass system. For S1, we did not calculate physical properties because S1 is base glass in this work and non-doped barium oxide. Hence, there is no value of the ion concentration. However, Polaron radius and interatomic distance are found to decrease with the concentration of BaO. In fact, the decrease in packing density was supported by the decrease in Polaron radius and interatomic distance. This result shows that the Ba<sup>2+</sup> ions are spread within the increase in glass network and the decrease in interatomic distance will lead to strong field strength in network structure [69,70,76]. In addition, the increase in field strength is due to the occurrence of strong link between the Ba<sup>2+</sup> and B<sup>-</sup> ions.

**Table 4.3 Ion concentration, Polaron radius, interatomic distance, and field strength as a function of BaO in glass system**

Glass samples	Physical properties			
	Ion concentration ( $\times 10^{21}$ ion/cm <sup>3</sup> )	Polaron radius ( $\times 10^{-8}$ Å)	Interatomic distance ( $\times 10^{-8}$ Å)	Field strength ( $\times 10^{16}$ cm <sup>2</sup> )
S1	-	-	-	-
S2	0.634	4.688	11.634	0.091
S3	1.212	3.778	9.378	0.140
S4	1.682	3.388	8.408	0.174
S5	2.138	3.127	7.761	0.204
S6	2.513	2.963	7.355	0.227
S7	2.840	2.845	7.061	0.247
S8	3.114	2.759	6.847	0.262

#### 4.4 Elastic properties

##### 4.4.1 Ultrasonic measurement

The ultrasonic wave was generated from a ceramic transducer with a resonant frequency at 4 MHz and acting as a transmitter-receiver at the same time. Bismuth oxide 5 mol% in the glass sample for previous work is the glass base (BaO 0 mol%) for this work, and then we add the concentration of barium oxide 5–35 mol% into the glass system. From the previous research, the longitudinal velocities of 0 mol% of bismuth oxide are 6109 m/s and decrease with the increase in the concentration of bismuth oxide. The value of longitudinal velocity in this work and previous work at S-5 (base glass for this work) is 5300 m/s and 5255 m/s respectively. this result is the same value for longitudinal velocity. In this work, the variation of longitudinal and shear velocity for this work as shown in Figure 4.3. It is observed that both velocity of glass samples has a tendency to decrease continuously with the concentration of BaO. The concentration of BaO filled in the glass network leads to a decrease in the longitudinal velocity and decreases more than the previous work. The longitudinal velocities of glass samples were decreased from 5300 m/s to 5004 m/s and shear velocities were decreased from

3282 m/s to 2859 m/s. It is observed that the barium oxide added leads to a decrease in shear velocity. In addition, the changes in ultrasonic velocities have related to the structure of glass and related to the number of non-bridging oxygens (NBOs). These results show that the number of non-bridging oxygens was increased in the network structure of glass with the concentration of BaO. Thus, the increase in the number of non-bridging oxygens is responsible for decreasing the connectivity of the glass network because  $BO_3$  structural units were broken and converted into  $BO_4$  units. It is well known that the amount of  $BO_3$  units in their structure is normally used to produce strong glasses and pursuing an equilibrium reaction  $BO_3 \leftrightarrow BO_4 + NBO$ .

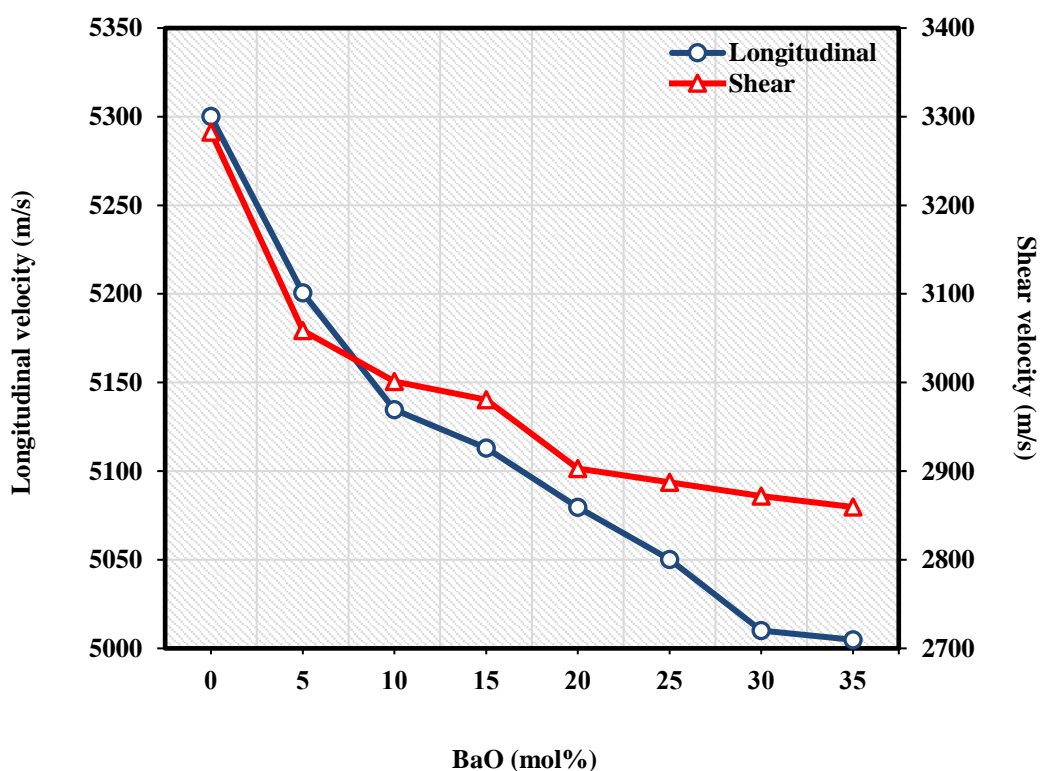
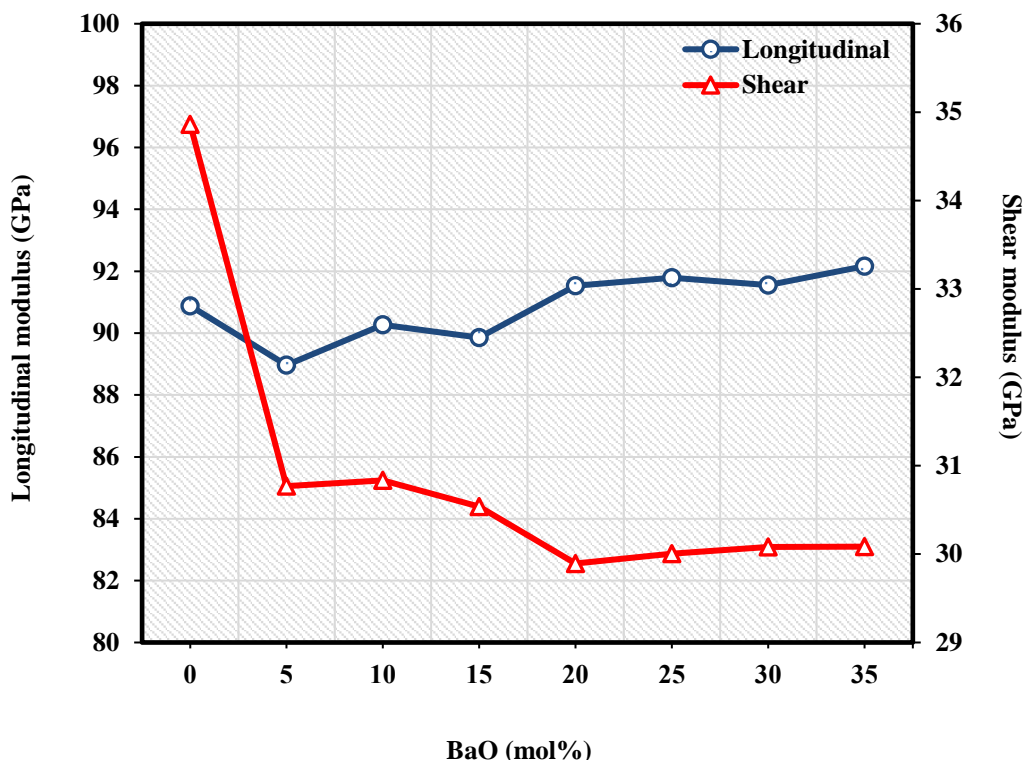


Figure 4.3 Longitudinal and shear velocity as a function of BaO contents

**Table 4.4 Density, molar volume, longitudinal velocity, and shear velocity as a function of Bi<sub>2</sub>O<sub>3</sub> in glass system for the previous research**

<b>Samples</b>	<b>Density (g/cm<sup>3</sup>)</b>	<b>Molar volume (cm<sup>3</sup>/mol)</b>	<b>Longitudinal velocity (m/s)</b>
S-0	2.5423	27.3321	6109
S-1	2.6758	27.4431	6027
S-2	2.8542	27.1101	5991
S-3	2.9759	27.3273	5548
S-4	3.1112	27.4071	5326
S-5	3.2352	27.5762	5255

Elastic moduli can be determined by using ultrasonic velocity data. Elastic properties such as longitudinal modulus, shear modulus, Bulk modulus, Young's modulus, Poisson's ratio, micro-hardness, softening temperature, and Debye temperature are extremely sensitive to any structural changes in the glass network. Figure 4.4 present the variation of longitudinal and shear modulus with different percentage of BaO mol%. The value of longitudinal modulus was decreased at 5 mol% of BaO from 90.88 GPa to 88.96 GPa and will continue increasing at 10 - 35 mol% from 90.26 GPa to 92.16 GPa. While the value of shear modulus was continually decreasing from 34.85 GPa to 30.08 GPa. This result due to the value of longitudinal modulus and shear modulus is depended on the density of glass and ultrasonic velocities of glass and supported by FTIR spectra in Figure 4.9. The obvious decrease in shear modulus is due to a decrease in the rigidity of glass samples. This result indicate that the cross-link density is decrease in network structure of glass and related to Poisson's ratio in Figure 4.7. Figure 4.5 Show the value of Young's modulus and bulk modulus with the concentration of BaO. The value of Young's modulus is associated with the difference in chemical bond and the bond strength in the glass network [77]. The value of Young's modulus changes from 82 GPa to 75 GPa. While the value of bulk modulus was increase from 64 GPa to 69 GPa with increasing of the concentration of BaO in the glass system.



**Figure 4.4 Longitudinal and shear modulus as a function of BaO contents**

The decrease in Young's modulus is due to the decrease in the value of ultrasonic velocities of glass and the change in the presence of large number of covalent bonds. These lead to less resistance to withstand changes in length when under lengthwise tension or compression. In addition, Young's modulus can be accounted for the change in the rigidity of the glass network, and it also related to the change in non-bridging oxygens in the glass network. Firstly, the decrease in Young's modulus with the increase of the concentration BaO is due to a decrease in longitudinal velocity and shear velocity. Secondly, Young's modulus decreased with the increase of the concentration BaO showed that the formation of the number of non-bridging oxygen (NBOs) was created in the glass structure. The number of non-bridging oxygen (NBOs) created in the glass structure is built from barium ions and bismuth ions filled in the glass system. In the last, the adding of barium oxide and bismuth oxide in the glass system is leads to a decrease in the average strength of the bond. These results show that the strength of glass decrease with the adding of BaO and  $\text{Bi}_2\text{O}_3$  in the glass network.

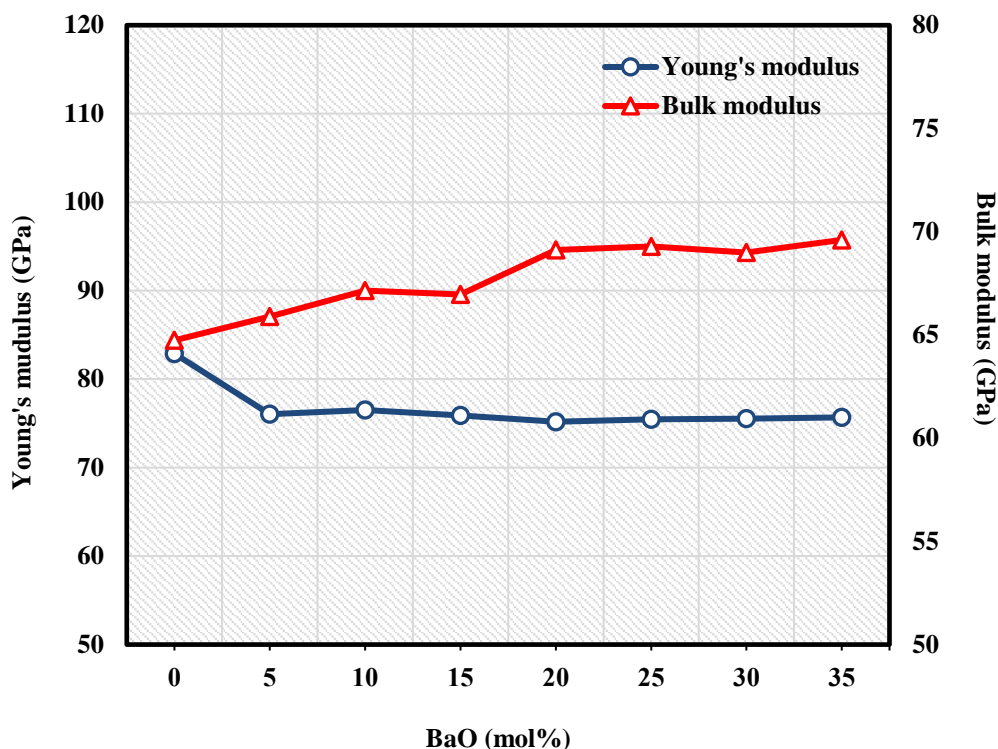


**Figure 4.5 Young's modulus and bulk modulus as a function of BaO contents**

The change in Bulk modulus has related to the change in the cross-linkage coordination of the glass network and bond stretching force constant [78]. Figure 4.6 are show the variation of softening temperature and Debye temperature with the concentration of BaO in the glass system. The value of softening temperature is indicating that the maximum temperature of glass before it permanently deforms. When we are adding BaO in the glass system, softening temperature decrease from 586 K to 520 K with the concentration of BaO in the glass system. This may be probably from the amount of barium oxide increased because the melting point of barium and bismuth is 730 and 271.3 degrees Celsius, respectively.

The value of Debye temperature is decrease from 906 K to 644 K with the concentration of BaO. It is known that Debye temperature represents the temperature at which all the low frequency atomic vibrational modes are excited. These results showed that the rigidity of the glass network was decreased and created the number of non-bridging oxygen (NBOs) in the glass network. Poisson's ratio is shown in Figure 4.6. Poisson's ratio is defined for any structure as the ratio of lateral to longitudinal strain produced when tensile forces are applied. Normally, the tensile strain created in the



glass network is affected by cross-links while the lateral strain greatly increases with decreasing the cross-link density. The value of Poisson's ratio varies from 0.18 to 0.25 with increasing the concentration of BaO in glass systems. As you can see in Table 4.5 found that Poisson's ratio changes from 0.188 to 0.235 when adding the concentration of BaO at 5 mol%. the large change of Poisson's ratio due to the greatly decrease in longitudinal and shear modulus from 0 mol% to 5 mol% of BaO. These results indicated that the number of non-bridging oxygens is created in the glass network and cross-links decreased with the increasing of BaO in the glass system. Moreover, the increase in number of non-bridging oxygens led to the open structure of glass and it indicates the glass structure is weak [79].

**Table 4.5 Experimental elastic moduli of glass samples**

Samples	<b>E</b> (GPa)	<b>K</b> (GPa)	<b><math>\sigma</math></b>	<b>H</b> (GPa)	<b><math>T_s</math></b> (K)	<b><math>\theta_D</math></b> (K)	<b><math>C_v</math></b> (J · mol <sup>-1</sup> K <sup>-1</sup> )
S1	82.88	64.73	0.188	7.23	584.33	906.87	68.971
S2	76.04	65.88	0.235	5.42	515.85	828.73	90.381
S2	76.50	67.13	0.240	5.33	504.98	796.71	101.726
S4	75.89	66.95	0.242	5.24	511.59	764.96	114.903
S5	75.18	69.11	0.257	4.83	492.89	728.20	133.246
S6	75.44	69.29	0.257	4.85	496.03	700.71	149.524
S7	75.52	68.99	0.255	4.90	505.36	672.72	168.990
S8	75.67	69.60	0.257	4.86	508.33	644.86	191.836

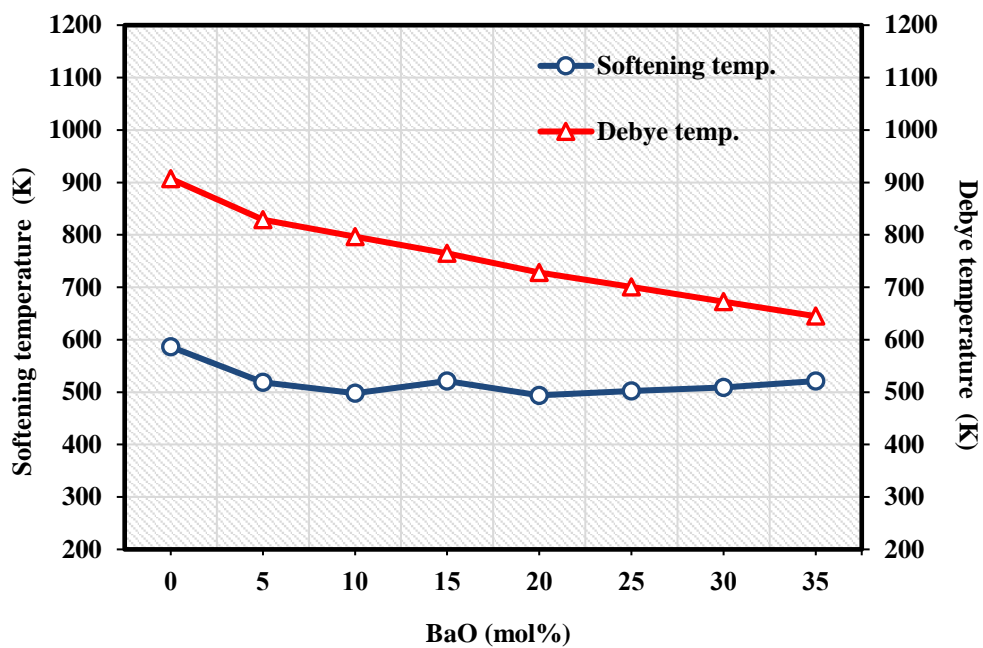


**Figure 4.6** Softening temperature and Debye temperature as a function of BaO contents

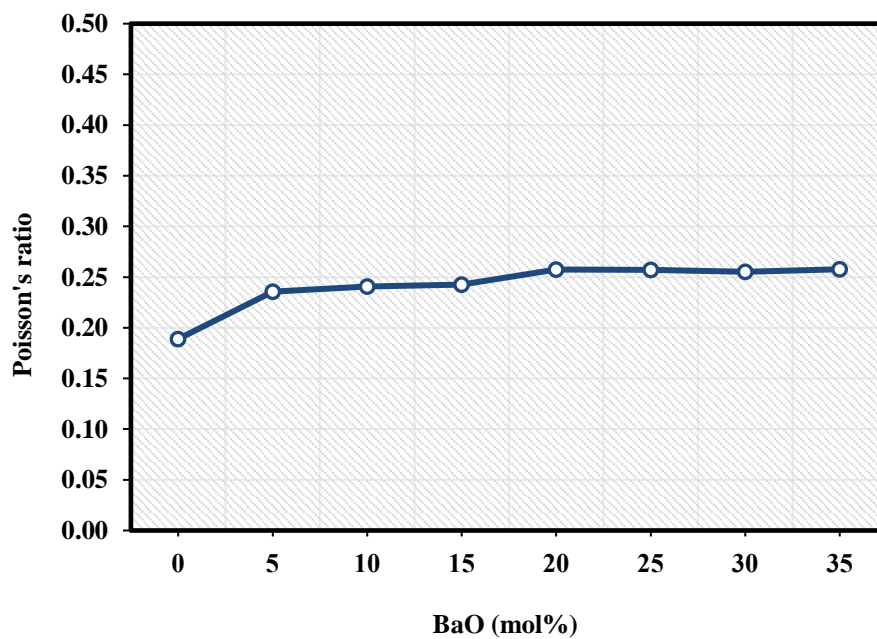


**Figure 4.7** Poisson's ratio as a function of BaO contents

Figure 4.8 describe the variation of microhardness as a function of BaO contents. Microhardness is the hardness of the material exposed to low applied loads and indicates that the resistance offered by the material to permanent indentation. It also decreases from 7.23 GPa to 8.46 GPa like the decrease in elastic moduli which indicates the elasticity of glass structure, and this may be due to the introduction of weak bonding. The decrease in microhardness indicates that the glass samples have decreasing in resistance to downforce. The formation of non-bridging oxygens and elastic moduli may be responsible for the behavior of the influence of BaO at higher concentrations.

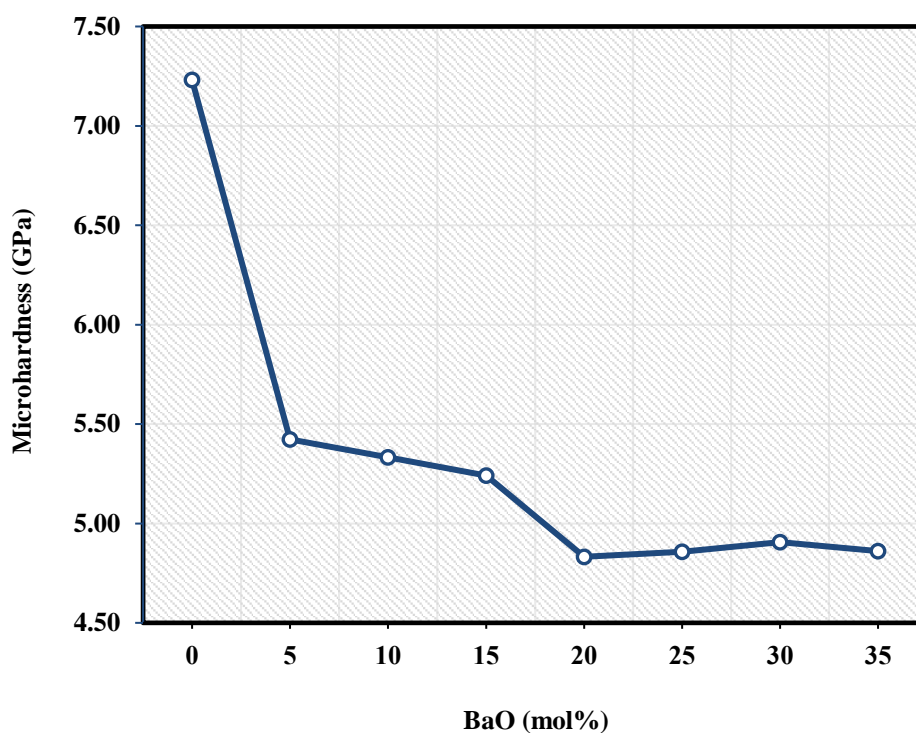


**Figure 4.8 Micro-hardness as a function of BaO contents**

Moreover, the elastic moduli result from the ultrasonic measurement compared with the elastic moduli calculation by Makishima-Mackenzie's model. The experimental elastic moduli of the glass sample are show in Table 4.1 and the theoretical elastic moduli of the glass sample as show in Table 4.2. In Figure 4.9, it can be observed that longitudinal modulus has a small change for experimental data. They decrease at 5 mol% of BaO and then, they increase at 10 - 35 mol% of BaO from 90.26 - 92.16 GPa. In theoretical calculation, the tendency of longitudinal modulus has decreased with the

concentration of BaO from 88.67 - 59.75 GPa. For shear modulus, the shear modulus of theoretical and experimental data has decreased all together with an increase in the concentration of BaO and as shows in Figure 4.10. They are a good agreement for theoretical value and experimental data. Young's modulus is present in Figure 4.11 and is decrease in theoretical and experimental data and has a value more than the theoretical value. This result shows that the barium ions have an influence on the structure of glass more than predicted from the theoretical calculation. Basically, the Young's modulus tends to increase with increasing connectivity of the glass structure. However, the value of Young's modulus decreases resulting in the reduced strength of the glass network and converting bridging oxygen (BO) atoms into non-bridging oxygen (NBO). For bulk modulus in Figure 4.12, the experimental data is an increase from 64.73 to 69.60 GPa with the increase in the concentration of BaO. But the theoretical value is decrease from 49.64 to 34.14 GPa with the adding of concentration of BaO. This may be attribute to fact that barium ions added to the glass network are an enhancement of the glass samples under pressure on all surfaces. Poisson's ratio is shows in Figure 4.13. In general, Poisson's ratio is in the range between 0 and 0.5 and related to the change in the term of cross-link density of the glass network. For example, the value of Poisson's ratio in a range between 0.1 - 0.2 has a high cross-link density. whereas high Poisson's ratio, such as 0.3 - 0.5, indicates the low cross-link density in the glass structure. In experimental data, Poisson's ratio is increasing as a function of BaO in the glass network. But Poisson's ratio of the theoretical value has a decrease with the concentration of BaO. When we compare Poisson's ratio between theoretical and experimental data, we found that the glass samples have a decrease in cross-link density more than the prediction of Poisson's ratio. These results indicate that the structure of glass has become less compact as tetrahedral coordination of boron with the concentration of BaO. However, the elastic moduli are different between experimental data and the theoretical value because the bonds of glass structure are destroyed by barium ions. Their bonds might have lower dissociation energy that was not considered in the theoretical calculation.

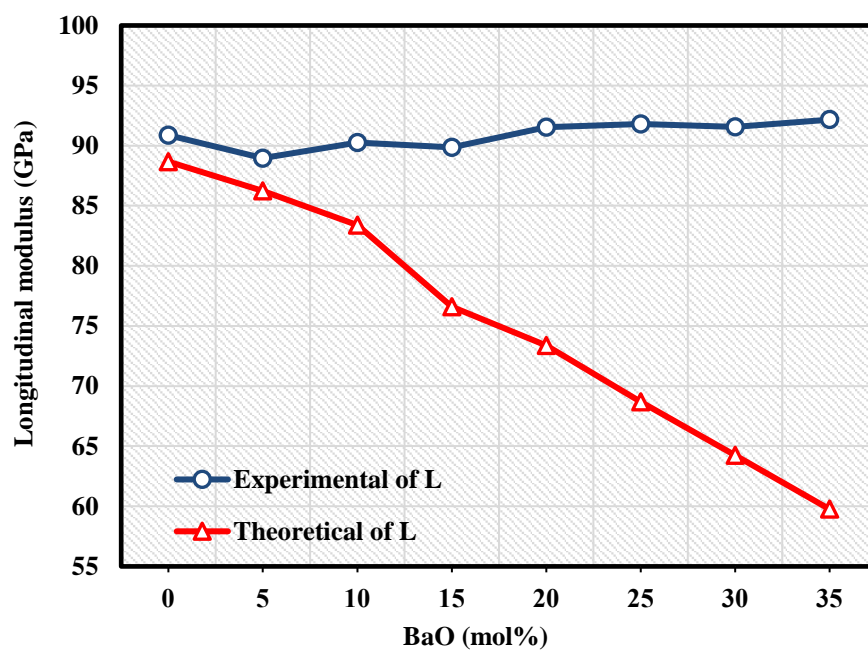


Figure 4.9 Longitudinal modulus compare with theoretical and experimental data

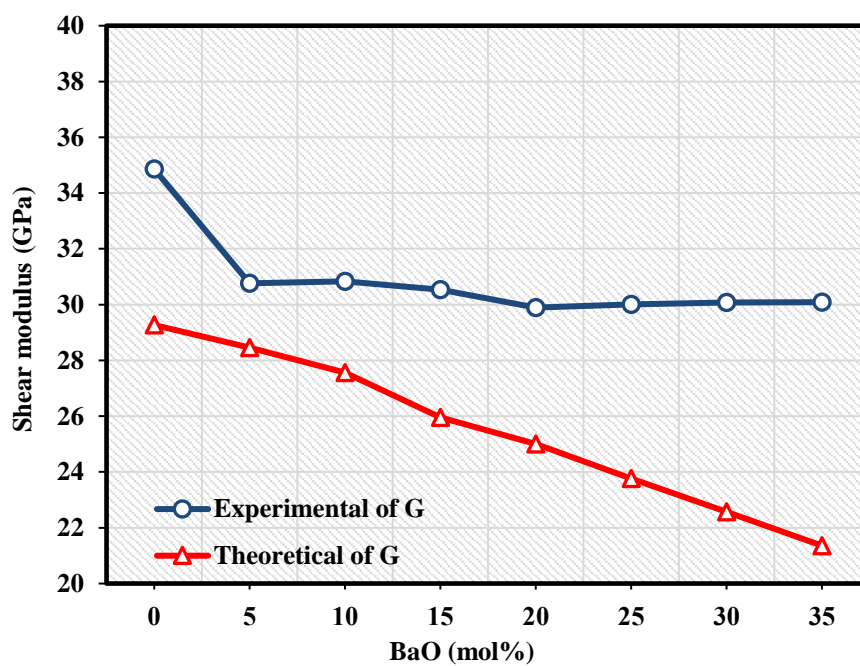


Figure 4.10 Shear modulus compare with theoretical and experimental data

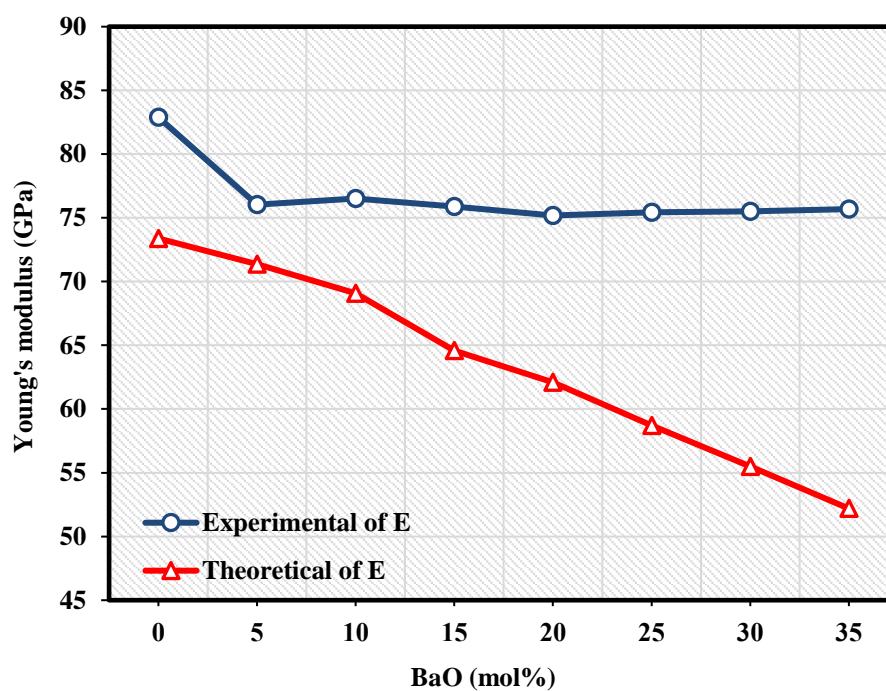


Figure 4.11 Young's modulus compare with theoretical and experimental data

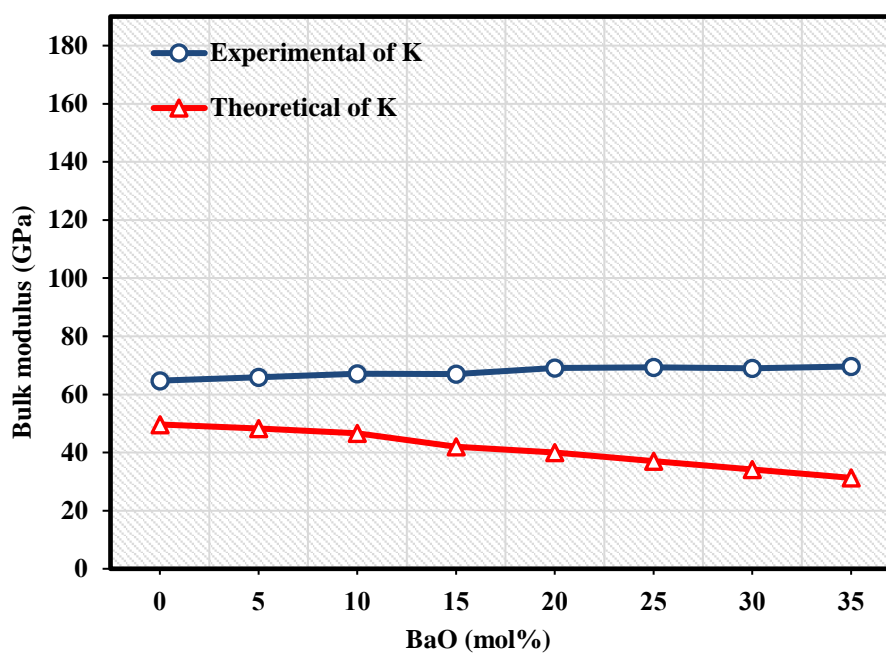


Figure 4.12 Bulk modulus compare with theoretical and experimental data

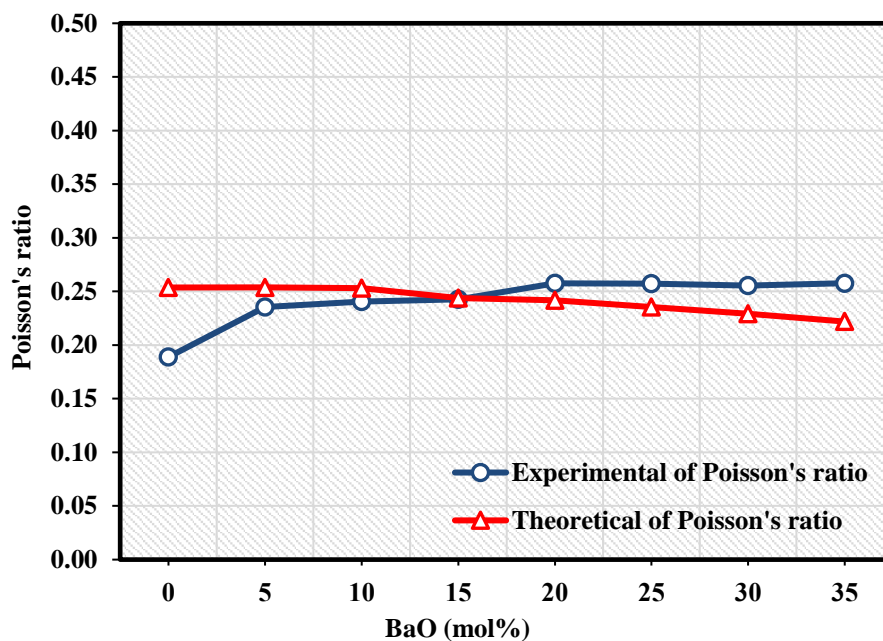


Figure 4.13 Poisson's ratio compare with theoretical and experimental data

Table 4.6 Experimental elastic moduli of glass samples

Samples	$L_{ex}$ (GPa)	$G_{ex}$ (GPa)	$E_{ex}$ (GPa)	$K_{ex}$ (GPa)	$H_{ex}$ (GPa)	$\sigma_{ex}$
S1	90.88	34.85	82.88	64.73	7.23	0.188
S2	88.96	30.77	76.04	65.88	5.42	0.235
S3	90.26	30.83	76.50	67.13	5.33	0.240
S4	89.85	30.53	75.89	66.95	5.24	0.242
S5	91.54	29.89	75.18	69.11	4.83	0.257
S6	91.79	30.00	75.44	69.29	4.85	0.257
S7	91.55	30.07	75.52	68.99	4.90	0.253
S8	92.16	30.08	75.67	69.60	4.86	0.257

**Table 4.7 Theoretical elastic moduli of glass samples**

Samples	$L_{th}$ (GPa)	$G_{th}$ (GPa)	$E_{th}$ (GPa)	$K_{th}$ (GPa)	$\sigma_{th}$
S1	88.67	29.26	73.38	49.64	0.2536
S2	86.25	28.45	71.35	48.30	0.2538
S3	83.38	27.56	69.08	46.63	0.2534
S4	76.60	25.96	64.57	41.99	0.2437
S5	73.38	25.00	62.08	40.05	0.2416
S6	68.67	23.76	58.71	36.99	0.2354
S7	64.23	22.56	55.47	34.14	0.2292
S8	59.75	21.35	52.19	31.27	0.2219

#### 4.5 Infrared spectral studies

FTIR spectroscopy is one of the techniques used to explain the glass structure and give the data about the vibrational modes of the molecules present in the amorphous system. The FTIR spectra of glass system as shown in Figure 4.9. The spectra were recorded in the wavenumber range of 400 - 2000  $\text{cm}^{-1}$ . Although, Figure 4.9 are shown in the range 400 - 1200  $\text{cm}^{-1}$  because of the vibrational modes of glass network is absorb in the range 400 - 1000  $\text{cm}^{-1}$ . The peak at 500  $\text{cm}^{-1}$  correspond to the formation of Ba-O bonds. The band at 470 – 480  $\text{cm}^{-1}$  reveals that the vibration of Si-O-Si and Bi-O bending vibrations in  $\text{BiO}_3$  pyramidal units. The absorption peak appearing at 620  $\text{cm}^{-1}$  have been assigned to B-O-Si stretching, Si-O-Si and O-Si-O bending. In addition, the absorption peak at 610  $\text{cm}^{-1}$  is attributed either to cationic vibrations in network and various modes of Bi-O vibration in  $\text{BiO}_6$ . The band around 700 – 710  $\text{cm}^{-1}$  represent the bending vibration of bridging oxygen between trigonal  $\text{BO}_3$  groups. The signal at approximately 780  $\text{cm}^{-1}$  is Si-O-Si stretching of  $\text{SiO}_4$  units, oxygen bridging between tetrahedral and trigonal boron. The peak in the region of 900  $\text{cm}^{-1}$  and 950  $\text{cm}^{-1}$  reveals that the vibration of B-O stretching in  $\text{BO}_4$  tetrahedra and asymmetric stretching vibrations of O-Si-O in SiO with two bridging oxygen. The broad absorption band at approximately 1010 – 1020  $\text{cm}^{-1}$  can be assigned to Si-O-Si and B-O-B stretching vibration. The signal at around 1050  $\text{cm}^{-1}$  is assigned to curve vibration of O-Si-O



stretching modes [80-82]. It can be observed from Figure 4.9, the glass sample at 0 mol% of BaO absorbs infrared in the wavenumber range of 480, 500, 540, 620, 640, 720, 900, 940, and 1000  $\text{cm}^{-1}$ . When we adding barium oxide at 5 mol% found that the glass sample absorbs a decrease in the wavenumber range of 620-640  $\text{cm}^{-1}$ . This means it absorbs the functional group of Si-O-Si decreased lead to the creation of non-bridging oxygens in the glass structure. in addition, these results relate to the longitudinal modulus decreased at 5 mol% of BaO. Next, at 10 mol% of BaO, the glass sample strongly absorbs in a wavenumber range of 620-640  $\text{cm}^{-1}$ . This result explains the creation of bridging oxygen in the glass structure because of Si-O-Si bonds and B-O-Si bonds increased. And then, the absorption bands decrease at 15 mol% of BaO in the wavenumber range of 620-640  $\text{cm}^{-1}$  lead to the value of longitudinal modulus decrease at 15 mol% of BaO. This result indicates that barium ions destroy the glass structure at 15 mol% of BaO. At 30 mol% of BaO, we found that the vibrational mode of  $\text{BO}_4$  is strongly absorbed in the wavenumber range of 940  $\text{cm}^{-1}$ . It leads to creation of the formation of non-bridging oxygen in the glass network. IR absorption spectra of glass are related to network bonds in glass structure. These results are due to the modifier oxide maybe destroy the network structure of glass and non-bridging oxygens are created in glass structure. In addition, the results are led to the change in structure of glass and elastic properties of glass. In this work, structural properties were studied by FTIR spectroscopy because these techniques can explain molecular vibrations of the functional group and the quantity of the functional group in glass samples. If the decrease in the absorption from the reference sample can indicate the bonds in the network decreased. If the absorption increased of a functional group from the reference sample reveal the bridging bonds increased. This can support the results from ultrasonic velocity measurement and confirm the results of elastic properties.

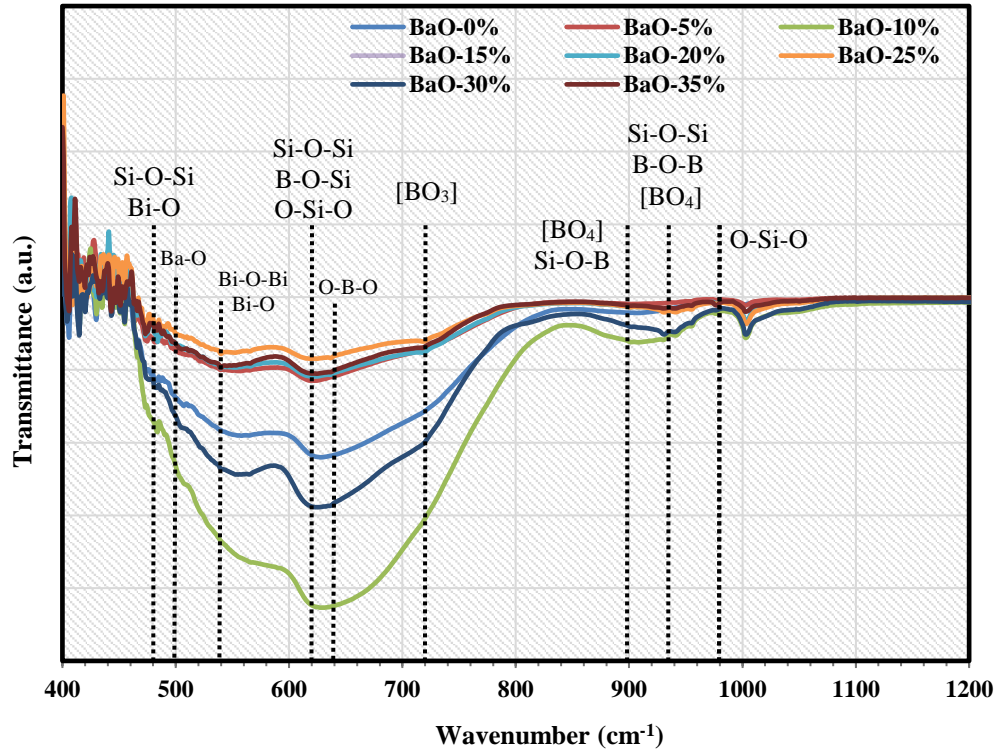


**Figure 4.14 The IR spectra of (75-x) HPSg – (20) Na<sub>2</sub>O – 5 Bi<sub>2</sub>O<sub>3</sub> – (x) BaO glass system**

## 4.6 Optical properties

### 4.6.1 Optical band gap

UV-Vis spectroscopy is a useful tool for studying the structural and optical properties of the glass. Visible light and ultraviolet optical absorption spectra were recorded for the glass samples in the wavelength region 200 - 1100 nm. The absorption spectra of the present glass system were plotted in Figure 4.15. As you can see in Figure 4.15, All glass sample is less absorbing the visible light at around 400 nm or transmit the visible light increases. This result leads to the transparency of glass samples. Optical band gap can be calculated from the absorption spectra data of glass samples by Mott and Davis relation [83]. The spectra consist of one transition bands which centered in the range 420 - 480 nm. Commonly, the optical band gap is presented in terms of direct band gap and indirect band gap. The value of optical band gap can be determined from the linear part of the curves extrapolating at  $(\alpha\hbar\omega)^2 = 0$  for direct band gap and  $(\alpha\hbar\omega)^{1/2} = 0$  for indirect band gap [84]. Figure 4.16 and Figure 4.17 are shown the graph for calculating the direct and indirect band gap, respectively. The value of direct

and indirect band gap lies in range 3.15 to 2.70 eV and 2.60 to 2.70 eV, respectively and collected in Table 4.8. Direct band gap decreases due to barium ions create the donor state between the valence band and conduction band. These results indicate that an electron can be easy to travel when barium ions increased in the glass network. An indirect band gap is a slight increase due to the addition of barium oxide. However, the value of indirect band gap has a tendency not to significant change. Thus, barium ions have an effect to direct band gap more than indirect band gap. It is known that the change in the optical band gap can be described by the change of network structure in the glass system. It is due to the increase of the number of non-bridging oxygens and bonding defects. It may be possible that BaO creates more  $\text{BO}_4$  units in the glass network.

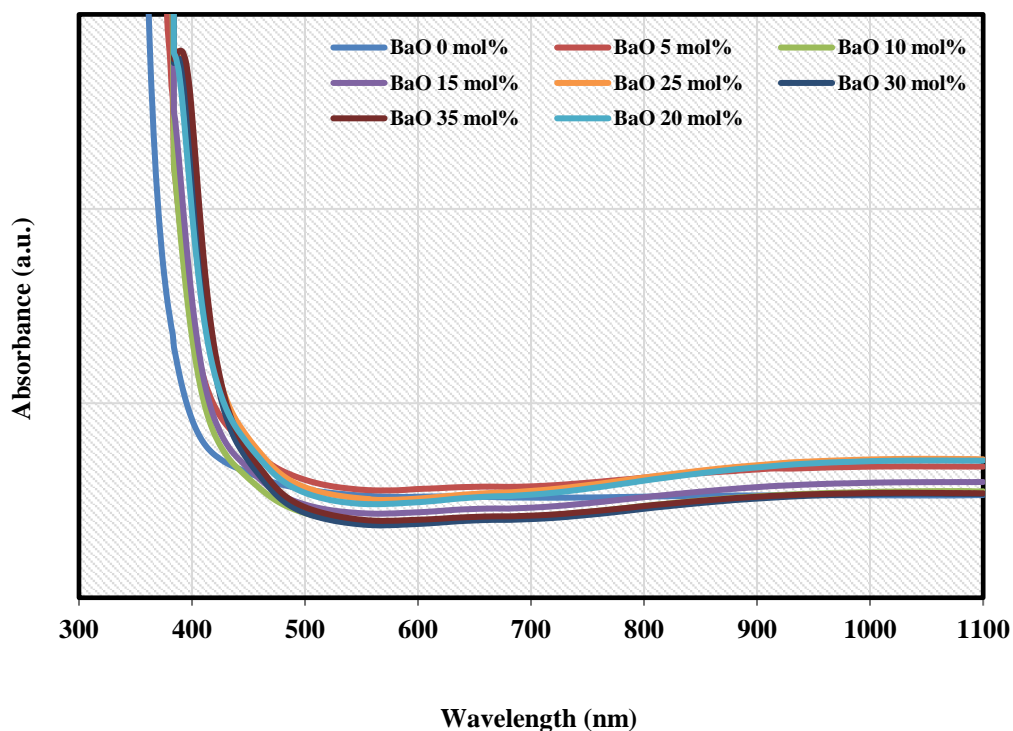


**Figure 4.15** Absorption spectra as a function of wavelength

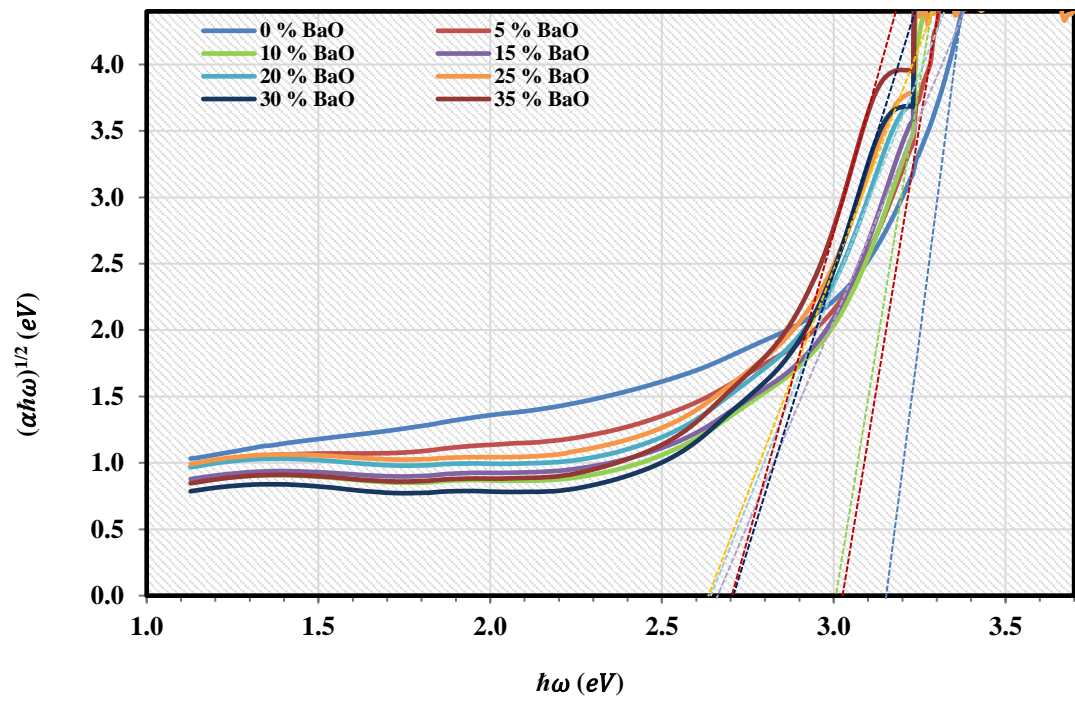


Figure 4.16 Direct band gap of glass samples

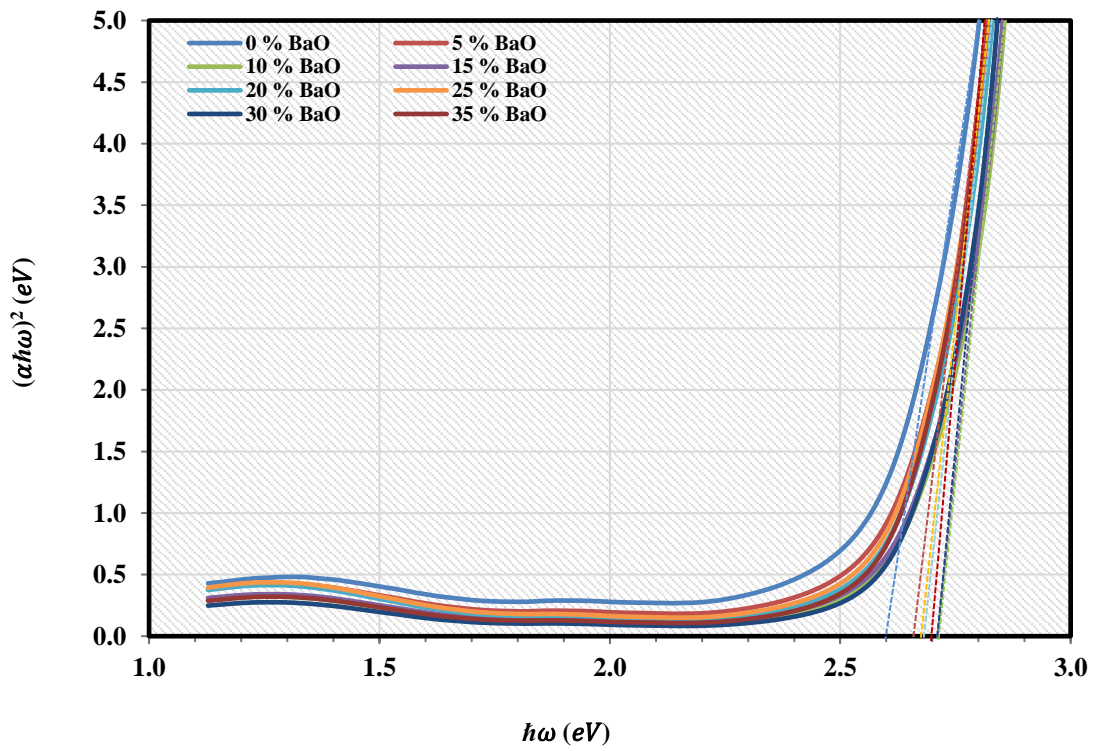


Figure 4.17 Indirect band gap of glass samples

### 4.6.2 Optical parameters

The optical properties such as refractive index, dielectric constant, optical dielectric constant, reflection loss, molar refractivity, metallization, and molar polarizability can be calculated from the value of the energy band gap and as shown in Table 4.8. The refractive index is an important parameter in optical properties of the glass [19]. It is known that the percentage of incident light undergoes reflection depends on the refractive index of the medium, and the incident light that is refracted undergoes a change in velocity of light. In this work, we calculate the refractive index of glass from the indirect band gap because the graph in Figure 4.17 has a value of R-squared close to 1 more than the direct band gap in Figure 4.16. The value of the refractive index of the glass sample decreases from 2.12 to 2.10 with the adding concentration of BaO. The slight difference in the refractive index indicates that barium ions hardly affect to the refractive index because the glass sample is good transparency. Moreover, the value of refractive index is related to determinant like polarizability and the number of non-bridging oxygen in the glass system [85]. In addition, other optical properties of glass can be influenced by the refractive index. The dielectric constant can be calculated by using formula  $\epsilon = n^2$ . The value of dielectric constant was decreased from 4.52 to 4.44 and the optical dielectric constant was decreased from 3.52 to 3.44 with an increase of BaO in the glass system. The dielectric constant decreases indicate that the glass sample has electric conduction increased when increasing the concentration of barium ions. Molar refraction of the glass sample is given by using the Lorentz-Lorentz equation and related to the structure of the glass network. The value of molar refraction was increased from  $14.89 \text{ cm}^3$  to  $17.12 \text{ cm}^3$ . The molar polarizability and metallization of the glass samples were increased from  $5.90 \times 10^{-24} \text{ pm}$  to  $6.79 \times 10^{-24} \text{ pm}$  and 0.459 to 0.465 with the increasing of BaO content in the glass system. The increase in metallization has increased the metallicity of the glass sample. Basically, the value of metallization is in the range of 0-1. If the nature of solids can be explained on the condition that  $R_m/V_m < 1$  (non-metal) and  $R_m/V_m > 1$  (metal). These results indicate that the glass network is created the number of non-bridging oxygen in the network former led to the change in optical properties.

**Table 4.8 Refractive index, dielectric constant, optical dielectric constant, reflection loss, molar refractivity, metallization, and molar polarizability as a function of BaO in glass system.**

Properties	Glass samples							
	S <sub>1</sub>	S <sub>2</sub>	S <sub>3</sub>	S <sub>4</sub>	S <sub>5</sub>	S <sub>6</sub>	S <sub>7</sub>	S <sub>8</sub>
Direct band gap	3.15	3.02	3.02	2.68	2.65	2.64	2.70	2.70
Indirect band gap	2.62	2.65	2.72	2.72	2.68	2.68	2.72	2.70
Refractive index	2.12	2.12	2.10	2.10	2.11	2.11	2.10	2.10
Dielectric constant	4.52	4.49	4.42	4.42	4.46	4.46	4.42	4.44
Optical dielectric constant	3.52	3.49	3.42	3.42	3.46	3.46	3.42	3.44
Reflection loss	0.40	0.40	0.39	0.39	0.40	0.40	0.39	0.40
Molar refractivity	14.89	15.26	15.16	15.73	15.95	16.33	16.62	17.12
Metallization	0.459	0.461	0.467	0.467	0.464	0.464	0.467	0.465
Molar polarizability (10 <sup>-24</sup> )	5.90	6.05	6.01	6.24	6.32	6.47	6.59	6.79

#### 4.7 Radiation properties

In this work, the radiation shielding parameter such as linear attenuation coefficient, mass attenuation coefficient, mean free path, and half value layer was measured and calculated at the photon energy of 662 keV, 1174 keV, and 1332 keV. The obtained results that the linear attenuation coefficient has increased with the increasing concentration of BaO in the glass system and photon energy. The value of linear attenuation coefficient and mass attenuation coefficient are shown in the Table 4.10. The linear attenuation coefficient depends on the thickness of the glass samples and photon energy. The mass attenuation coefficient can be calculated by the value of linear attenuation coefficient and density of glass. The value of mass attenuation coefficient is increase with the increasing of the concentration of BaO. However, at the 1332 keV, the value of the mass attenuation coefficient is a small increase and almost unchanged in slope. Figure 4.18 show the value of the mass attenuation coefficient at the photon energy and compare with the glass sample in previous work.

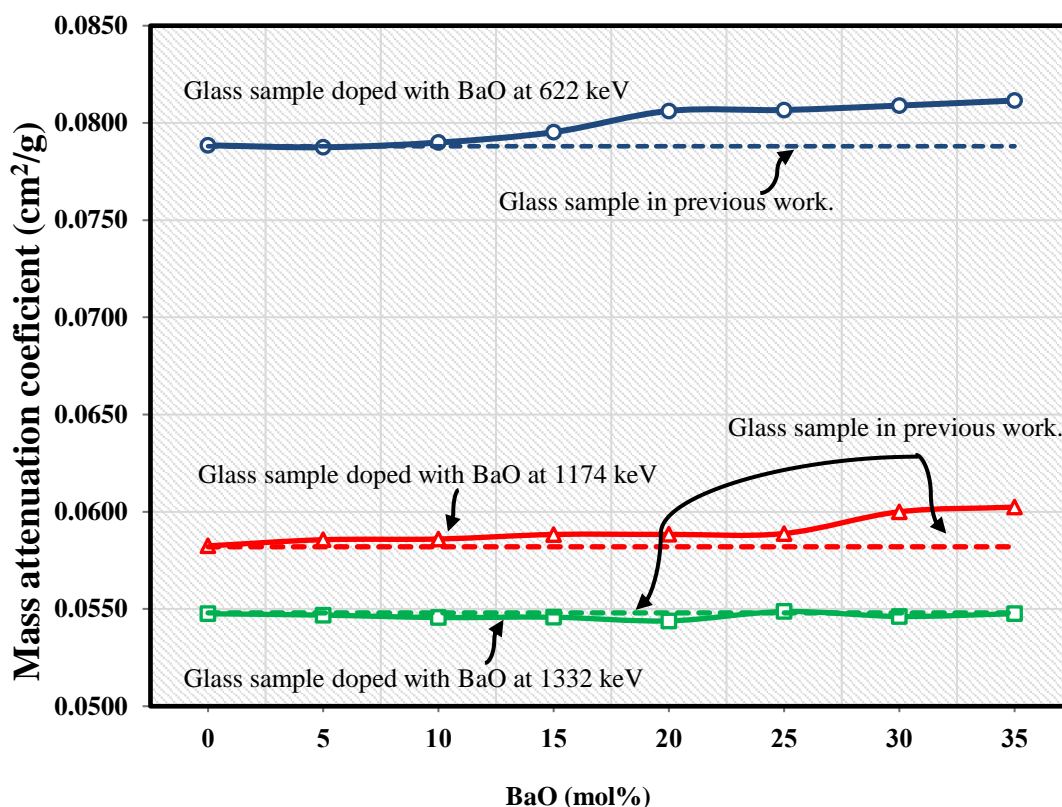


**Figure 4.18 Comparison the mass attenuation coefficient between the glass samples in previous work and doped with BaO at 662, 1174, and 1332 keV**

When adding the BaO into the glass system is lead to the increase in density of glass sample due to BaO has a high molecular weight (153.326 g/mol). Density of glass have the effect on gamma attenuation. Thus, the mass attenuation coefficient increases with the adding the concentration of barium oxide at the photon energy of 622 keV and 1174 keV. However, the mass attenuation coefficient at 1332 keV is a slight change because of the high energy of the photon. In addition, the increase in photon energy led to deep penetration and pass-through in the glass sample. these results are led to slight differences in the value of the mass attenuation coefficient. And then, we compare the mass attenuation coefficient between the glass sample in previous work and doped with BaO. We found that the mass attenuation coefficient of the glass sample doped with different the concentration of BaO have a value more than the glass sample in previous work at 662 keV and 1174 keV. This result indicates that barium ions create more interaction of gamma ray and are due to the higher of Compton scattering processes in higher photons energy. K.kirdsiri and et al[57] reported that the barium oxide filled in

the glass networks can create the higher Compton interaction than the glasses doped with the lead oxide and bismuth oxide. At 1332 keV, the mass attenuation coefficient of the glass sample doped with different the concentration of BaO and the glass sample in previous work are not different values.

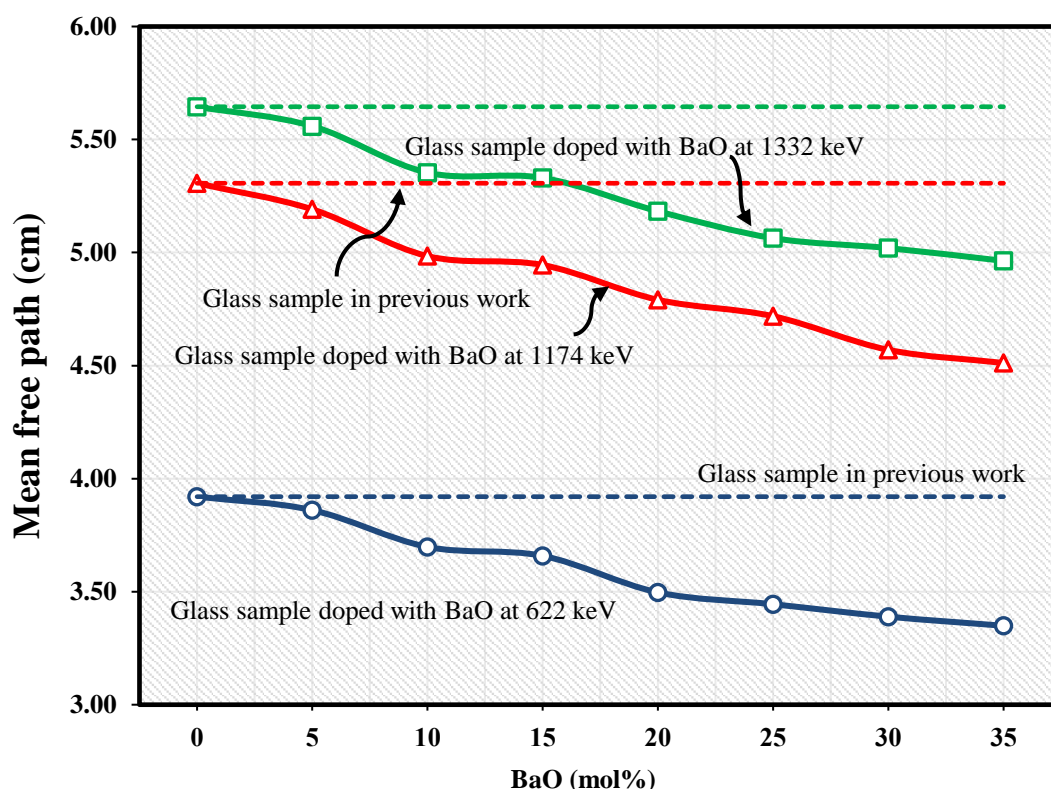


**Figure 4.19 Comparison of mfp of glass samples with different concentration of barium oxide and mfp of previous work**

The value of mean free path as shown in Figure 4.19. Mean free path decreased from 3.9201 cm to 3.3490 cm at the 662 keV of photon energy with the increase of the concentration of BaO. At 1174 keV of photon energy, the value of mean free path decreased from 5.3066 cm to 4.5116 cm and decreased from 5.6450 cm to 4.9632 cm for 1332 keV of photon energy. These results show that the adding of barium oxide into the glass system can be improve the radiation shielding properties of glass due to barium ions can increase the interaction of gamma ray with glass samples. The average distance of the photon particle which travels through before interaction is decreasing because the photon particles transfer energy to the other atom or more collisions of a photon particle.



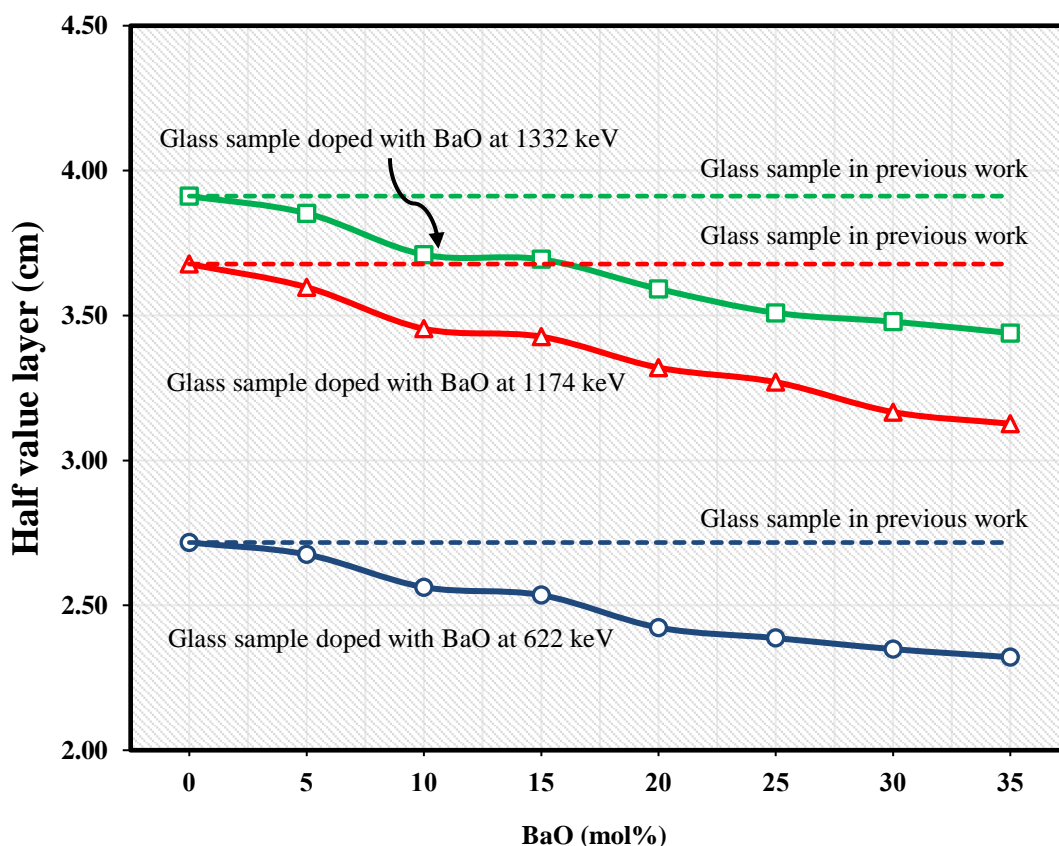


**Figure 4.20 Comparison of HVL of glass samples with different concentration of barium oxide and HVL of previous work**

However, the value of the mean free path is increased with the comparison of the different photon energy (662 keV, 1174 keV, and 1332 keV). This result found that the glass sample has a decrease in radiation attenuation with the increasing of photon energy. Table 4.11 show the value of mean free path and HVL of all glass sample with the different photon energy. In the many research, they are reported that the low value of the mean free path is led to a good for shielding of the radiation. When comparing with the previous work (5 mol% of  $\text{Bi}_2\text{O}_3$  and without barium oxide) found that the value of mean free path of the glass samples doped with BaO is lower than the previous work at 662 keV, 1174 keV, and 1332 keV. These results indicate that the glass system in previous work can be improved the radiation shielding properties by adding barium oxide.

Concerning half value layer, this parameter indicates that the thickness of the material in the cm unit penetrated by 50% of photon energy. Figure. 4.20 are show the value of HVL in different energy. It has been found that the value of HVL decrease from 2.7166 to 2.3265 cm, 3.6775 to 3.1265 cm, and 3.9120 to 3.4395 cm at the energy of 662 keV, 1174 keV, and 1332 keV, respectively. It is known that half value layer parameter depends on the density and energy of the photons. Thus, adding of barium oxide in the glass system is effect to the increase in the value of density of glass samples and improve the gamma ray shielding properties. In higher energy, the value of HVL has a value more than the low energy because the energy of photons can deep penetration in glass samples. In addition, we compare the HVL with the glass sample in previous work. These results show that the glass sample doped with BaO can attenuate the gamma ray and better than the glass sample in previous work (non-doped barium oxide). Figure 4.21 shows that the half value layer of glass samples compare with different concrete such as ordinary concrete, barite concrete, serpentite concrete, chromite concrete, and ferrite concrete at the energy of 662 keV. As you can see in Figure 4.21, we found that the HVL of glass samples is decrease and better than ordinary concrete, barite concrete, serpentite concrete, chromite concrete, except ferrite concrete at the energy of 662 keV. Half value layer may be influenced by barium ions and bismuth ions in the glass system and lead to an increase in attenuation of gamma ray. Barium and bismuth have a high atomic number which is effective in the three mechanisms (Photoelectric effect, Compton scattering, and pair production) for shielding properties. At 1174 keV, the glass sample at 35 mol% of BaO is better than ordinary concrete, barite concrete, serpentite concrete, chromite concrete, except ferrite concrete at the energy of 1174 keV and as shows in Figure 4.22. However, the glass sample is better than barite concrete when we add the barium oxide at 15 mol%. At 1332 keV, all glass samples have a tendency of the line graph like the glass sample at the energy of 662 keV and 1174 keV. The chemical compositions of concretes are given in Table 4.9. The chemical composition of concrete has a lot of silicon, barium, magnesium, chromium, and iron of the ordinary concrete, barite concrete, serpentite concrete, chromite concrete, and ferrite concrete, respectively.

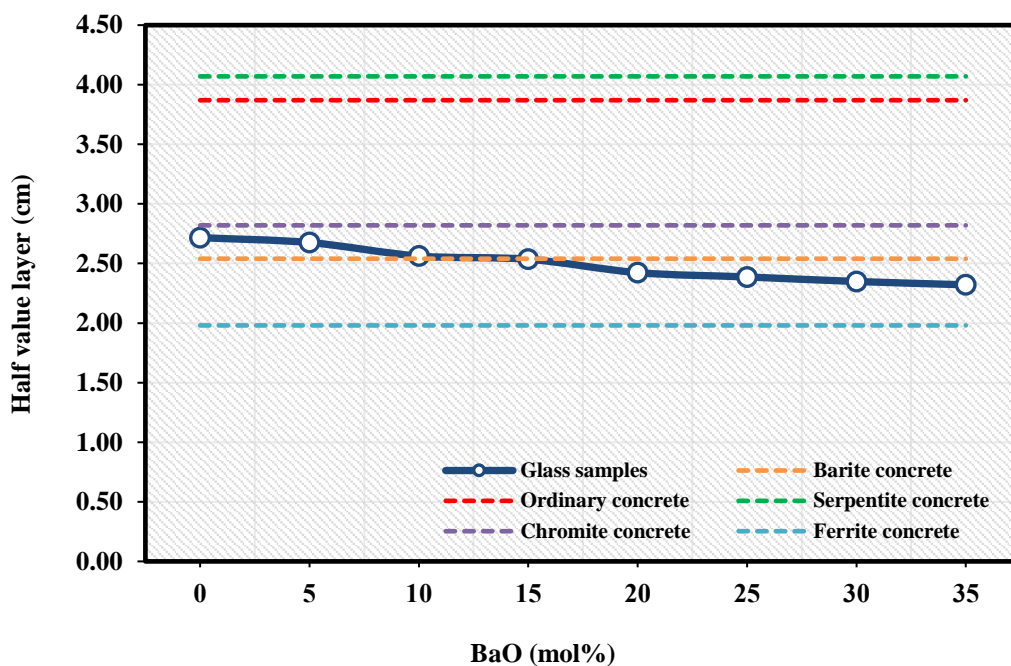


**Figure 4.21** The variation of HVL of glass samples compare to different concrete with different concentration of barium oxide at 662 keV

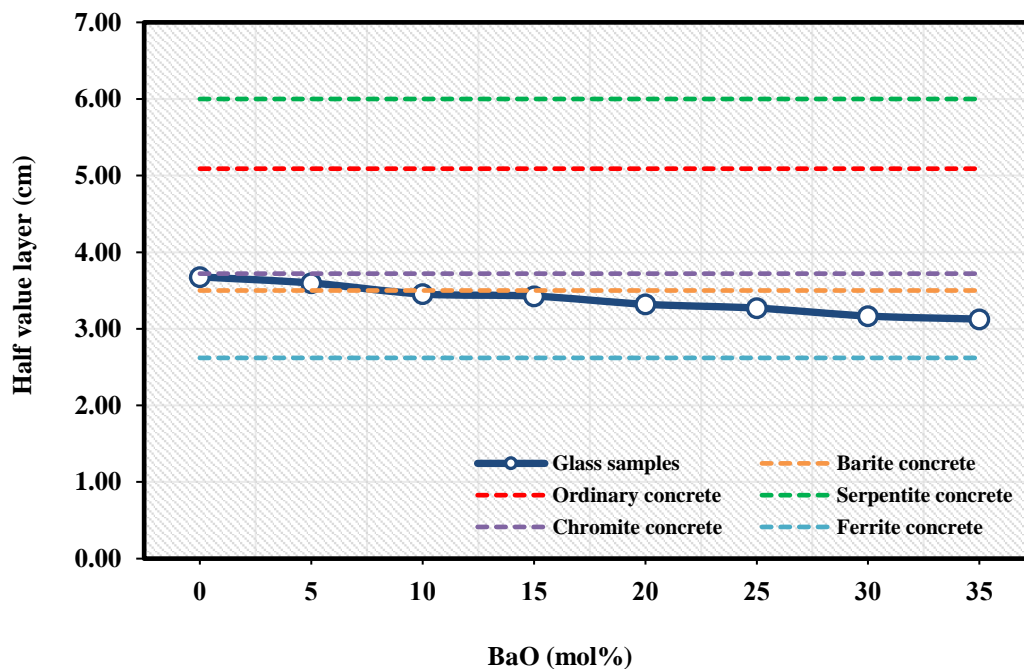


**Figure 4.22** The variation of HVL of glass samples compare to different concrete with different concentration of barium oxide at 1174 keV

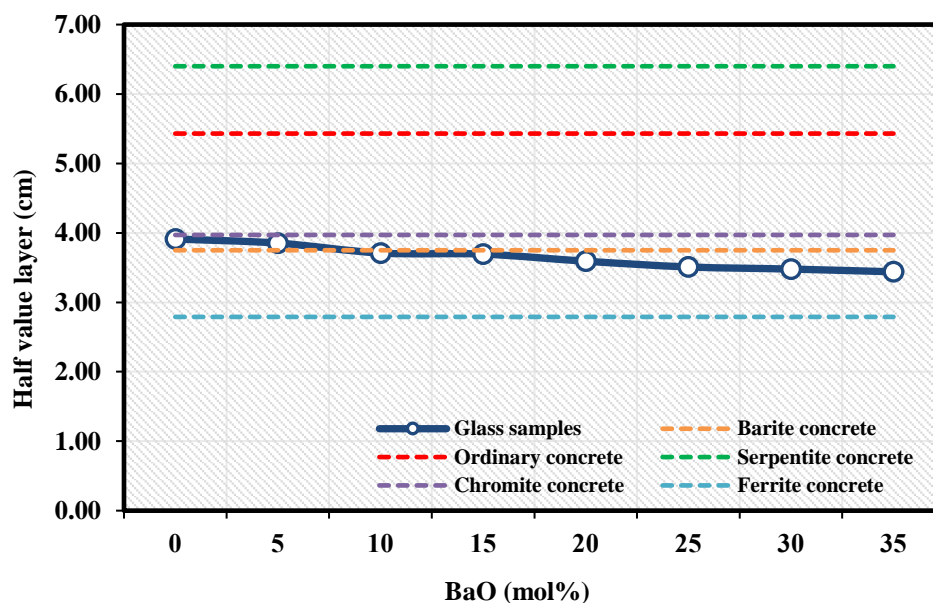


**Figure 4.23** The variation of HVL of glass samples compare to different concrete with different concentration of barium oxide at 1332 keV

**Table 4.9** Chemical compositions of concretes

Weight fraction elements	Ordinary concrete	Barite concrete	Serpentine concrete	Chromite concrete	Ferrite concrete
H	0.1000	0.0083	0.0128	-	0.0280
B	-	0.0115	0.0061	-	-
C	0.0010	-	-	0.0006	-
O	0.5291	0.3475	0.5136	0.3670	0.4554
Na	0.0160	-	-	0.0088	-
Mg	0.0020	0.0022	0.1705	0.1705	0.0019
Al	0.0338	0.0044	0.0215	0.0215	0.0038
Si	0.3370	0.0148	0.1587	0.0443	0.0128
S	-	0.0997	0.0046	0.0061	0.0007
K	0.0130	-	-	-	-
Ca	0.0440	0.0834	0.0677	0.0364	0.0595
Cr	-	-	-	0.3423	-
Fe	0.0140	0.0047	0.0441	0.0804	0.4378
Ba	-	0.4237	-	-	-

However, the value of HVL of glass samples is higher than HVL of ferrite concrete in all the concentrations of BaO at 662 keV, 1174 keV, and 1332 keV. These results may be due to the high density of ferrite concrete and the composition of ferrite concrete. The chemical composition of ferrite concrete in the weight fraction is 0.0595 of calcium, 0.4378 of ferrite, 0.0128 of silicon and as shown in the Table 4.9. Ferrite concrete has a large quantity of Iron which leads to an increase in the density of concrete and more interaction of gamma ray. HVL of ferrite is 1.98 cm, 2.62 cm, and 2.79 cm at the photon energy of 662 keV, 1174 keV, and 1332 keV, respectively. Thus, ferrite concrete has a good for radiation shielding properties and better than the glass doped BaO in the glass system for this work.

**Table 4.10 The value of linear attenuation coefficient and mass attenuation coefficient**

Samples	Linear attenuation coefficient ( $\text{cm}^{-1}$ )			Mass attenuation coefficient ( $\text{cm}^2/\text{g}$ )		
	662 keV	1174 keV	1332 keV	662 keV	1174 keV	1332 keV
S1	0.2550	0.1884	0.1771	0.0788	0.0582	0.0548
S2	0.2590	0.1926	0.1798	0.0787	0.0586	0.0547
S3	0.2704	0.2006	0.1867	0.0790	0.0586	0.0546
S4	0.2733	0.2022	0.1875	0.0795	0.0588	0.0546
S5	0.2859	0.2087	0.1929	0.0806	0.0588	0.0544
S6	0.2903	0.2119	0.1974	0.0807	0.0589	0.0549
S7	0.2950	0.2188	0.1992	0.0809	0.0600	0.0546
S8	0.9858	0.2216	0.2014	0.0812	0.0602	0.0548

**Table 4.11 The value of the mean free path and HVL**

Samples	Mean free path (cm)			Half value layer (cm)		
	662 keV	1174 keV	1332 keV	662 keV	1174 keV	1332 keV
S1	3.9201	5.3066	5.6450	2.7166	3.6775	3.9120
S2	3.8606	5.1912	5.5593	2.6754	3.5975	3.8526
S3	3.6977	4.9844	5.3533	2.5625	3.4541	3.7098
S4	3.6583	4.9440	5.3305	2.5352	3.4268	3.6940
S5	3.4967	4.7911	5.1829	2.4232	3.3202	3.5917
S6	3.4444	4.7185	5.0638	2.3869	3.2699	3.5092
S7	3.3893	4.5696	5.0199	2.3488	3.1667	3.4788
S8	3.3490	4.5116	4.9632	2.3209	3.1265	3.4395

#### 4.7.1 Theoretical calculation method

In addition, the radiation shielding parameter in terms of the mass attenuation coefficients can be calculated by using the WinXcom program and Fluka program. The mass attenuation coefficients of glass systems can be predicted by using the theoretical calculation method. WinXcom program and Fluka program is used widely in radiation shielding fields, mechanism in radiation interaction, and understanding the radiation attenuation when the photons pass through the glass samples. For the WinXCom program, we can define a substance of compounds or mixtures which the substance determination list comes with a predefined list of the elements in the periodic table ( $Z=1-100$ ). WinXCom program calculate based on a standard energy grid, spaced approximately logarithmically. The results of the program provide total cross-sections and attenuation coefficients as well as incoherent and coherent scattering, photoelectric absorption, and pair production. The Fluka program calculate based on Monte Carlo (MC) techniques for the interaction, transport of particles, nuclei in the matter, and to estimate the shielding properties. Figure 4.24 shown that the value of mass attenuation coefficients compares with the experimental data, WinXcom data, and Fluka data at the energy of 662 keV. It has been found that the mass attenuation coefficients of the experimental data from the narrow beam transmission method is higher than the mass attenuation coefficients from WinXcom and Fluka program at 15 mol% of BaO. The results from both programs are an increase in the mass attenuation coefficients and good

agreement for the data of mass attenuation coefficients at 662 keV of the photon energy. However, at 1174 keV, the mass attenuation coefficients increase with increasing of BaO in the glass network while the value from both programs are decreases with the concentration of BaO increased and as shows in Figure 4.25. The increase in mass attenuation coefficients of experimental data may be due to the Compton scattering process increased. These results indicated that the barium oxide added in the glass network can create the Compton scattering increased. However, the difference between theoretical value and experimental data is 2% which is exceedingly small of changes.

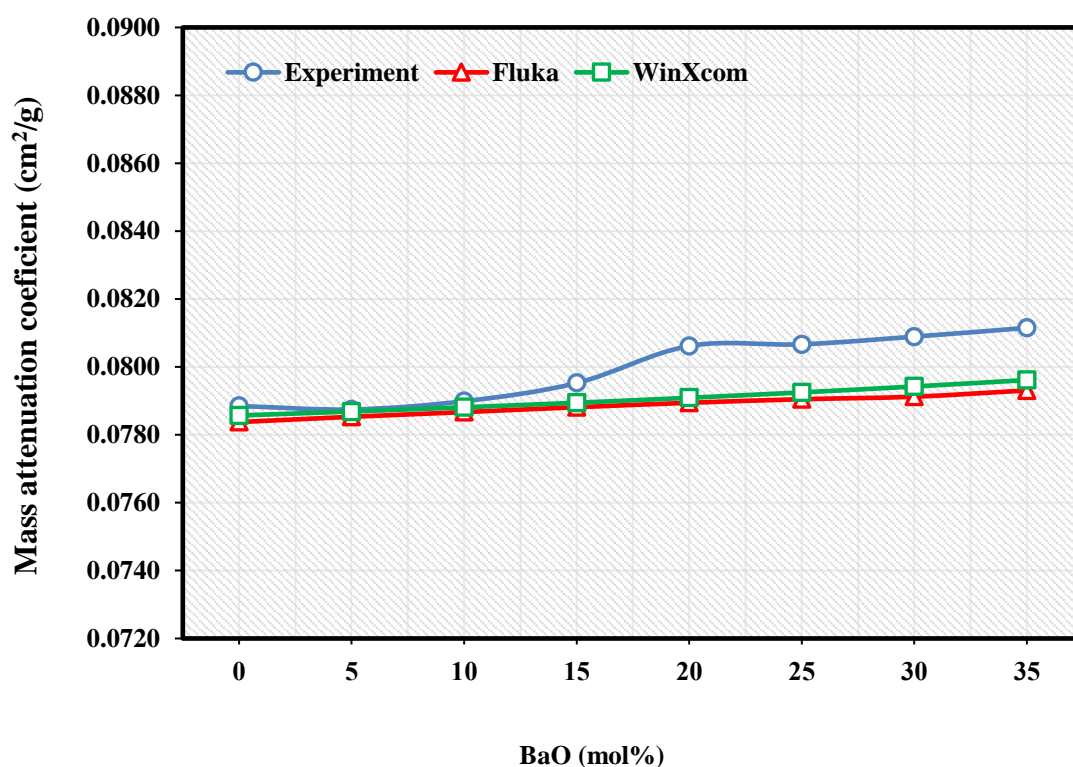


**Figure 4.24 Comparison of the mass attenuation coefficients between experimental data, WinXcom data, and Fluka data at the energy of 662 keV**

At 1332 keV, the mass attenuation coefficients are higher than the theoretical calculation method and as shows in Figure 4.26. The experiment data of mass attenuation coefficients at 10 mol% of BaO is higher than the theoretical value in both programs. And in addition, the theoretical data of the Fluka program and WinXcom program show that the value of mass attenuation coefficients of WinXcom data is higher than the value of Fluka data and the data of both programs are good agreement.

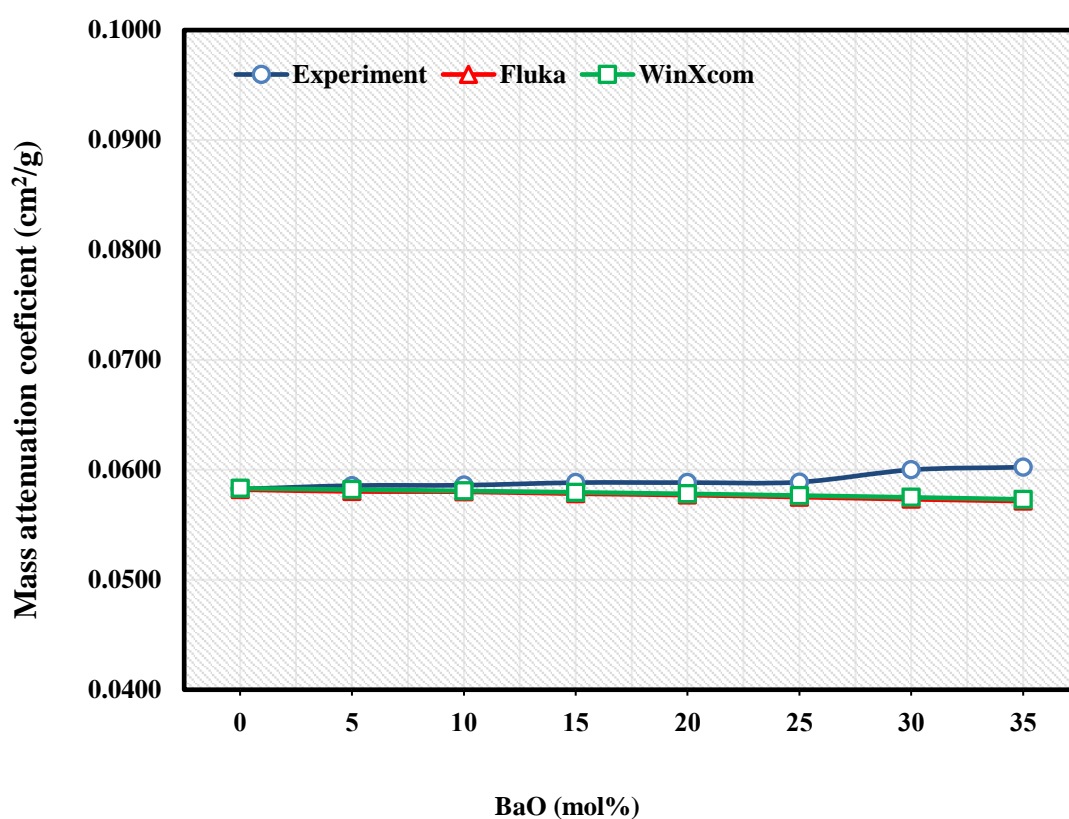
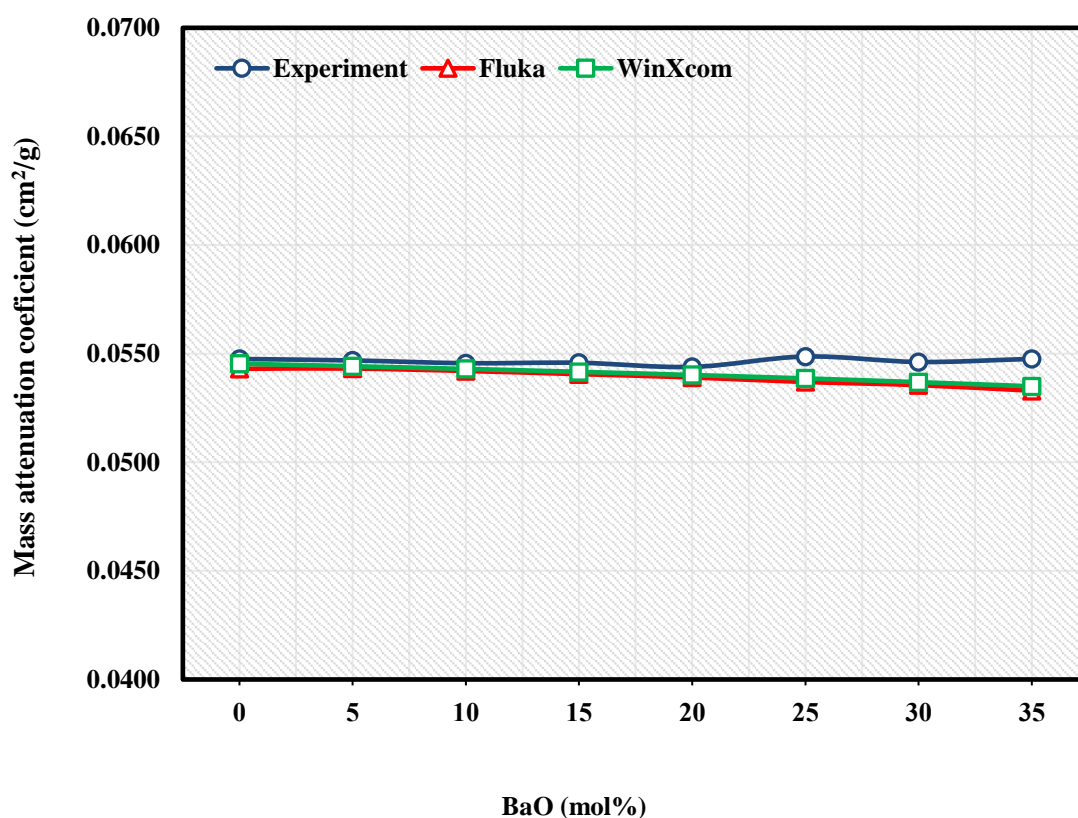


**Figure 4.25 Comparison of the mass attenuation coefficients between experimental data, WinXcom data, and Fluka data at the energy of 1174 keV**



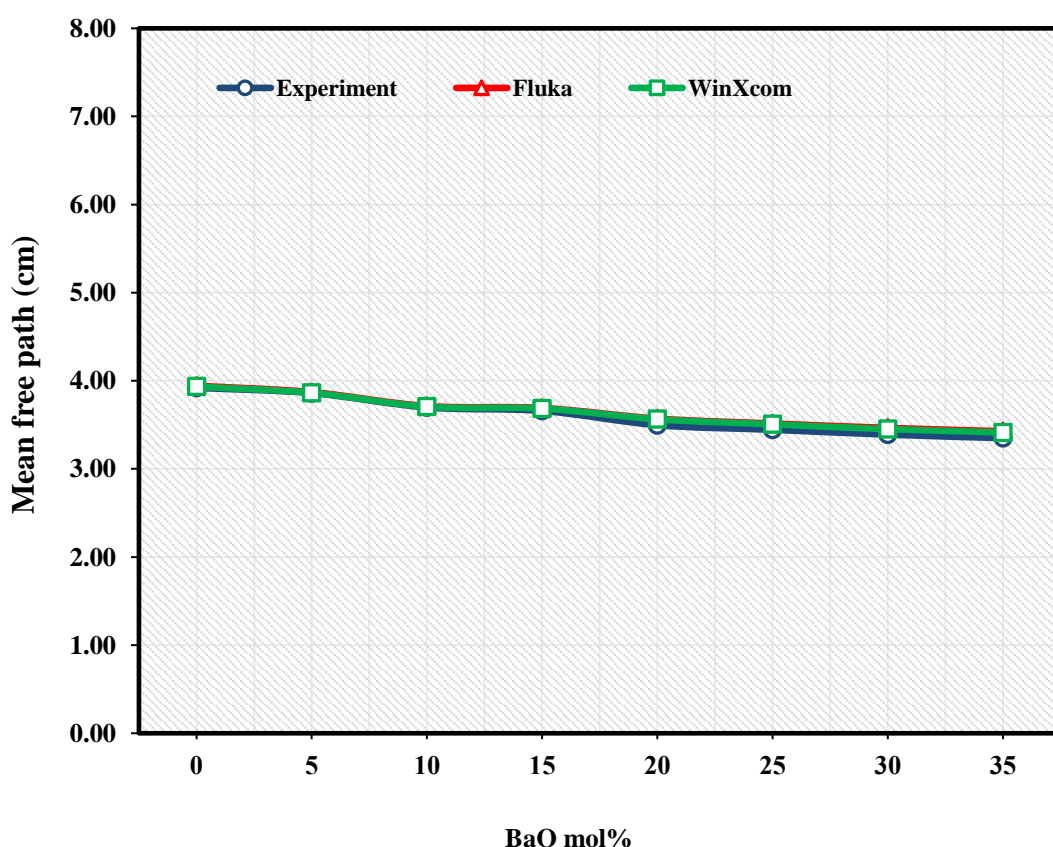
**Table 4.12** The value of mass attenuation coefficients between WinXcom and Fluka data

Samples	WinXcom			Fluka		
	662 keV	1174 keV	1332 keV	662 keV	1174 keV	1332 keV
S1	0.0786	0.0583	0.0545	0.0784	0.0582	0.0543
S2	0.0787	0.0582	0.0544	0.0785	0.0580	0.0543
S3	0.0788	0.0581	0.0543	0.0787	0.0580	0.0542
S4	0.0789	0.0580	0.0542	0.0788	0.0578	0.0541
S5	0.0791	0.0578	0.0540	0.0789	0.0577	0.0539
S6	0.0792	0.0577	0.0539	0.0790	0.0575	0.0537
S7	0.0794	0.0575	0.0537	0.0791	0.0573	0.0536
S8	0.0796	0.0573	0.0535	0.0793	0.0572	0.0533



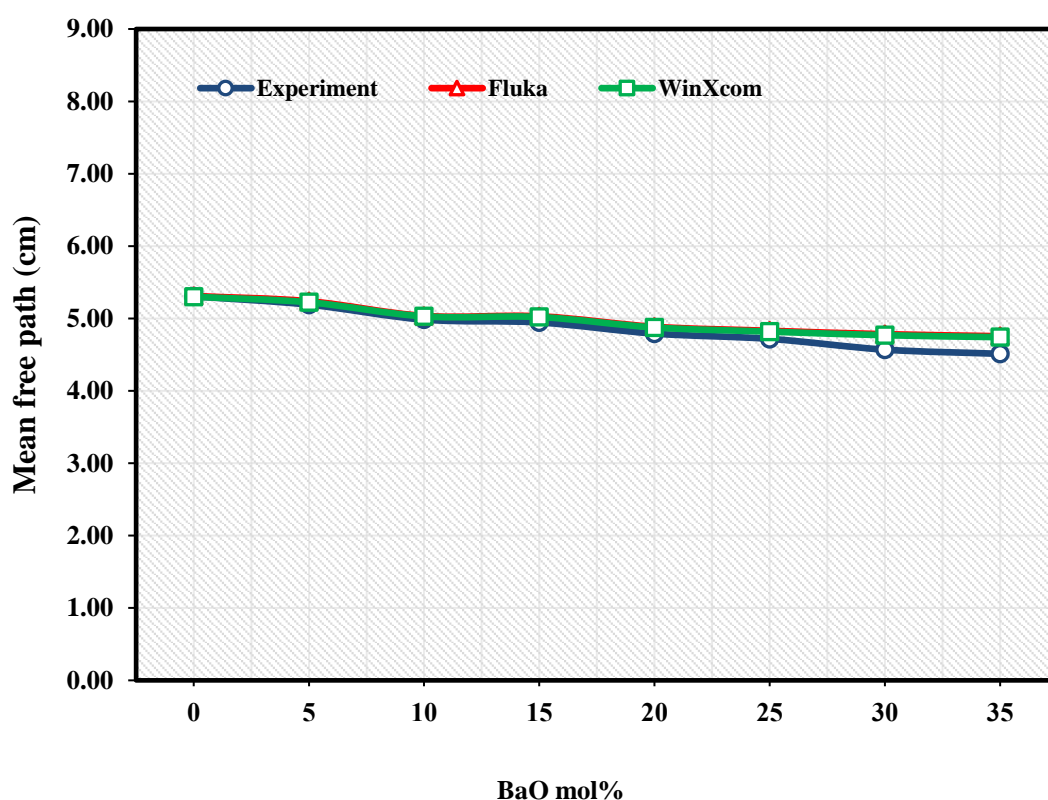
**Figure 4.26** Comparison of the mass attenuation coefficients between experimental data, WinXcom data, and Fluka data at the energy of 1332 keV

Figure 4.27 shows that the value of mean free path compares between experimental data, WinXcom data, and Fluka data at the energy of 622 keV. At 622 keV, the value of the mean free path of glass samples decreases from 3.92 to 3.34 cm for experimental data. For theoretical calculation methods, the mean free path of glass samples decreases from 3.94 to 3.42 cm and 3.93 to 3.41 cm for Fluka program and WinXcom program, respectively. The mean free path of the Fluka program is higher than the mean free path of WinXcom data and are good agreement in both programs. The low value of the mean free path shows that the adding of BaO in the glass network is an influence on the gamma ray shielding properties of glass samples. However, the mean free path from experimental data is lower than theoretical data. These results show that the barium ions are effect to the glass network more than the prediction from both programs and mean free path is depend on density of glass and mass attenuation coefficient.



**Figure 4.27 Comparison of the mean free path between experimental data, WinXcom data, and Fluka data at the energy of 622 keV**

At 1174 keV, we found that the value of the mean free path is decreased from 5.31 to 4.75 cm and 5.30 to 4.74 cm for Fluka program and WinXcom program, respectively. The mean free path from experimental data is decreased from 5.30 to 4.5 cm and is good agreement for the three-way of the calculations. Comparison of the mean free path between experimental data, WinXcom data, and Fluka data at the energy of 1174 keV as shown in Figure 4.28. The value of the mean free path in the blue line has lower than the green line and the red line. In addition, Figure 4.29 are present the comparison of the mean free path between experimental data, WinXcom data, and Fluka data at the energy of 1332 keV. The trend of the graph in Figure 4.29 is like the trend of the graph in Figure 4.28. The value of the mean free path of glass samples at 1332 keV have decrease in the trend from 5.69 to 5.09 cm and 5.66 to 5.08 cm for Fluka program and WinXcom program, respectively.



**Figure 4.28 Comparison of the mean free path between experimental data, WinXcom data, and Fluka data at the energy of 1174 keV**

**Table 4.13** The value of mean free path between WinXcom and Fluka data

Samples	WinXcom			Fluka		
	662 keV	1174 keV	1332 keV	662 keV	1174 keV	1332 keV
S1	3.9340	5.3008	5.6677	3.9438	5.3109	5.6920
S2	3.8636	5.2236	5.5863	3.8712	5.2384	5.5972
S3	3.7061	5.0289	5.3794	3.7128	5.0357	5.3886
S4	3.6852	5.0202	5.3714	3.6914	5.0309	5.3819
S5	3.5642	4.8760	5.2186	3.5709	4.8853	5.2294
S6	3.5059	4.8186	5.1587	3.5148	4.8303	5.1743
S7	3.4520	4.7686	5.1069	3.4651	4.7830	5.1198
S8	3.4137	4.7420	5.0803	3.4269	4.7552	5.0996

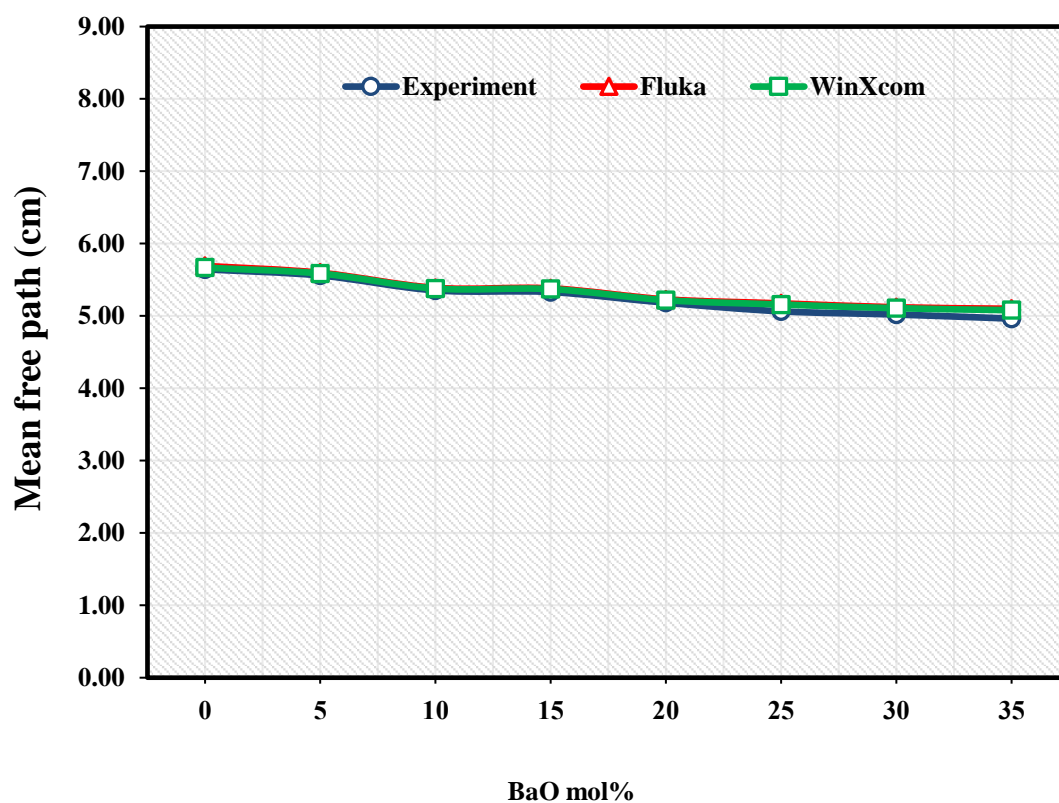
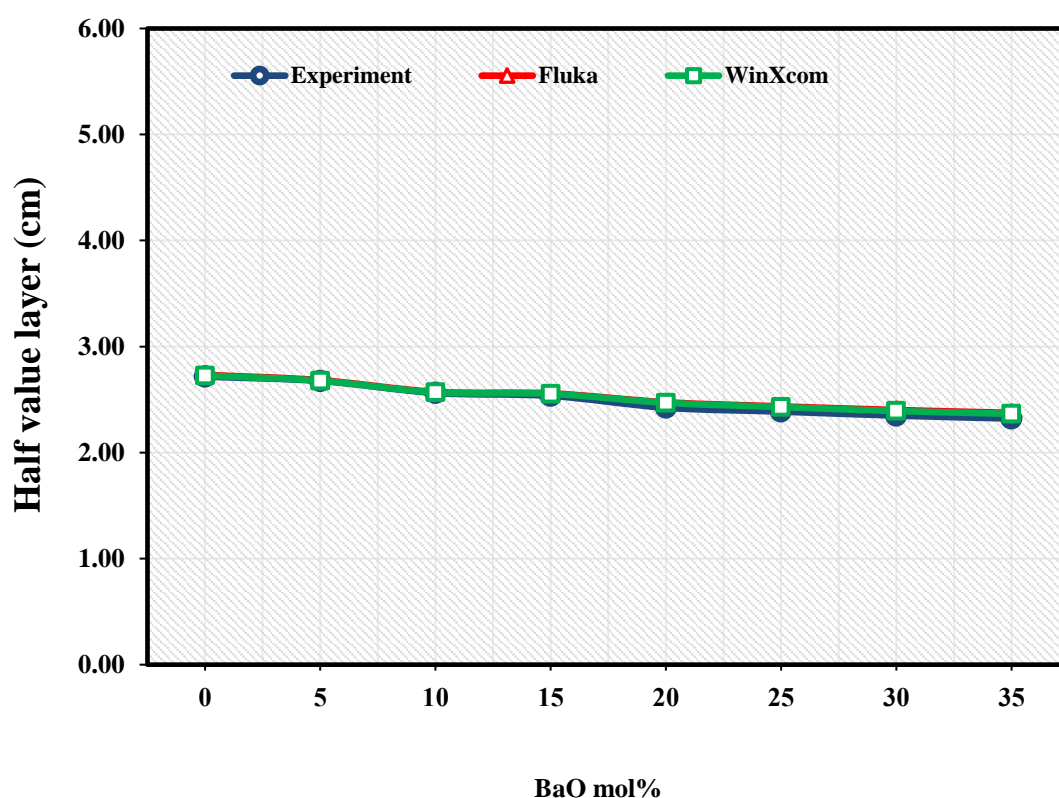
**Figure 4.29** Comparison of the mean free path between experimental data, WinXcom data, and Fluka data at the energy of 1332 keV

Figure 4.30 as shows the comparison of the half value layer between experimental data, WinXcom data, and Fluka data at the energy of 622 keV. From the Figure 4.30, it has been found that the half value layer of glass samples has a decrease in the trend of the graph when adding the concentration of barium oxide in the glass system. Half value layer of glass samples at photons energy of 622 keV decreases from 2.71 to 2.32 cm with an increase in the concentration of barium oxide in the glass network. For radiation shielding properties, the low of the value of half value layer is better for radiation shielding application materials. However, the results predicted from both programs have the higher the value of experimental data. The value of half value layer at 622 keV of photons energy decreases from 2.73 to 2.37 cm and 2.72 to 2.36 cm for Fluka program and WinXcom program, respectively. In addition, the results in both programs are good agreement between the experimental data and theoretical calculation methods.



**Figure 4.30 Comparison of the half value layer between experimental data, WinXcom data, and Fluka data at the energy of 622 keV**

In 1174 keV of photons energy, half value layer of glass samples decreases with the increase of the concentration of barium oxide in the glass network and as shown in Figure 4.31. The results from the three paths calculated in Figure 4.31 are good agreement. The experimental data is shown in the blue line and decrease from 3.67 to 3.12 cm with the barium oxide filled in the glass network. The results of both programs are higher than the experimental data and the trend in the graph is decreased from 3.68 to 3.29 cm and 3.67 to 3.28 cm for Fluka program and WinXcom program, respectively. Furthermore, at 1332 keV, half value layer of the glass samples decreases from 3.91 to 3.43 cm with the concentration of barium oxide in the glass network. Figure 4.32 shows the comparison of the half value layer between experimental data, WinXcom data, and Fluka data at the energy of 1332 keV. the value of half value layer from experimental data, calculation in Fluka program, and calculation in WinXcom are good agreement and decrease with the increase in the concentration of barium oxide in the glass network. For theoretical calculation methods, the value of half value layer decrease from 3.94 to 3.53 cm and 3.92 to 3.52 cm for Fluka program and WinXcom program, respectively. These results show that the barium oxide filled in the glass system can improve the radiation shielding properties of the glass samples. In addition, if adding of barium oxide in the glass systems are led to the thick reduced because the radiation shielding properties are increased.

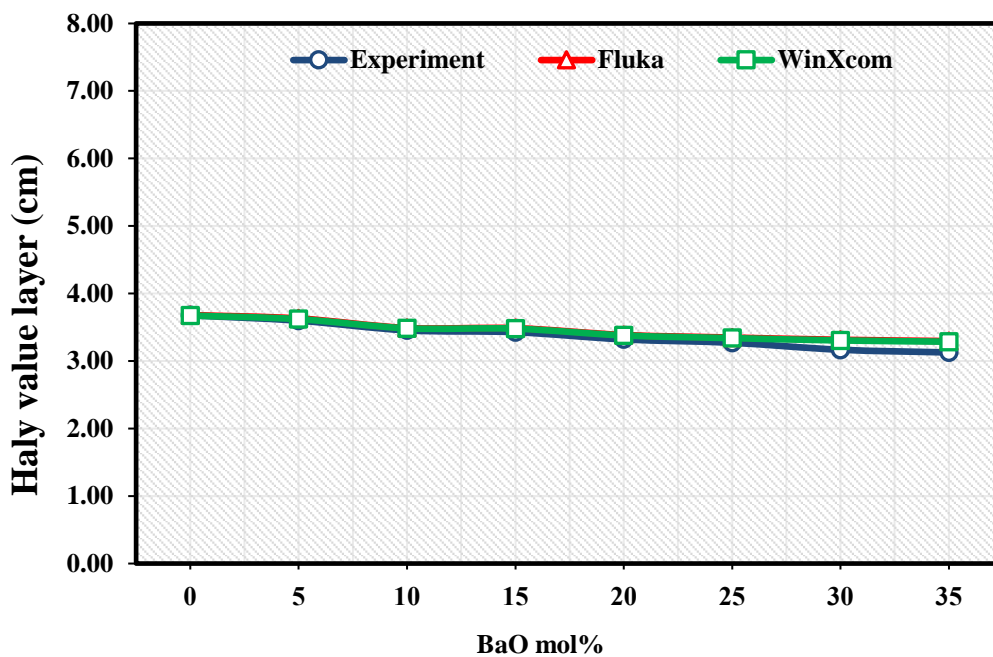


Figure 4.31 Comparison of the half value layer between experimental data, WinXcom data, and Fluka data at the energy of 1174 keV

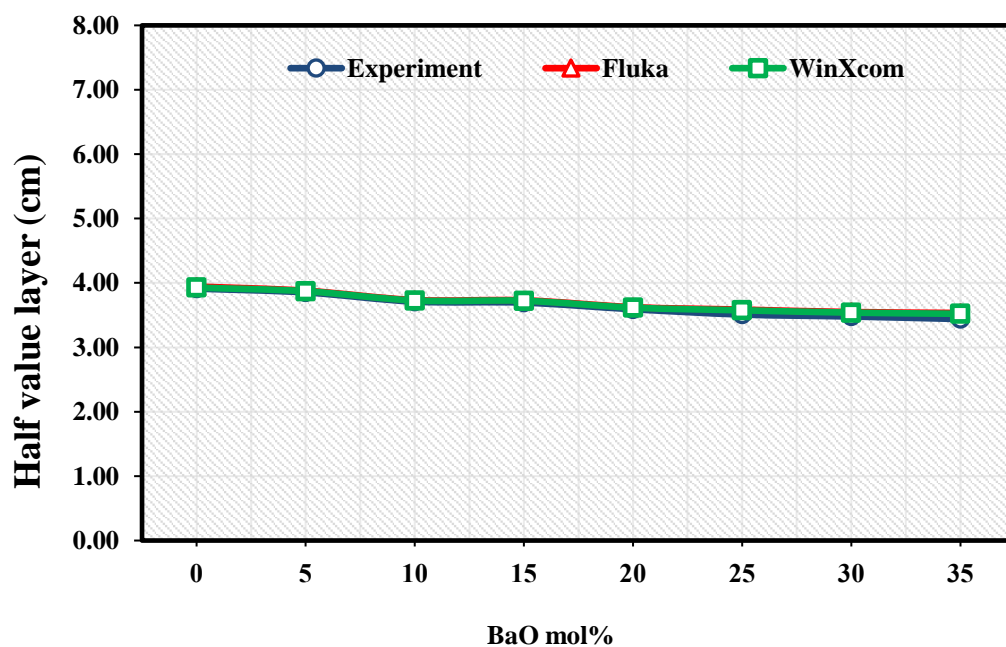


Figure 4.32 Comparison of the half value layer between experimental data, WinXcom data, and Fluka data at the energy of 1332 keV

**Table 4.14 The value of half value layer between WinXcom and Fluka data**

<b>Samples</b>	<b>WinXcom</b>			<b>Fluka</b>		
	<b>662 keV</b>	<b>1174 keV</b>	<b>1332 keV</b>	<b>662 keV</b>	<b>1174 keV</b>	<b>1332 keV</b>
S1	2.7262	3.6734	3.9277	2.7330	3.6804	3.9446
S2	2.6775	3.6199	3.8713	2.6828	3.6322	3.8788
S3	2.5683	3.4850	3.7279	2.5729	3.4897	3.7343
S4	2.5538	3.4790	3.7224	2.5581	3.4864	3.7296
S5	2.4699	3.3791	3.6165	2.4746	3.3855	3.6240
S6	2.4295	3.3392	3.5750	2.4357	3.3474	3.5858
S7	2.3922	3.3046	3.5391	2.4013	3.3146	3.5480
S8	2.3657	3.2862	3.5206	2.3748	3.2953	3.5340



## CHAPTER 5

### CONCLUSION

#### 5.1 Structural properties

High pressure sodium lamp glass can be recycled for this work and was used instead of borosilicate glasses because they have a high percent of  $B_2O_3$  like borosilicate glasses. The glass samples were prepared in  $(75-x)$  HPSg –  $(20)$   $Na_2O$  –  $5$   $Bi_2O_3$  –  $(x)$   $BaO$  system and has a clear and without bubbles inside the glass. The color of glass samples is a result of bismuth oxide in the glass system. These results are led to the yellow-green color of the glass samples which we called lemon-lime color. However, the color of the glass sample in this work has changed in lemon-lime color increase when we compare with the glass samples in previous research. Density and molar volume increase with the adding concentration of  $BaO$  in the glass system. Furthermore, the density and molar volume was greatly increased when we compare with the glass samples in previous research. This result due to barium oxide and bismuth oxide filled in the glass system. For the structure of glass, the number of non-bridging oxygen (NBO) is created by barium ions adding. NBO created in the glass network is leads to a decrease in the rigidity of glass due to the value of Young's modulus and micro-hardness decrease. From the FTIR data, it was found that the glass network is absorbing and vibrate the various modes of functional group in the range of  $700 - 710\text{ cm}^{-1}$ , and  $900 - 950\text{ cm}^{-1}$ . This region reveals that the NBOs are created in the glass network and these results confirmed by the ultrasonic technique data. Moreover, we compare the elastic moduli between theoretical value from Makishima-Mackenzie's model and experimental data. We found that the value of elastic moduli is good agreement except Poisson's ratio because the glass samples have a decrease in cross-link density more than the prediction of Poisson's ratio. These results indicate that the structure of glass has become less compact as tetrahedral coordination of boron with the concentration of  $BaO$ .

## 5.2 Optical properties

From the UV – Vis spectroscopy data, the optical band gap is in the range of 3.15 to 2.70 eV and 2.60 to 2.70 eV for direct and indirect band gap, respectively. The decrease in the direct band gap indicates that BaO creates more  $\text{BO}_3$  units in the glass network. In addition, the refractive index of glass samples is approximately 2.10 to 2.12. The optical parameter such as refractive index, dielectric constant, optical dielectric constant, reflection loss, molar refractivity, metallization, and molar polarizability is related to the number of non-bridging oxygen in the glass system and influenced by barium ions.

## 5.3 Radiation properties

The linear attenuation coefficient and mass attenuation coefficient are increase with increasing the concentration of BaO in glass systems, but they decrease with the increase of photon energy. The value of mean free path and half value layer decreases with increasing the concentration of BaO in the glass system. However, at the photon energy of 1174 keV and 1332 keV, the MFP and HVL is higher than the MFP and HVL of glass sample at 662 keV. Moreover, if compared the HVL with different type of concrete found that the HVL of glass samples is better than ordinary concrete, barite concrete, chromite concrete, and serpentite concrete in 662 keV, 1174 keV, and 1332 keV. For ferrite concrete, the glass samples are higher than the value of HVL of ferrite concrete. This shows that the radiation shielding of glass samples is better than the ordinary concrete, barite concrete, chromite concrete, and serpentite concrete except ferrite concrete. However, radiation shielding properties of glass samples is greatly improved when we add the barium oxide in the glass system and better than the glass samples in the previous work. The mass attenuation coefficient at 1174 keV and 1332 keV is an increase when barium oxide filled in S-5 samples (previous work) whilst mean free path and half value layer at 622 keV, 1174 keV, and 1332 keV are decreased when we compare with the previous work. These results show that the barium oxide filled in the S-5 sample can improve the radiation shielding properties of glass samples and better than glass samples in the previous work for radiation shielding properties term. Moreover, the theoretical calculation methods present that the value of the radiation

shielding parameter is a good agreement with the experimental data. These results support the results from a narrow beam transmission method.

## **REFERENCES**

## REFERENCES

- [1] E. Zorla and et al. “Radiation shielding properties of high performance concrete reinforced with basalt fibers infused with natural and enriched boron”, **Nuclear Engineering and Design**. 313: 306-318; March, 2017.
- [2] M. Dong and et al. “A novel comprehensive utilization of vanadium slag: as gamma ray shielding material”, **Journal of Hazardous Materials**. 318: 751-757; November, 2016.
- [3] S.A.M. Issa and A.M.A. Mostafa. “Effect of  $\text{Bi}_2\text{O}_3$  in borate-tellurite-silicate glass system for development of gamma-rays shielding materials”, **Journal of Alloys and Compounds**. 695: 302-310; February, 2017.
- [4] El-Sayed A. Waly and et al. “Gamma-ray mass attenuation coefficient and half value layer factor of some oxide glass shielding materials”, **Annals of Nuclear Energy**. 96: 26-30; October, 2016.
- [5] P. Kaur, D. Singh. “Heavy metal oxide glasses as gamma rays shielding material”, **Nuclear Engineering and Design**. 307: 364-376; October, 2016.
- [6] A. Khanna and et al. “Structural study of bismuth borosilicate, aluminoborate and aluminoborosilicate glasses by  $^{11}\text{B}$  and  $^{27}\text{Al}$  MAS NMR spectroscopy and thermal analysis”, **Journal of Non-Crystalline Solids**. 373-374: 34-41; August, 2013.
- [7] T. Maeder. “Review of  $\text{Bi}_2\text{O}_3$  based glasses for electronics and related applications”, **International Materials Reviews**. 58: 3-40; January, 2013.
- [8] M. Kurudirek and et al. “Effect of  $\text{Bi}_2\text{O}_3$  on gamma ray shielding and structural properties of borosilicate glasses recycled from high pressure sodium lamp glass”, **Journal of Alloys and Compounds**. 745: 355-364; May, 2018.
- [9] Reza Bagheri, Alireza Khorrami Moghaddam. “Gamma Ray Shielding Study of Barium - Bismuth - Borosilicate Glasses as Transparent Shielding Materials using MCNP-4C Code, XCOM Program, and Available Experimental Data”, **Nuclear Engineering and Technology**. 49(1): 216 – 223; February, 2017.

## REFERENCES (CONTINUED)

- [10] Sarawut Burinram. **Investigation of elastic properties of bismuth borosilicate glass**. Special project; Department of Physics, Faculty of science, Ubon Ratchathani University, 2016.
- [11] James Michael Curran and et al. **Forensic Interpretation of Glass Evidence 1st Edition**. Florida: CRC Press, 2001.
- [12] Dictionary by Merriam-Webster. “glass”,  
<http://www.merriamwebster.com/dictionary/glass>. April 20, 2013.
- [13] Taylor w.c. and et.al. “THE CONSTITUENTS OF MARINE SPONGES .8. MINOR DITERPENOID METABOLITES OF APLYSILLA-ROSEA AND A. VAR. SULFUREA”, **Australian Journal of Chemistry**. 50(9): 895-902; April, 1997.
- [14] ASTM International. **Standard Test Methods for Chemical Analysis of Glass Sand**. ASTM C146 - 94a. April 20, 2014.
- [15] Jiraphan Datchanipetch. **Physical properties and structures of chromium doped bismuthglasses**. Master’s Thesis: Chiangmai University, 2011.
- [16] William D. Callister. **Fundamentals of Materials Science and Engineering: An Integrated Approach 4th Edition**. Hoboken: John Wiley & Sons Inc., 2001.
- [17] M Hasanuzzaman and et al. **Properties of Glass Materials**. Amsterdam: Elsevier inc., 2016.
- [18] William D. Callister and David G. Rethwisch. **Materials Science and Engineering An Introduction**. Hoboken: John Wiley & Sons Inc., 2010.
- [19] James E. Shelby. **Introduction to glass science and technology**. London: The royal society of chemistry, 1997.
- [20] J. David Musgraves and et al. **Crystallization and Glass-Ceramics**. New York: Springer Link; 113-167, 2019.
- [21] D.H. Kim and et al. “Phase separation in metallic glasses”, **Progress in Materials Science**. 58(8): 1103–1172; October, 2013.

## REFERENCES (CONTINUED)

- [22] Bryan R. Wheaton and Alexis G. Clare. “Evaluation of phase separation in glasses with the use of atomic force microscopy”, **Journal of Non-Crystalline Solids**. 353(52-54): 4767–4778; December, 2007.
- [23] Alexander J. and et al. “On the origins of strain inhomogeneity in amorphous materials”, **Scientific Reports**. 8: 1574; January, 2018.
- [24] L. Bloomfield. **How Things Work: The Physics of Everyday Life**. New York: Wiley, 2001.
- [25] L. M. Baucio. **Engineered Materials Reference Book**. Ohio: ASM International, 1994.
- [26] L. D. Pye and et al. **Borate glasses: structure, properties, application**. New York: Plenum Press, 1978.
- [27] G. W. Morey. **The Properties of Glass**. New York: Reinhold Publishing Corp., 1954.
- [28] J. Swenson and L. Borjesson. “Magnetic structure of  $\text{NpPd}_2\text{Al}_3$ : Relevance to the coexistence of superconductivity and magnetism in  $\text{UPd}_2\text{Al}_3$ ”, **Physical Review Journals**. B55: 1138; January, 1997.
- [29] J. W. Zwanziger. “Microstructure and modification in borate and tellurite glasses”, **Journal of Non-Crystalline Solids**. 157: 192–193; December, 1995.
- [30] Michael I. Ojovan, William E. LeeStepan, N. Kalmykov. **An Introduction to Nuclear Waste Immobilisation**. Amsterdam: Elsevier inc., 2019.
- [31] N. Mehta. “Applications of chalcogenide glasses in electronics and optoelectronics: A review”, **Journal of Scientific & Industrial Research**. 65: 777-786; October, 2006.
- [32] J. Lucas. “HALIDE GLASSES”, **Journal of Non-Crystalline Solids**. 80: 83–91; January, 1986.
- [33] Samir Y. Marzouk. “Ultrasonic and infrared measurements of copper-doped sodium phosphate glasses”, **Materials Chemistry and Physics**. 114(1): 188–193; March, 2009.

## REFERENCES (CONTINUED)

- [34] M.S. Gaafar and S.Y. Marzouk. “Mechanical and structural studies on sodium borosilicate glasses doped with  $\text{Er}_2\text{O}_3$  using ultrasonic velocity and FTIR spectroscopy”, **Physica B**. 388(1-2): 294-302; January, 2007.
- [35] D. Krause. **Condensed Matter and Materials Data**. New York: Springer Link, 2005.
- [36] M.K. Halimah and et al. “Optical properties of lithium borate glass  $(\text{Li}_2\text{O})_x(\text{B}_2\text{O}_3)_{1-x}$ ”, **Sains Malays**. 43(6): 899–902; June, 2014.
- [37] V. Dimitrov and S. Sakka. “Electronic oxide polarizability and optical basicity of simple oxide”, **Journal of Applied Physics**. 79: 1736–1740; August, 1996.
- [38] A.M. Noorazlan and et al. “Effect of erbium nanoparticles on optical properties of zinc borotellurite glass system”, **Journal of Nanomaterials**. 168, November, 2013.
- [39] Z.A.S. Mahraz and et al. “Band gap and polarizability of borotellurite glass: Influence of erbium ions”, **Journal of Molecular Structure**. 1072: 238-241; August, 2014.
- [40] Ashok Kumar and et al. “Physical, structural, optical and gamma ray shielding behavior of  $(20+x) \text{PbO} - 10 \text{BaO} - 10 \text{Na}_2\text{O} - 10 \text{MgO} - (50-x) \text{B}_2\text{O}_3$  glasses”, **Physica B: Physics of Condensed Matter**. 552: 110 – 118; January, 2019.
- [41] Xinyu Zhao and et al. “Electronic polarizability and optical basicity of lanthanide oxides”, **Physica B: Physics of Condensed Matter**. 392: 132-136; April, 2017.
- [42] Salah Hassan Alazoumi and et al. “Optical properties of zinc lead tellurite glasses”, **Results in Physics**. 9: 1371-1376; June, 2018.
- [43] Priyanka Goyal and et al. “The effect of  $\text{SiO}_2$  content on structural, physical and spectroscopic properties of  $\text{Er}^{3+}$  doped  $\text{B}_2\text{O}_3\text{--SiO}_2\text{--Na}_2\text{O--PbO--ZnO}$  glass systems”, **Journal of Non-Crystalline Solids**. 463(1): 118-127; May, 2017.
- [44] John Schroeder. “Brillouin scattering and pockels coefficients in silicate glasses”, **Journal of Non-Crystalline Solids**. 40(1-3): 549-566; July, 1980.



## REFERENCES (CONTINUED)

- [45] R. El-Mallawany and et al. “Ultrasonic studies of  $(\text{TeO}_2)_{50} - (\text{V}_2\text{O}_5)_{50-x} - (\text{TiO}_2)_x$  glasses”, **Materials Chemistry and Physics**. 95(2-3): 321–327; February, 2006.
- [46] M.A. Sidkey and M.S. Gaafar. “Ultrasonic studies on network structure of ternary  $\text{TeO}_2 - \text{WO}_3 - \text{K}_2\text{O}$  glass system”, **Physica B**. 348(1-4): 46 –55; May, 2004.
- [47] D. Souri. “DSC and elastic moduli studies on tellurite-vanadate glasses containing antimony oxide”, **The European Physical Journal B**. 84: 47-51; November, 2011.
- [48] Gordon Gilmore. **Practical Gamma-Ray Spectrometry**.  
[http://www.uct.ac.za/sites/default/files/image\\_tool/images/281/we\\_frahn\\_library/Courses/Nuclear\\_Physics\\_For\\_Power\\_Eng/Laboratory\\_Classes/gilpgrs2-c02.pdf](http://www.uct.ac.za/sites/default/files/image_tool/images/281/we_frahn_library/Courses/Nuclear_Physics_For_Power_Eng/Laboratory_Classes/gilpgrs2-c02.pdf). April, 2011.
- [49] John Lilley. **Nuclear Physics: Principles and applications**(1st edition). Hoboken: Wiley, 2001.
- [50] G. Nelson and D. Reilly. **Gamma-Ray Interactions with Matter**.  
<https://faculty.washington.edu/agarcia3/phys575/Week2/Gamma%20ray%20interactions.pdf>. April, 2019.
- [51] Satya Prakash. **Nuclear Physics**. 2<sup>nd</sup> ed. Uttar Pradesh: Pragati prakashan, 2011.
- [52] Attix and Frank Herbert. **Introduction to Radiological Physics and Radiation Dosimetry**. Hoboken: Wiley, 1986.
- [53] James E. Parks. **The Compton Effect, Compton Scattering and Gamma-Ray Spectroscopy**. Knoxville: University of Tennessee, 2015.
- [54] Adnan Küçükönder, and Saniye Tekerek. “Measurement of total electronic cross-section, total atomic cross-section, effective atomic numbers and effective electron densities for some Sm compounds”, **AIP Conference Proceedings** **2042**. P. 020025(1-5), Bodrum: Turkey, 2018.

## REFERENCES (CONTINUED)

- [55] A Pacific Energy Center Factsheet. **High Pressure Sodium Lamps**.  
[https://www.lightingassociates.org/i/u/2127806/f/tech\\_sheets/high\\_pressure\\_sodium\\_lamps.pdf](https://www.lightingassociates.org/i/u/2127806/f/tech_sheets/high_pressure_sodium_lamps.pdf). May, 2019.
- [56] Kulwant Singh and et al. “Gamma-ray attenuation coefficients in bismuth borate glasses”, **Nuclear Instruments and Methods in Physics Research B**. 194(1): 1–6; July, 2002.
- [57] K. Kirdsiri and et al. “Comparative study of silicate glasses containing Bi<sub>2</sub>O<sub>3</sub>, PbO and BaO: Radiation shielding and optical properties”, **Annals of Nuclear Energy**. 38(6): 1438-1441; June, 2011.
- [58] Y. Al-Hadeethi and M. I. Sayyed. “Analysis of borosilicate glasses doped with heavy metal oxides for gamma radiation shielding application using Geant4 simulation code”, **Ceramics International Part A**. 45(18): 24858-24864; December, 2019.
- [59] Narveer Singh and et al. “Comparative study of lead borate and bismuth lead borate glass systems as gamma-radiation shielding materials”, **Nuclear Instruments and Methods in Physics Research Section B: Beam Interactions with Materials and Atoms**. 225(3): 305-309; September, 2004.
- [60] C. Bootjomchai and et al. “Gamma-ray shielding and structural properties of barium-bismuth-borosilicate glasses”, **Radiation Physics and Chemistry**. 81(7): 785-790; July, 2012.
- [61] Reza Bagheri and et al. “Determination of gamma-ray shielding properties for silicate glasses containing Bi<sub>2</sub>O<sub>3</sub>, PbO, and BaO”, **Journal of Non-Crystalline Solids**. 479(1): 62-71; January, 2018.
- [62] Reza Bagheri and et al. “Gamma Ray Shielding Study of Barium–Bismuth–Borosilicate Glasses as Transparent Shielding Materials using MCNP-4C Code, XCOM Program, and Available Experimental Data”, **Nuclear Engineering and Technology**. 49(1): 216-223; February, 2017.

## REFERENCES (CONTINUED)

- [63] M. Kurudirek and et al. “Effect of  $\text{Bi}_2\text{O}_3$  on gamma ray shielding and structural properties of borosilicate glasses recycled from high pressure sodium lamp glass”, **Journal of Alloys and Compounds**. 745(15): 355-364; May, 2018.
- [64] Abolfazl Khodadadi and Reza Taherian. “Investigation on the radiation shielding properties of lead silicate glasses modified by ZnO and BaO”, **Materials Chemistry and Physics**. 251(1): 123136; September, 2020.
- [65] N. Chanthima and et al. “Development of BaO–ZnO– $\text{B}_2\text{O}_3$  glasses as a radiation shielding material”, **Radiation Physics and Chemistry**. 137: 72-77; August, 2017.
- [66] S. Kaewjaenga and et al. “Effect of BaO on Optical, Physical and Radiation Shielding Properties of  $\text{SiO}_2 - \text{B}_2\text{O}_3 - \text{Al}_2\text{O}_3 - \text{CaO} - \text{Na}_2\text{O}$  Glasses System”, **Procedia Engineering**. 32: 1080 – 1086; November, 2012.
- [67] O. Agar and et al. “An investigation on shielding properties of BaO,  $\text{MoO}_3$  and  $\text{P}_2\text{O}_5$  based glasses using MCNPX code”, **Results in Physics**. 12: 629–634; March, 2019.
- [68] Color Code. **Lemon lime/#e3ff00 Hex Color Code**.  
<https://encycolorpedia.com/e3ff00>. 7 August 2020.
- [69] S.A. Azizan and et al. “Physical and optical properties of  $\text{Dy}^{3+}$ :  $\text{Li}_2\text{O}$ – $\text{K}_2\text{O}$ – $\text{B}_2\text{O}_3$  glasses”, **Journal of Molecular Structure**. 1076(5): 20–25; November, 2014.
- [70] R.S. Gedam and D.D. Ramteke. “Influence of  $\text{CeO}_2$  addition on the electrical and optical properties of lithium borate glasses”, **Journal of Physical Chemistry Solids**. 7410(10): 1399–1402; October, 2013.
- [71] A. Rajiv and et al. “Thermal and Optical properties of Sodium-Phospho-Zinc-Neodymium oxide glass system”, **Journal of Advanced Scientific Research**. 5(2): 32-39; October, 2014.
- [72] E. S. Moustafa and et al. “Structural and optical properties of lithium borobismuthate glasses”, **Journal of Physics and Chemistry of solids**. 69(9): 2281 –2287; September, 2008.

## REFERENCES (CONTINUED)

- [73] R. Laopaiboon and C. Bootjomchai. “Thermoluminescence studies on alkali-silicate glass doped with dysprosium oxide for use in radiation dosimetry measurement”, **Journal of Luminescence**. 158: 275-280; February, 2015.
- [74] A. Rajiv and et al. “Thermal and Optical properties of Sodium-Phospho-Zinc-Neodymium oxide glass system”, **Journal of Advanced Scientific Research**. 5(2): 32-39; October, 2014.
- [75] E. S. Moustafa and et al. “Structural and optical properties of lithium borobismuthate glasses”, **Journal of Physics and Chemistry of solids**. 69(9): 2281 –2287; September, 2008.
- [76] R. Laopaiboon and C. Bootjomchai. “Thermoluminescence studies on alkali-silicate glass doped with dysprosium oxide for use in radiation dosimetry measurement”, **Journal of Luminescence**. 158: 275-280; February, 2015.
- [77] R. Laopaiboon and et al. “The effects of gamma irradiation on the elastic properties of soda lime glass doped with cerium oxide”, **Journal of Alloys and Compounds**. 666: 292-300; May, 2016.
- [78] H. Afifi and S. Marzouk. “Ultrasonic velocity and elastic moduli of heavy metal tellurite glasses”, **Materials chemistry and physics**. 80(2): 517-523; May, 2003.
- [79] A. A. Higazy and B. Bridge. “Elastic constants and structure of the vitreous system  $\text{Co}_3\text{O}_4$  - $\text{P}_2\text{O}_5$ ”, **Journal of Non-Crystalline Solids**. 72: 81-108; May, 1985.
- [80] Markus Diantoro and et al. “The Role of  $\text{Fe}_2\text{O}_3$  and Light Induced on Dielectric Properties of Borosilicate Glass”, **Journal of Physics: Conference Series**. 846: 012007; November, 2015.
- [81] C. Bootjomchai and et al. “Structural investigation of borosilicate recycled-barium–bismuth glasses under the influence of gamma-irradiation through ultrasonic and FTIR studies”, **Nuclear Engineering and Design**. 248: 28–34; July, 2012.

## REFERENCES (CONTINUED)

- [82] Samir Y. Marzouk and et al. “Linear and non-linear optics and FTIR characteristics of borosilicate glasses doped with gadolinium ions”, **Optical Materials**. 35(12): 2077–2084; October, 2013.
- [83] M.K. Halimah and et al. “Optical properties of lithium borate glass  $(\text{Li}_2\text{O})_x(\text{B}_2\text{O}_3)_{1-x}$ ”, **Sains Malays**. 43(6): 899–902; June, 2014.
- [84] K.Maheshvaran and P.K.Veeran. “Structural and optical studies on  $\text{Eu}^{3+}$  doped boro-tellurite glasses”, **Solid State Sciences**. 17: 54-62; March, 2013.
- [85] Fouad El-Diasty et al. “Optical band gap studies on lithium aluminum silicate glasses doped with  $\text{Cr}^{3+}$  ions”, **Journal of Applied Physics**. 100: 093511; November, 2006.
- [86] Gaofeng Shao. “Thermal shock behavior and infrared radiation property of integrative insulations consisting of  $\text{MoSi}_2$ /borosilicate glass coating and fibrous  $\text{ZrO}_2$  ceramic substrate”, **Surface and Coatings Technology**. 270: 154-163; May 2015.
- [87] M.K. Halimah and C. Eevon. “Comprehensive study on the effect of  $\text{Gd}_2\text{O}_3$  NPs on elastic properties of zinc borotellurite glass system using non-destructive ultrasonic technique”, **Journal of Non-Crystalline Solids**. 511: 10-181; May 2019.
- [88] A. Makishima and J.D. Mackenzie. “Direct calculation of Young's modulus of glass”, **Journal of Non-Crystalline Solids**. 12: 35–45; May 1973.
- [89] A. Makishima and J.D. Mackenzie. “Calculation of bulk modulus, shear modulus and Poisson's ratio of glass”, **Journal of Non-Crystalline Solids**. 17: 147–157; March 1975.
- [90] C. Bootjomchai and et al. “Gamma-ray shielding and structural properties of barium–bismuth–borosilicate glasses”, **Radiation Physics and Chemistry**. 81(7): 785-790; July 2012.
- [91] J.Dutchaneephet and et al. “Spectroscopic property and color of bismuth silicate glasses with addition of 3d transition metals”, **Materials letters**. 229: 174-177; October, 2018.

## REFERENCES (CONTINUED)

- [92] M.K.Halimah and et al. “Influence of bismuth oxide on gamma radiation shielding properties of boro-tellurite glass”, **Journal of Non-Crystalline Solid**. 512: 140-147; May, 2019.
- [93] J. Park and H. J. Kim. “X-ray and photon luminescence of bismuth-borate glasses”, **Journal of Korea Physical Society**. 59: 657-660; August 2011.

## **APPENDICES**

## **APPENDIX A**

### **TOOLS**



## Material and instrument in research



**Figure A.1 Electronic balance (Precisa d05M-200A) having an accuracy of 0.0001 g**



**Figure A.2 Compound clay crucible**



**Figure A.3 Stainless steel mold**



**Figure A.4 Electric furnace was developed by GTEC.**



**Figure A.4 Annealing furnace was developed by GTEC.**



**Figure A.5 Grinding and polishing machine was developed by GTEC.**



**Figure A.6 Ultraviolet-visible spectrophotometer (PerkinElmer instruments system 2000) at Chemistry Department, Faculty of science, Ubon Ratchathani University**



**Figure A.7 Ultrasonic flaw detector (SONATEST: SITESCAN 230)**



**Figure A.8 Fourier Transform Infrared (FTIR) Spectrophotometer (Scientific Instrument Center, Ubon Ratchathani University)**



**Figure A.9 Power supply (model 31060: Canberra)**



**Figure A.10 Amplifier (model 2022: Canberra)**



**Figure A.11 Multichannel Analyses (MCA)**

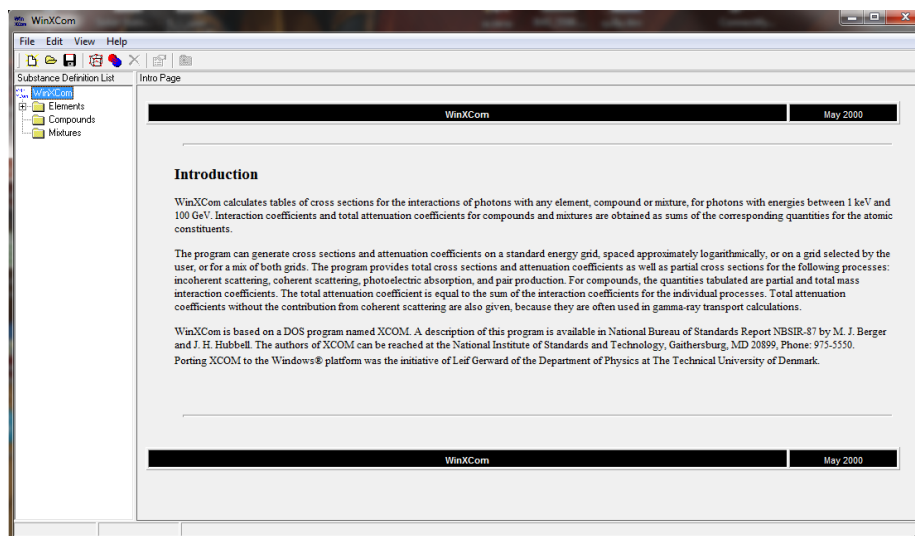


**Figure A.12 WinXcom program**



**Figure A.13 High pressure sodium lamp**

**APPENDIX B**  
**PUBLICATION / PROCEEDING**



## PUBLICATION / PROCEEDING

- [1] **Y. Jaichueai**, C. Bootjomchai, J. Laopaiboon and R. Laopaiboon, 2015, “Effect of doping  $\text{Cu}_2\text{O}$  on elastic and structural properties of  $90\text{RWG} - 10\text{Na}_2\text{O} - x\text{Cu}_2\text{O}$  glasses”, Siam Physics Congress, Krabi, Thailand
- [2] **Y. Jaichueai**, J. Laopaiboon, C. Bootjomchai, C. Yenchai and R. Laopaiboon, 2016, “Investigation of  $90\text{RWG} - 10\text{Na}_2\text{O} - 0.01\text{Cu}_2\text{O}$  thermoluminescence dosimeter on the effective atomic number and elastic properties”, Siam Physics Congress, Ubon ratchathani, Thailand
- [3] **Y. Jaichueai**, L. Singsawat, C. Bootjomchai, O. Jaiboon, J. Laopaiboon, U. Patakham and R. Laopaiboon, 2017, “The investigation of  $x\text{CaO} - (50-x)\text{SrO} - 50\text{B}_2\text{O}_3$  glass systems added with CaO from cassava rhizome on elastic and structural properties”, Journal of Science and Technology Ubon Ratchathani University, Vol. 19, 153-162.
- [4] M. Kurudirek, **N. Chutithanapanon**, R. Laopaiboon, C. Yenchai, C. Bootjomchai, 2018, “Effect of  $\text{Bi}_2\text{O}_3$  on gamma ray shielding and structural properties of borosilicate glasses recycled from high pressure sodium lamp glass”, Journal of alloys and compounds, 745, 355-364.
- [5] N. Suebsing, **N. Chutithanapanon**, P. Juntarat, R. Laopaiboon and C. Bootjomchai, 2018, “An investigation of structural and elastic properties of soda-lime glasses doped with rare earth oxide”, Journal of Physics: Conference Series, 1144 012129.
- [6] **N. Chutithanapanon**, R. Laopaiboon, C. Bootjomchai, 2019, “Investigation of the optical properties of borosilicate glass recycled from high-pressure sodium lamp glasses (HPSg): Compositional dependence by adding  $\text{Bi}_2\text{O}_3$ ” Journal of physics and chemistry of solids, 132, 244-251.
- [7] **Y. Jaichueai**, C. Bootjomchai, J. Laopaiboon and R. Laopaiboon, 2019, “Elastic Properties of Recycled Soda-lime Glasses Doped with Copper(I)oxide ( $\text{Cu}_2\text{O}$ ) Studied by Ultrasonic Technique and Fourier Transform Infrared Spectroscopy”, Journal of Science and Technology Ubon Ratchathani University, Vol. 19, 119-128.

**VITAE**

<b>NAME</b>	Mr. Natsupon Chutithanapanon
<b>ADDRESS</b>	31/1 Obtom, Samko, Angthong, Thailand, 14160
<b>DATE OF BIRTH</b>	December 17, 1991
<b>CONTACT</b>	N.chutithanapanon@gmail.com
<b>EDUCATION</b>	2014-1016: Master of Science in Physics (M.Sc. Physics), Ubon Ratchathani University, Ubon Ratchathani, Thailand 2010-2014: Bachelor of Science in Physics (B.Sc. Physics), Ubon Ratchathani University, Ubon Ratchathani, Thailand
<b>SCHOLARSHIP</b>	Royal Golden Jubilee PhD project (RGJ) under the Thailand research fund of the royal Thai government (grant no. PHD/0060/2560)
<b>PUBLICATION</b>	5 papers 2 proceedings of the international conferences